ACTA GEOLOGICA

ACADEMIAE SCIENTIARUM HUNGARICAE

REDIGIT

E. SZÁDECZKY-KARDOSS

TOMUS IV

AKADÉMIAI KIADÓ
BUDAPEST
1957

ACTA GEOLOGICA

ACADEMIAE SCIENTIARUM HUNGARICAE

REDIGIT

SZÁDECZKY-KARDOSS E.

TOMUS IV FASCICULUS 1

MAGYAR TUDOMÁNYOS AKADÉMIA

BUDAPEST, 1956

ACTA GEOLOGICA

A MAGYAR TUDOMÁNYOS AKADÉMIA FÖLDTANI KÖZLEMÉNYEI

SZERKESZTŐSÉG ÉS KIADÓHIVATAL: BUDAPEST, V., ALKOTMÁNY U. 21

Az *Acta Geologica* orosz, francia, német és angol nyelven közöl értekezéseket a földtan és rokon tudományok köréből.

Az *Acta Geologica* változó terjedelmű füzetekben jelenik meg, több füzet alkot évenként egy kötetet.

A közlésre szánt kéziratok, géppel írva, a következő címre küldendők:

Acta Geologica, Budapest, 62. Postafiók 440.

Ugyanerre a címre küldendő minden szerkesztőségi és kiadóhivatali levelezés.

Az *Acta Geologica* előfizetési ára kötetenként belföldre 80 forint, külföldre 110 forint. Megrendelhető a belföld számára az «Akadémiai Kiadó»-nál (Budapest, V., Alkotmány utca 21. Bankszámla 04-878-111-46), a külföld számára pedig a «Kultúra» Könyv- és Hírlap-Külkereskedelmi Vállalatnál (Budapest, VI., Sztálin út 12. Bankszámla: 43-790-057-181), vagy külföldi képviseleteinél és bizományosainál.

«*Acta Geologica*» публикует научные статьи из области геологических наук на русском, французском, английском и немецком языках.

«*Acta Geologica*» выходит отдельными выпусками разного объема. Несколько выпусков составляют ежегодно один том.

Предназначенные для публикации рукописи (в напечатанном на машинке виде) следует направлять по адресу:

Acta Geologica, Budapest, 62. Postafiók 440.

По этому же адресу направлять всякую корреспонденцию для редакции и администрации.

Подписная цена «*Acta Geologica*» — 110 форинтов за том. Заказы принимает предприятие по внешней торговле книг и газет «Kultúra» (Budapest, VI., Sztálin út. Текущий счет № 43-790-057-181), или его заграничные представительства и уполномоченные.

DÉTERMINATION DES VALEURS NUMÉRIQUES POUR LE MOMENT D'INERTIE, LE MOMENT ANGULAIRE ET L'ÉNERGIE CINÉTIQUE ROTATOIRE DE L'ATMOSPHÈRE TERRESTRE

Par

L. AUJESZKY

INSTITUT MÉTÉOROLOGIQUE DE HONGRIE, BUDAPEST

I. Introduction

La Terre (et, liée à elle, l'atmosphère) étant soumise à une rotation autour de l'axe terrestre, il est évident qu'on doit considérer, pour chacun de ces systèmes matériels, comme données physiques fondamentales les trois grandeurs suivantes : le moment d'inertie du système (relativement à l'axe terrestre), le moment angulaire du mouvement rotatoire, et l'énergie cinétique de la rotation.

Or, pour l'ensemble du globe terrestre (y compris l'atmosphère) les valeurs numériques approximatives de ces trois quantités sont bien connues.* Par contre, le moment d'inertie de l'atmosphère et les deux autres quantités se rapportant à l'atmosphère n'ont pas encore été, à notre connaissance, déterminées.

Le fait curieux que ces données fondamentales de l'atmosphère terrestre sont restées, jusqu'ici, numériquement inconnues, s'explique d'une part par le caractère onéreux des calculs arithmétiques qu'on doit surmonter afin de résoudre ce problème. De plus, le désir de connaître les valeurs du moment angulaire et de l'énergie rotatoire a été, pendant très longtemps, effacé par la conception fausse que les couches supérieures de l'atmosphère pourraient posséder une vitesse angulaire différente de celle des couches inférieures, ce qui aurait introduit de nouvelles complications au traitement mathématique du problème.

Or, ce dernier scrupule a été entièrement dissipé par les recherches météorologiques exécutées au cours de ces dernières années. On peut, aujourd'hui, considérer comme un fait établi que la masse entière de l'atmosphère (y compris même les couches ionosphériques) participe, d'une manière complète, à la rotation de la Terre avec une commune valeur de la vitesse angulaire. Cette vitesse angu-

* Déterminations du moment d'inertie du globe terrestre :
P. M. S. BLACKETT, Nature, Mai 17, 1947.
J. BARNÓTHY. Nature, Juin 15, 1946 (approximation plutôt rudimentaire).
Le moment d'inertie étant connu, les valeurs des deux autres quantités s'ensuivent par un calcul élémentaire, à partir de la connaissance de la vitesse angulaire.

laire comporte, pour l'époque géologique actuelle, la valeur suivante :

$$\omega = 7{,}29 \cdot 10^{-5} \text{ rad/sec} \tag{1}$$

elle a possédé, toutefois, une valeur bien supérieure pendant les époques géologiques anciennes (au moins le quadruple de la valeur actuelle).

L'essentiel du problème (et la principale difficulté) réside dans la détermination de la valeur numérique du moment d'inertie de l'atmosphère en rotation. En ce qui suit, nous développons une méthode pour accomplir cette tâche, méthode par laquelle nous allons démontrer les faits suivants :

A) Ordre de grandeur du moment d'inertie de l'atmosphère terrestre :

$$10^{39} \text{ gr cm}^2$$

B) A partir de quelques hypothèses géophysiques bien fondées, nous allons déduire que la valeur numérique du moment d'inertie de l'atmosphère (Θ_a) doit être comprise entre les limites :

$$1{,}41 \cdot 10^{39} < \Theta_a < 1{,}57 \cdot 10^{39} \text{ gr cm}^2 \tag{2}$$

contenant une détermination de cette valeur avec une exactitude de 10% environ.

Comme le moment angulaire (S_a) et l'énergie rotatoire (E_a) sont liés à Θ_a par les formules élémentaires :

$$S_a = \omega \Theta_a \tag{3}$$

$$E_a = \frac{\omega^2}{2} \Theta_a \tag{4}$$

on obtient immédiatement à partir de l'inégalité (2), les résultats suivants :

C) L'ordre de grandeur du moment angulaire de l'atmosphère est de

$$10^{35} \text{ gr cm}^2\text{rad/sec}$$

et l'ordre de grandeur de l'énergie cinétique rotatoire de l'atmosphère est de

$$10^{30} \text{ erg}$$

D) Les valeurs numériques du moment angulaire (S_a) et de l'énergie rotatoire (E_a) pour l'atmosphère se trouvent entre les limites :

$$1{,}03 \cdot 10^{35} \text{ gr cm}^2\text{rad/sec} < S_a < 1{,}15 \cdot 10^{35} \text{ gr cm}^2\text{rad/sec} \tag{5}$$

$$3{,}73 \cdot 10^{30} \text{ erg} < E_a < 4{,}74 \cdot 10^{30} \text{ erg} \tag{6}$$

en supposant, toutefois, que les hypothèses — expliquées ci-dessous — servant à déduire l'inégalité (2) soient valables.

II. Simplifications couramment adoptées

Afin de déduire les résultats énoncés sous *A)* et *B)*, nous ne faisons usage que des simplifications suivantes, utilisées, d'ailleurs, couramment en météorologie.

Pour obtenir l'énoncé *A)*, on a besoin de trois simplifications :

1. Qu'il est permis de traiter la Terre en *sphère*, c'est-à-dire, que les dimensions de la Terre peuvent se caractériser par une seule quantité (le rayon terrestre, désigné par a_0) ;

2. qu'il est permis de traiter l'atmosphère terrestre en sphère-creuse, c'est-à-dire, que les dimensions de l'atmosphère peuvent être caractérisées par les deux quantités a_0 (rayon intérieur) et H (hauteur de l'atmosphère) ;

3. qu'il est permis de supposer, dans l'atmosphère, une distribution de masses laquelle ne contient des inhomogénéités que suivant la verticale, et dans laquelle il y a une parfaite homogénéité horizontale.

De ces présomptions, 1 et 2 sont reconnues entièrement en météorologie puisqu'elles représentent une si bonne approximation à l'état véritable, que les erreurs émanant de leur acceptation sont inférieures à la limite d'exactitude avec laquelle les autres grandeurs météorologiques fondamentales (par exemple la température, la masse de l'atmosphère) peuvent être mesurées.

La présomption 3 est également très acceptable, puisque dans l'atmosphère, de grandes inhomogénéités de densité n'existent que suivant la verticale, — la diminution très rapide de la densité vers le haut étant une conséquence de la compressibilité de l'air soumis à la pesanteur.

Pour obtenir les résultats exprimés par le côté gauche de l'inégalité double du paragraphe *B)*, (c'est-à-dire pour établir une limite inférieure pour la valeur du moment d'inertie) aucune autre simplification ne sera utilisée.

Afin de démontrer la validité de la partie droite de l'inégalité double du paragraphe *B)*, il serait nécessaire de faire usage, hormis les simplifications 1 et 2, d'une présomption ultérieure, selon laquelle :

4. L'altitude (l'épaisseur) de l'atmosphère est inférieure à un-cinquième du rayon du globe terrestre :

$$H < 0{,}2\ a_0 \tag{7}$$

Comme les énoncés *C)* et *D)* sont des conséquences de *A)* et *B)*, il s'ensuit, que :

l'énoncé *C)* ainsi que les deux limites inférieures données sous *D)* ne reposent que sur les présomptions 1, 2 et 3 ;

mais pour la validité des limites supérieures du paragraphe *B)*, il est nécessaire encore d'accepter la présomption 4.

III. Détermination du moment d'inertie de l'atmosphère terrestre

Une des explications du fait remarquable que le moment d'inertie a été déterminé pour le globe terrestre par plusieurs auteurs (cités plus haut), tandis qu'il n'a pas été, jusqu'ici, déterminé pour l'atmosphère, doit être cherchée dans la distribution verticale compliquée des masses atmosphériques.

Cette distribution est caractérisée, d'une part, par la diminution extrêmement rapide de la densité avec la hauteur. Rappelons en cette connexion que l'atmosphère possède une hauteur de 1000 km au moins, mais que 50% de la masse de l'atmosphère se trouvent concentrés dans la couche inférieure qui n'a que 6 km d'épaisseur. D'autre part, la variation de la densité suivant la verticale ne peut être décrite par une expression analytique uniformément valable à toutes les altitudes, puisque l'atmosphère se compose d'une série de domaines superposés l'un à l'autre (à savoir, la troposphère, la stratosphère, quatre domaines mésosphériques successives, l'ionosphère,* l'exosphère) pour lesquelles des expressions analytiques spéciales sont valables, donnant pour chaque domaine la densité en fonction de l'altitude. Les différences entre ces expressions analytiques, utilisables pour un domaine vertical déterminé de l'atmosphère, ne se bornent pas aux valeurs numériques des coefficients : il s'agit de fonctions entièrement différentes. Par exemple, pour la troposphère, on a une diminution de la densité suivant une puissance de l'altitude (approximativement la sixième puissance), tandis que pour d'autres domaines, dont la stratosphère, on doit recourir à une fonction exponentielle.

Pour une masse dont la distribution est tellement irrégulière, c'est une tâche bien compliquée de calculer, par une méthode directe, la valeur du moment d'inertie. En conséquence, nous avons préféré de choisir une voie indirecte, consistant dans la recherche de limites inférieures et supérieures d'une exactitude suffisante.

Il est connu, que le moment d'inertie (relativement à un axe passant par le centre) d'une sphère-creuse de densité homogène, possédant un rayon intérieur a et une épaisseur H, est exprimé par la formule

$$\Theta = \frac{2}{5} \frac{(a+H)^5 - a^5}{(a+H)^3 - a^3} DV \tag{8}$$

D étant la densité (possédant la même valeur à tous les points du corps) et V le volume :

$$V = \frac{4\Pi}{3} [(a+H)^3 - a^3] \tag{9}$$

* Ce terme a été remplacé récemment, suivant une décision de l'UGGI, par la dénomination thermosphère.

Au cas d'une sphère-creuse de densité non-homogène, on peut toujours considérer une sphère-creuse d'épaisseur élémentaire (da) comme possédant le moment d'inertie (élémentaire) :

$$d\Theta = \frac{2}{5}\,\frac{(a+da)^5 - a^5}{(a+da)^3 - a^3}\,DdV \tag{10}$$

avec

$$dV = 4\Pi a^2 da \tag{11}$$

En appliquant, à la formule (10), le théorème binomial, et en négligeant les quantités de second ordre, nous obtenons :

$$d\Theta = \frac{2}{5}\,\frac{5\,a^4}{3\,a^2}\,DdV = \frac{2}{3}\,a^2 DdV \tag{12}$$

ou bien, conformément à (11),

$$d\Theta = \frac{8\Pi}{3}\,a^4 Dda \tag{13}$$

Il s'ensuit, qu'on va obtenir le moment d'inertie d'une sphère-creuse, d'une distribution inhomogène de densité (mais ne possédant que des inhomogénéités verticales), par intégration de la formule (13) :

$$\Theta = \frac{8\Pi}{3}\int_{a=a_0}^{a_0+H} a^4 Dda \tag{14}$$

Cette expression semble être applicable, en principe, aussi au cas de l'atmosphère terrestre. Toutefois, il serait nécessaire de substituer, à la place de a_0, le rayon terrestre, à la place de H, la hauteur de l'atmosphère, et à la place de D, une formule explicite et unique décrivant la variation de la densité en fonction de l'altitude, figurant comme la variable d'intégration. Or, la valeur de H (mesurée par la distance du centre de la Terre), n'est pas encore connue et, pour D, il n'existe pas, comme nous l'avons remarqué, une formule unique valable pour toutes les hauteurs de l'atmosphère, formule par laquelle la variation de cette quantité pourrait s'exprimer en fonction de la distance du centre de la Terre. Par suite, l'intégrale (14) n'est pas directement utilisable pour obtenir une valeur numérique du moment d'inertie de l'atmosphère.

C'est en raison de ces circonstances que nous avons été amenés à la recherche d'une approximation au moyen de limites supérieures et inférieures.

Les procédés pour obtenir des valeurs inférieures et supérieures à la valeur réelle du moment d'inertie seront fondés sur le même principe. On va s'appuyer sur la considération que tout changement dans la répartition verticale des masses atmosphériques sera accompagné par un changement du moment d'inertie de la manière suivante : la subsidence de masses d'air résulte, en général, en une diminution du moment d'inertie, et l'ascension de l'air est suivie, en général, par une augmentation de cette quantité. On démontre la validité de ces assertions par la circonstance qu'un mouvement vertical descendant représente, en général, un approchement de masses à l'axe terrestre, (à l'exception du cas quand l'air situé exactement au-dessus du pôle exécute une descente verticale), ce qui amène, par définition, la diminution du moment d'inertie. Se servant du même raisonnement, on trouve que par l'ascension de masses il doit se produire une augmentation du moment d'inertie.

Il en résulte que si l'on calcule le moment d'inertie à partir d'un modèle imaginaire de l'atmosphère lequel montre une distribution verticale fictive des masses, distribution dans laquelle toutes les masses élémentaires occupent une altitude inférieure à celle qu'elles occupent dans l'atmosphère réelle : on va aboutir à une valeur Θ_1 du moment d'inertie de ce modèle, valeur qui sera certainement inférieure à celle du moment d'inertie de l'atmosphère réelle Θ_a. Similairement, si l'on exécute des calculs à partir d'un modèle dans lequel les masses se trouvent, systématiquement, en une altitude plus grande que dans l'atmosphère réelle, on va aboutir à une valeur Θ_2 laquelle est nécessairement supérieure à la valeur réelle — mais inconnue — Θ_a. On pourra donc délimiter la valeur inconnue Θ_a par une inégalité double :

$$\Theta_1 < \Theta_a < \Theta_2 \tag{15}$$

On s'efforce naturellement à trouver des modèles qui pourront permettre une calculation relativement simple des valeurs Θ_1 et Θ_2 et livrant, en même temps, des valeurs Θ_1 et Θ_2 très rapprochées l'une de l'autre, c'est-à-dire, permettant, à l'aide de l'inégalité (15), une bonne approximation de la valeur Θ_a. Pour satisfaire à ces exigeances, nous allons employer les modèles suivants de la distribution verticale des masses.

a) *Déduction d'une approximation inférieure* Θ_1. Si la masse entière de l'atmosphère pouvait être ramenée au niveau du sol et concentrée en une sphère-creuse de minceur élémentaire, le moment d'inertie de ce corps serait certainement inférieur à Θ_a, puisque le modèle pourrait être réalisé à partir de l'atmosphère réelle par la descente de toutes les masses d'air jusqu'au niveau du sol.

Un tel changement de la distribution verticale des masses se produirait dans le cas si l'atmosphère, sujette à une perte de chaleur énorme, devait se liquéfier en toute son étendue. Comme la densité de l'air liquide diffère peu de

celle de l'eau, cette couche d'air liquide posséderait, sur un globe parfaitement sphérique et plane, seulement une épaisseur de 10 mètres, ce qui peut être regardé (en comparaison aux dimensions de la Terre elle-même) comme une couche de minceur presque élémentaire.

On se trouve donc autorisé à considérer le moment d'inertie de la sphère-creuse élémentaire comme une valeur Θ_1 certainement inférieure à Θ_a. D'autre part, la détermination numérique de cette valeur de Θ_1 est facilement exécutée, puisqu'elle peut être tirée de la formule générale (12) valable pour toutes les sphères-creuses élémentaires, en substituant, à la place de a, la valeur du rayon terrestre a_0, et, à la place de la masse $D \cdot dV$ la masse M_a de l'atmosphère :

$$\Theta_1 = \frac{2}{3} a_0^2 M_a \tag{16}$$

Il ne reste que de substituer les valeurs bien connues :

$$a_0 \sim 6{,}37 \cdot 10^8 \text{ cm} \tag{17a}$$

$$M_a \sim 5{,}2 \cdot 10^{21} \text{ gr} \tag{17b}$$

En exécutant les calculs numériques, on obtient, comme approximation inférieure du moment d'inertie de l'atmosphère :

$$\Theta_1 = 1{,}41 \cdot 10^{39} \text{ gr cm}^2 \tag{18}$$

b) *Déduction d'une approximation supérieure* Θ_2. Afin d'obtenir une approximation supérieure d'une exactitude suffisante, il est nécessaire d'utiliser un modèle un peu plus compliqué. Nous allons séparer l'atmosphère, en imagination, en deux sphères-creuses (une «inférieure» et une «supérieure»), de masses égales à $M_a/2$ chacune. La surface de séparation coïncide donc approximativement avec la surface isobarique de 500 millibars, située, on le sait, en une altitude entre 5 et 6 kilomètres.

Pour ce qui suit, nous nous servirons des symboles suivants : l'épaisseur de la sphère-creuse inférieure sera désignée par αa_0, la hauteur entière de l'atmosphère par βa_0 ; les quantités α et β représentent donc les épaisseurs de la sphère-creuse inférieure et de l'atmosphère entière, exprimées en unités de longuer a_0.

En désignant le moment d'inertie de la sphère-creuse inférieure par Θ_i et celui de la supérieure par Θ_s, on a, par suite de l'additivité des moments d'inertie

$$\Theta_a = \Theta_i + \Theta_s \qquad (19)$$

Nous allons construire, à l'aide du principe exposé en haut, des approximations supérieures pour les deux moments d'inertie Θ_i et Θ_s. La somme de ces deux approximations supérieures doit fournir, conformément à (19), une approximation supérieure de la quantité Θ_a.

Des approximations supérieures pour les deux moments d'inertie peuvent être dérivées, à partir du principe utilisé dans les calculs précédents, par l'établissement d'un modèle imaginaire de la répartition verticale des masses, répartition dans laquelle les masses sont déplacées vers le haut relativement à leur position dans l'atmosphère réelle. Nous allons réaliser un tel modèle en distribuant, dans les mêmes volumes, mais avec une densité homogène la même masse $M_a/2$, qui se trouve, dans le cas réel, distribuée avec une très grande inhomogénéité verticale.

Les deux modèles étant de densité homogène, on peut aisément obtenir, à partir de l'équation (8), leur moment d'inertie, en exécutant les substitutions suivantes :*

Pour la sphère-creuse inférieure :

$$\begin{gathered} a = a_0 \\ H = \alpha\, a_0 \\ a + H = (1 + \alpha)\, a_0 \\ DV = M_a/2 \end{gathered} \qquad (21)$$

Pour la sphère-creuse supérieure :

$$\begin{gathered} a = a_0 + \alpha\, a_0 \\ H = (\beta - \alpha)\, a_0 \\ a + H = (1 + \beta)\, a_0 \\ DV = M_a/2 \end{gathered} \qquad (22)$$

* Il eût été, naturellement, plus aisé de procéder au lieu de la séparation de l'atmosphère en deux parties, directement à établir un modèle dans lequel la masse entière de l'atmosphère se trouve distribuée, avec une densité uniforme, dans le même volume que possède l'atmosphère réelle. Toutefois, ce calcul beaucoup plus simple ne peut livrer une approximation d'exactitude suffisante; elle n'aboutit qu'à l'approximation superieure bien rudimentaire de

$$\Theta_2 = 1{,}74 \cdot 10^{39} \text{ gr cm}^2 \qquad (20)$$

tandis qu'au moyen de la séparation de l'atmosphère en deux parties et de l'application de modèles spéciaux à chacune d'elles, on va obtenir des approximations entièrement satisfaisantes.

On en tire les approximations suivantes :

$$\Theta_i < \frac{2}{5}\,\frac{(1+\alpha)^5-1}{(1+\alpha)^3-1}\,\alpha_0^2\,\frac{M_a}{2} = \frac{1}{5}\,\frac{(1+\alpha)^5-1}{(1+\alpha)^3-1}\,\alpha_0^2 M_a \qquad (23)$$

$$\Theta_s < \frac{2}{5}\,\frac{(1+\beta)^5-(1+\alpha)^5}{(1+\beta)^3-(1+\alpha)^3}\,\alpha_0^2\,\frac{M_0}{2} = \frac{1}{5}\,\frac{(1+\beta)^5-(1+\alpha)^5}{(1+\beta)^3-(1+\alpha)^3}\,\alpha_0^2 M_a \qquad (24)$$

Par addition des approximations supérieures des deux sphères-creuses (23) et (24), on a, conformément à (19), une approximation supérieure de Θ_a :

$$\Theta_a < \frac{a_0^2 M_a}{5}\left\{\frac{(1+\alpha)^5-1}{(1+\alpha)^3-1} + \frac{(1+\beta)^5-(1+\alpha)^5}{(1+\beta)^3-(1+\alpha)^3}\right\} \qquad (25)$$

Il nous reste encore de procéder à une évaluation numérique des expressions se trouvant au côté droit des inégalités (23) et (24), et introduire les valeurs trouvées en la formule finale (25).

Quant à l'expression figurant sous (23), il est évident qu'elle doit s'accroître d'une façon monotone avec α. D'autre part, l'expression se trouvant à la droite de la formule (24) croît avec β, mais elle diminue avec la croissance de la quantité α. Or, on va obtenir une inégalité d'une validité à fortiori, par le procédé de remplacer, en (23), la valeur véritable de la quantité α par une valeur plus élevée ; de même, on aura, à partir de (24), une inégalité, valable également à fortiori, en remplaçant, dans cette inégalité, β par une valeur plus élevée, et en même temps α par une valeur plus basse.

Comme α signifie l'épaisseur de la sphère-creuse inférieure (correspondant, comme nous l'avons dit, à une valeur entre 5 et 6 km), mais exprimée en unités de rayon terrestre, on a certainement

$$\frac{5}{6370} < \alpha < \frac{6}{6370} \qquad (26)$$

D'autre part, notre présomption (7) sur l'épaisseur de l'atmosphère nous fournit.

$$\beta < 0{,}2 \qquad (27)$$

Les inégalités (26) et (27) assurent le moyen d'introduire, dans (23), une valeur certainement supérieure à α, et, dans (24), une valeur certainement supérieure à β et, en même temps, une valeur certainement inférieure à α, ce

qui conduit, en raison de ce que nous avons démontré, aux inégalités, valables *a fortiori*

$$\Theta_i < 1{,}6786\,\frac{a_0^2 M_a}{5} \tag{28}$$

$$\Theta_s < 2{,}0455\,\frac{a_0^2 M_a}{5} \tag{29}$$

et, par addition, on a

$$\Theta_a = \Theta_i + \Theta_s < 3{,}7241\,\frac{a_0^2 M_a}{5} \tag{30}$$

Enfin, en substituant les valeurs numériques couramment utilisées pour a_0 et M_a, nous obtenons

$$\Theta_a < 1{,}57 \cdot 10^{39}\ \text{cm}^2\text{gr} \tag{31}$$

L'approximation inférieure (18) et l'approximation supérieure (31), prises ensemble, fournissent la vérification de l'énoncé contenu dans la formule (2) laquelle était à prouver.

IV. Influence de notre incertitude concernant la hauteur de l'atmosphère sur les résultats obtenus dans cet article

La validité des résultats concernant les ordres de grandeur et les valeurs numériques du moment d'inertie (Θ_a), du moment angulaire (S_a) et de l'énergie cinétique rotatoire (E_a) de l'atmosphère terrestre, énoncés aux paragraphes *A)*, *B)*, *C)* et *D)* au début de l'article, a été démontrée au Chapitre III. par un raisonnement aboutissant à la vérification des approximations numériques inférieure et supérieure de la formule (2), ce qui fournissait aussi les valeurs numériques de S_a et E_a par l'application des formules élémentaires (3) et (4). Dans la dernière partie de la déduction du Chapitre III, nous avons fait usage de l'hypothèse que la hauteur de l'atmosphère terrestre ne dépasse pas la valeur de 1274 km. Or, une connaissance certaine de la hauteur de l'atmosphère n'est pas à notre disposition à l'heure qu'il est. Conséquemment, on pourrait s'imaginer que des découvertes nouvelles concernant la limite de l'atmosphère pourraient, à l'avenir, ébranler la validité des résultats obtenus. Il est donc nécessaire de se faire une idée sur les modifications qu'un tel événement pourrait apporter à nos conclusions.

Un traitement de cette question apparaît d'autant plus désirable, puisque l'histoire de la météorologie nous enseigne qu'il était nécessaire, au cours de l'évolution de nos connaissances sur l'atmosphère, de faire constamment reculer, à des hauteurs toujours plus grandes, l'altitude qu'on pouvait reconnaître comme la limite supérieure de l'atmosphère terrestre. Même de nos jours, se rencontrent dans la littérature des hypothèses selon lesquelles l'épaisseur de l'atmosphère devrait surpasser de beaucoup la valeur généralement acceptée de 1000 km environ.

Nous allons démontrer que la solution de cette question se peut formuler de la manière suivante :

1. Les résultats se rapportant aux ordres de grandeur énoncés sous *A)* et *C)* sont valables non seulement pour une épaisseur de l'atmosphère inférieure à 1274 km ($\beta < 0{,}2$), mais elles sont également correctes pour des valeurs de β beaucoup plus élevées.

2. Les approximations inférieures, données sous *B)* et *D)*, sont correctes indépendamment de l'épaisseur de l'atmosphère.

3. Les approximations supérieures de *B)* et *D)* ne sont plus valables pour les valeurs élevées de β.

De ces trois assertions, (2) et (3) ne sont que des conséquences évidentes du fait que, pour obtenir les approximations inférieures, nous ne faisons aucun usage d'une hypothèse concernant la valeur de β, tandis que pour déduire les approximations supérieures, nous devions, dans la formule (25), laquelle était encore indépendente de la valeur de β, introduire la valeur 0,2. Or, ce dernier procédé serait inadmissible si l'hypothèse $\beta \leqq 0{,}2$ était fausse, puisque (25) augmente, d'une façon monotone, avec β.

Pour démontrer l'assertion (1), selon laquelle les ordres de grandeur restent valables même pour des valeurs de β surpassant notablement 0,2, nous allons utiliser, de nouveau, le fait que l'expression au côté droit de l'inégalité (25) croît d'une manière monotone avec la grandeur β. Par conséquent, il suffit de prouver qu'il existe des valeurs β notablement plus élevées que 0,2, pour lesquelles l'ordre de grandeur de cette expression ne dépasse pas 10^{39} unités CGS.

Pour obtenir cette preuve, nous allons considérer une épaisseur dix fois plus grande que la valeur généralement acceptée aujourd'hui, c'est-à-dire, nous allons substituer, à (25), la valeur $\beta = 2$ correspondant à une atmosphère dont l'épaisseur serait le double de la valeur du rayon de la Terre.

En exécutant cette substitution, on a toujours

$$\Theta_a < \frac{a_0^2 M_a}{5} \left\{ \frac{(1+\alpha)^5 - 1}{(1+\alpha)^3 - 1} + \frac{3^5 - (1+\alpha)^5}{3^3 - (1+\alpha)^3} \right\}$$

Or, la première expression figurant dans la parenthèse est, comme nous l'avons établi sous (28), inférieure à 1,68. Quant à l'expression suivante, nous

allons l'augmenter, comme nous l'avons fait plus haut, en substituant, à la place de a, la valeur plus petite de 5/6370. Après avoir exécuté les calculs numériques et substitué, pour a_0 et M_a, les données citées sous (17a) et (17b), nous obtenons $4{,}6 \cdot 10^{39}$. Par là, nous avons prouvé, que même si l'atmosphère possédait une épaisseur dix fois plus grande relativement à la valeur considérée aujourd'hui comme la valeur la plus probable, l'ordre de grandeur du moment d'inertie de l'atmosphère serait toujours de 10^{39} CGS et la valeur numérique serait, même en ce cas extrême, inférieure à $5 \cdot 10^{39}$.

RÉSUMÉ

L'objet de l'article consiste à déterminer les valeurs de quelques données physiques fondamentales de l'atmosphère terrestre, numériquement inconnues jusqu'ici.

L'atmosphère exécute une rotation avec la même vitesse angulaire et autour du même axe que toutes les autres masses de notre planète. Par conséquent, on doit considérer, comme des données physiques fondamentales pour l'atmosphère et pour le globe entier, les valeurs respectives des grandeurs suivantes : du moment d'inertie relativement à l'axe terrestre ; du moment angulaire de la rotation ; et de l'énergie cinétique rotatoire.

Dans le cas du globe terrestre, la valeur numérique de ces quantités est déjà connue ; d'autre part, pour le moment d'inertie, le moment angulaire et l'énergie cinétique rotatoire de l'atmosphère, nous ne possédons jusqu'ici aucune valeur numérique, et même les ordres de grandeur restaient inconnues.

Par des considérations élémentaires, décrites dans l'article, nous avons obtenu les résultats suivants : en acceptant quelques hypothèses de simplification, couramment employées en météorologie, on trouve que les ordres de grandeur sont :

pour le moment d'inertie de l'atmosphère terrestre, 10^{39} gr cm^2
pour le moment angulaire de l'atmosphère, 10^{35} cm^2 rad/sec
pour l'énergie cinétique rotatoire de l'atmosphère, 10^{30} ergs.

L'essentiel de ce travail a consisté dans une approximation numérique de la valeur du moment d'inertie, puisque les autres deux quantités peuvent être obtenues à partir de la connaissance du moment d'inertie, par des calculs arithmétiques élémentaires. La difficulté qui empêchait, jusqu'ici, la détermination du moment d'inertie de l'atmosphère, réside dans la grande inhomogénéité de la distribution des masses atmosphériques suivant la verticale.

La méthode utilisée à surmonter cette difficulté s'appuie à la construction des approximations inférieures et supérieures à la valeur réelle du moment d'inertie de l'atmosphère.

On trouve que la valeur numérique du moment d'inertie de l'atmosphère est située entre les deux quantités $1{,}41 \cdot 10^{39}$ et $1{,}57 \cdot 10^{39}$ gr cm^2, l'approximation supérieure n'étant valable que pour une atmosphère dont l'épaisseur ne dépasse pas un-cinquième de la valeur du rayon terrestre. Ces approximations représentent la valeur du moment d'inertie de l'atmosphère avec une exactitude de 10% environ.

A partir de ce résultat, on a pour le moment angulaire (S_a) et pour l'énergie cinétique de rotation (E_a) les relations suivantes :

$$1{,}03 \cdot 10^{35}\text{CGS} < S_a < 1{,}15 \cdot 10^{35}\text{CGS}$$

$$3{,}73 \cdot 10^{30}\text{erg} < E_a < 4{,}14 \cdot 10^{30}\text{erg}$$

En supposant que la hauteur de l'atmosphère soit beaucoup plus grande que les valeurs aujourd'hui généralement acceptées, on trouve que l'exactitude des approximations supérieures diminue, mais les ordres de grandeur ne devraient pas être modifiés.

ОПРЕДЕЛЕНИЕ МОМЕНТА ИНЕРЦИИ, УГЛОВОГО МОМЕНТА И КИНЕТИЧЕСКОЙ ЭНЕРГИИ ВРАЩЕНИЯ АТМОСФЕРЫ

Л. АУЙЕСКИ

Резюме

В статье приводится определение некоторых основных физических данных атмосферы, которые в литературе до сих пор не встречаются.

Атмосфера находится в вращательном движении вокруг оси Земли с той же угловой скоростью, как и остальные массы вещества Земли. Поэтому существенными физическими данными атмосферы, а также всей Земли являются следующие величины: момент инерции, прводимый к земной оси, импульс вращения, происходящий из осевого вращения, а также кинетическая энергия осевого вращения.

Вышеуказанные три величины в отношении *всей Земли* уже известны, но момент инерции, импульс вращения и кинетическая энергия вращения *атмосферы* до сих пор не были определены, и даже в отношении порядка этих величин мы находились в полной неосведомленности.

Автор в своей статье устанавливает, что — в случае действительности приближенных представлений, привычных и общепринятых в метеорологии — порядок этих величин является следующим:

Порядок момента инерции атмосферы: 10^{39} г см^2

Порядок импульса вращения атмосферы: 10^{35} г см^2/сек.

Порядок кинетической энергии вращения атмосферы: 10^{30} эрг.

Существенной фазой определения вышеуказанных величин оказалось определение момента инерции, так как остальные две величины — со знанием угловой скорости — из момента инерции уже получаются при помощи элементарных тривиальных формул. Однако момент инерции атмосферы относительно земной оси до сих пор еще не был определен, так как крайне неравномерное вертикальное распределение масс атмосферы причинило трудности вычислению.

В статье приводится способ для преодоления этого затруднения. Идея данного способа заключается в том, что для момента инерции атмосферы изготовляются нижняя и верхняя оценки.

В качестве нижней оценки была получена следующая величина: $1{,}41 \cdot 10^{39}$ г см^2. Верхняя оценка получалась равной $1{,}57 \cdot 10^{39}$ г см^2 опираясь на предположение, что мощность атмосферы не превышает пятую часть длины радиуса Земли. Таким образом численная величина момента инерции атмосферы была определена с точностью примерно в 10%.

Из этих нижней и верхней оценок момента инерции получаются следующие более точные оценки импульса вращения (S_a) и кинетической энергии вращения (E_a) атмосферы:

$$1{,}03 \cdot 10^{35} \text{ CGS} < S_a < 1{,}15 \cdot 10^{35} \text{ CGS}$$

$$3{,}73 \cdot 10^{30} \text{ эрг} < E_a < 4{,}14 \cdot 10^{30} \text{ эрг}$$

Если высота атмосферы оказалась бы значительно больше пятой части радиуса Земли, приведенная величина верхней оценки также становилась бы большей, однако можно выявить, что результаты в отношении *порядка величин* в этом случае также являются правильными.

A 40—50 YEAR PERIOD IN THE SECULAR VARIATION OF THE GEOMAGNETIC FIELD

BY

GY. BARTA

STATE GEOPHYSICAL SURVEY OF HUNGARY, BUDAPEST

Introductory

It is an old experience that the orientation and the intensity of the geomagnetic field is varying in time. This is evident from chronologically arranging and comparing the results of the measurements performed at the same place at distant dates. The study of this phenomenon requires, however, long series of observations. Unfortunately, no series of sufficient length and reliability are available to this purpose.

Apart from a few Chinese records of the magnetic declination, our first data arrangeable in series do not date back earlier than the middle of the 15th century. During centuries these data were merely of an informatory character. No great expectations may be attached to them, because the measuring instruments and methods of those times were quite primitive.

Compared to the methods of measuring declination, those of the inclination and horizontal intensity are still more recent. Though magnetic inclination was mentioned already in 1544 by George HARTMANN, it was only in the middle of the 18th century that the improvement of the inclinatorium serving for measuring inclination advanced as much as to offer measuring results of satisfactory accuracy. No method of an absolute measurement of the magnetic intensity was known before 1832, when GAUSS published his measuring method of the horizontal intensity.

The longest and most complete series of observations on declination and inclination is that of London. Representing these data in a coordinate system, makes the periodic character of the variation obvious. Similar but much shorter series of observations made at other places present, however, curves of different shape. From this it may be concluded that the London series may possibly represent only the European secular variation whilst the variations might have been of different nature at other points of the Earth.

On the basis of the London series the period of the secular variation of the geomagnetic field is estimated at 480 years. However, this figure cannot be very accurate for the available series of declination measurements covers

but one single period. The determination of a period is greatly hindered by the uncertainty of the initial data and by the shortness of the series of inclination and horizontal intensity. Moreover, the establishment of a period is dependent also upon the method applied. This is why different values concerning the length of the period are met with in literature. Weighing the prevailing circumstances we may state that the observation series available for studies requiring greater accuracy are not longer than 100 years.

The methods to be applied to the examination of the secular variation of the geomagnetic field may also be different according to the special features of the variation. A comparison of the magnetic charts plotted at various dates reveals the regional distribution of the variation in time, in other words, on the basis of the charts we can draw the isopors of the magnetic components. The isoporic charts show that over great territories of the Earth the secular variation has the same trend. But taking into consideration that magnetic charts have not very often been prepared, further, that the observations used for the preparation have been made at widely different dates and reduced, in turn, by means of data furnished by observatories situated at considerably wide distances, we cannot expect isoporic charts to mirror the delicate details of the variation of the geomagnetic field.

The most precise representation of the magnetic field of the Earth is offered by spherical functions, the coefficients of which cover the peculiarities of the field: the first degree terms the magnitude and direction of the geomagnetic moment, the second degree the excentricity of the dipole, whilst the higher degree the different harmonic deformations of the field. The computation of the coefficients is based on various world charts drawn at different dates. Thus, it is natural that the secular variation is expressed by the coefficients. The expansion in series referring to different dates shows that the geomagnetic poles shift slowly to the west and the magnetic moment of the Earth has been decreasing during the last century.

The secular variation established in this way refers to the entire Earth, for the variation in the coefficients shows the smoothed variations in the individual areas. This is partly advantageous, for it affords conclusions of general validity, partly it is disadvantageous, since due to smoothing some of the minor local details of the variation disappear. There is also another inconvenience of this method namely, that these kinds of expansions have not often been performed and that the data of the charts serving as a basic material for the expansions contain as already mentioned several interpolations in time and space, which are fraught with more or less uncertainties. Even coefficients of spherical functions referring to the same date may show substantial differences when using charts based upon different data.

Data taken from the charts are by no means as accurate as the annual mean values furnished by one observatory. Namely the latter data measured

with the same instrument under identical circumstances, mostly for a long space of time, generally by the same observer, contain no extrapolation for time and space, these data may, therefore, be submitted to more detailed examinations. The observation series of an observatory reflect the variation at that place more precisely and clearly than the above mentioned processes, which involve a number of interpolations and adjustments. From the aggregate of observation series of many observatories it is then possible to compose a mosaic picture of the secular variation even for the whole surface of the Earth.

The accurate determination of the period of the total secular variation encounters difficulties owing to the relatively short observation series available. On the other hand, the more accurate observation series established in the last hundred years allow us to point out some phenomena of shorter duration in the secular variation and to take the conclusions to be drawn from them under examination.

The method applied

From the eighties of the last century we dispose of comparatively numerous observatories furnishing in general data of an accuracy adequate for studies of the minute peculiarities in the secular variation. Plotting the mean annual values of one magnetic element in a coordinate system may offer to some extent a picture of the secular change concerned, in the form of a curve rather irregular in shape. This is only natural, for one cannot expect the wave character of a variation of half-millennial cycle be expressed by a series of observations not exceeding some 70—80 years. Though the curve clearly shows the course of the variation at one single point of the Earth, this kind of representation is not suitable yet to draw inferences of general validity.

The first step of our method is an approximation to the series of the magnetic components observed in the single observatories, with the use as an approximating function of a power series of the time, by determining its coefficients with the method of the least squares. This was based on the assumption that the periodic function covering the variations of a long secular period may be along a relatively short time-interval well substituted by a power series. The determination of this series serves only to supply a sort of normal variation, on the basis of which we may test the minor though regularly recurring properties of the variation. The power series was used to facilitate computations, a trigonometrical function of unknown period, phase, and amplitude, being not able to offer substantial advantages against the technical difficulties involved.

The curve plotted of the series of differences between the observed and the approximating values shows a certain regularity to the extent that apparently the wave of the secular variation is superposed with a wave of a shorter period.

At observatories of the temperate zones the superimposing wave has a period of about 44 years, its amplitude is different with each observatory, but larger by far than the accuracy of the measurements (10—20′ in the declination, 200 gamma in the components of intensity).

In order to investigate this wave, we worked up the annual mean values of all observatories possessing observation series longer than 40 years. Since the examined series cannot be essentially shorter than the period of the wave, the number of the available series is considerably restricted. Choosing the degree of approximation requires some care, for an exaggerated approximation may distort the residual wave against the original one. Notwithstanding, a linear approximation is not suited for use with long series of observations, since the straight line plotted according to the approximating function does not follow at all the curved course of the main secular wave and, accordingly, it deforms also the superimposed wave. Very long series require a third degree approximation to completely filter the main wave out of the secular course. On this account, overlapping degrees of approximation, depending on the lengths of the observation series were established. To series of a period of 40—56 years a linear, to those of 44—79 years a quadratic, and to those of 73—105 years a cubic approximation was applied. Apart from a few exceptions we found that the waves obtained by adapting different degrees, scarcely diverge from each other. Thus, the series of altogether 36 observatories were comprised in our investigations (D, I, H, Y, X, Z and T elements and components, respectively) by availing of the data from the papers [3] and [4]. The observatories the records of which were taken under examination are listed in Table I. The wave presents itself in all elements and components, but for purposes of a representation of vector diagrams the components X, Y, Z are better suited than the other elements. For this reason in the present paper attention is turned to the former ones.

In order to illustrate the process of our investigations we communicate in detail the results of the computations referring to the components and the total intensity(X, Y, Z and T) recorded by the observatory at Chambon la Forêt. The observation series used in the computations are to be found in column 1 and 4 of Table II, and III. We approximated these series by the following second degree power series :

$$X = +18847 + 26{,}72t - 0{,}1728t^2 \qquad 1a$$

$$Y = -\ 5543 + 16{,}91t + 0{,}4219t^2 \qquad 1b$$

$$Z = +42244 - 39{,}74t + \ 4551t^2 \qquad 1c$$

$$T = +46591 - 27{,}65t + 0{,}3216t^2 \qquad 1d$$

where $t = \text{date} - 1882$.

Table I

Investigated observatories and data

	φ	λ	Interval	Degree of approximation	Remark
Oslo	+59,9°	+ 10,7°	1843—1930	3	only D, H, X, Y
Slutzk	+59,7	+ 30,5	1869—1941	2,3	
Sitka	+57,1	+224,7	1902—1950	1,2	
Wyssokaja Doubrawa	+56,7	+ 61,1	1887—1944	2	D 1844—1944
Rude Skov	+55,8	+ 12,5	1892—1949	2	
Stonyhurst	+53,8	+357,5	1865—1943	2,3	I, T, Z 1876—1943
Witteveen	+52,8	+ 6,7	1891—1947	2	
Zuy	+52,5	+104,0	1887—1945	2	
Niemegk	+52,1	+ 12,7	1890—1949	2	
Clausthal	+51,8	+ 10,3	1845—1918	2,3	only D
Abinger	+51,2	+ 359,6	1846—1950	3	
Manhay	+50,3	+ 5,7	1892—1950	2	only D
Prague	+50,1	+ 14,4	1830—1926	3	only D
Chambon-la-Forêt	+48,0	+ 2,3	1883—1950	2	
Budapest—Ógyalla	+47,9	+ 18,2	1871—1944	2,3	1871—1944 (broken)
Agincourt	+43,8	+280,7	1899—1950	1,2	
Karsani	+41,8	+ 44,7	1879—1934	1,2	Z, T, I 1880—1934
Capodimonte	+40,9	+ 14,3	1882—1921	1	only I
Coimbra	+40,2	+351,6	1868—1944	2,3	I, Z, T 1867—1940
Cheltenham	+38,7	+283,2	1902—1950	1,2	
San Miguel	+37,8	+334,3	1911—1950	1	
San Fernando	+36,5	+353,8	1891—1950	2	D 1881—1950
Kakioka	+36,2	+140,2	1897—1950	1,2	
Zo-Se	+31,1	+121,2	1875—1947	2,3	
Helwan	+29,9	+ 31,3	1903—1944	1	
Au-Tau	+22,4	+114,0	1884—1939	1,2	
Honolulu	+21,3	+201,9	1902—1950	1,2	
Alibag	+18,6	+ 72,9	1846—1949	3	
San Juan	+18,4	+293,9	1903—1950	1,2	
Batavia	− 6,2	+106,8	1884—1944	2	
Apia	−13,8	+188,2	1905—1950	1,2	
Tananarivo	−18,9	+ 47,5	1902—1950	1,2	
Mauritius	−20,1	+ 57,6	1893—1950	2	
Pilar	−31,7	+296,1	1905—1950	1,2	
Toolangi	−37,5	+145,5	1893—1949	2	D until 1950
Amberley	−43,2	+172,7	1902—1950	1,2	

Table II

The secular variation of the X- and Y-component in the observatory Chambon la Forêt

Year	1	2	3	4	5	6
	X_m	X_c	ΔX	Y_m	Y_c	ΔY
1883....	18829	18873	−44	−5535	−5526	− 9
1884....	18839	18900	−61	−5495	−5508	+ 13
1885....	18860	18925	−65	−5463	−5489	+ 26
1886....	18881	18951	−70	−5434	−5469	+ 35
1887....	18920	18976	−56	−5409	−5448	+ 39
1888....	18953	19001	−48	−5388	−5427	+ 39
1889....	18986	19025	−39	−5367	−5404	+ 37
1890....	19016	19050	−34	−5340	−5381	+ 41
1891....	19039	19073	−34	−5311	−5357	+ 46
1892....	19073	19097	−24	−5285	−5332	+ 47
1893....	19118	19120	− 2	−5263	−5306	+ 43
1894....	19136	19142	− 6	−5233	−5280	+ 47
1895....	19177	19165	+12	−5209	−5252	+ 43
1896....	19206	19187	+19	−5184	−5224	+ 40
1897....	19245	19209	+36	−5163	−5195	+ 32
1898....	19277	19230	+47	−5142	−5165	+ 23
1899....	19310	19251	+59	−5125	−5134	+ 9
1900....	19349	19272	+77	−5111	−5102	− 9
1901....	19386	19292	+94	−5098	−5070	− 28
1902....	19410	19312	+98	−5084	−5036	− 48
1903....	19427	19332	+95	−5063	−5002	− 61
1904....	19443	19351	+92	−5041	−4967	− 74
1905....	19456	19370	+86	−5018	−4931	− 87
1906....	19474	19388	+86	−4997	−4894	−103
1907....	19482	19407	+75	−4966	−4857	−109
1908....	19486	19425	+61	−4930	−4818	−112
1909....	19488	19442	+46	−4889	−4779	−110
1910....	19509	19459	+50	−4851	−4739	−112
1911....	19526	19476	+50	−4806	−4698	−108
1912....	19541	19493	+48	−4758	−4656	−102
1913....	19552	19509	+43	−4702	−4614	− 88
1914....	19554	19525	+29	−4646	−4570	− 76
1915....	19549	19540	+ 9	−4589	−4526	− 63
1916....	19547	19555	− 8	−4530	−4481	− 49
1917....	19548	19570	−22	−4475	−4435	− 40
1918....	19551	19585	−34	−4421	−4388	− 33
1919....	19552	19599	−47	−4364	−4340	− 24
1920....	19562	19612	−50	−4308	−4292	− 16

	1	2	3	4	5	6
	X_m	X_c	ΔX	Y_m	Y_c	ΔY
1921....	19579	19626	−47	−4249	−4242	− 7
1922....	19584	19639	−55	−4184	−4192	+ 8
1923....	19601	19652	−51	−4120	−4141	+ 21
1924....	19614	19664	−50	−4050	−4089	+ 39
1925....	19624	19676	−52	−3980	−4036	+ 56
1926....	19629	19688	−59	−3910	−3983	+ 73
1927....	19648	19699	−51	−3845	−3928	+ 83
1928....	19654	19710	−56	−3776	−3873	+ 97
1929....	19658	19721	−63	−3716	−3817	+101
1930....	19660	19731	−71	−3652	−3760	+108
1931....	19675	19741	−66	−3594	−3702	+108
1932....	19688	19751	−63	−3531	−3643	+112
1933....	19701	19760	−59	−3471	−3584	+113
1934....	19714	19769	−55	−3415	−3523	+108
1935....	19724	19777	−53	−3353	−3462	+109
1936....	19738	19786	−48	−3296	−3400	+104
1937....	19747	19794	−47	−3240	−3337	+ 97
1938....	19760	19801	−41	−3188	−3273	+ 85
1939....	19780	19808	−28	−3139	−3209	+ 70
1940....	19800	19815	−15	−3091	−3143	+ 52
1941....	19816	19822	− 6	−3041	−3077	+ 36
1942....	19845	19828	+17	−2995	−3010	+ 15
1943....	19853	19834	+19	−2946	−2942	− 4
1944....	19876	19839	+37	−2900	−2873	− 27
1945....	19890	19844	+46	−2852	−2804	− 48
1946....	19889	19849	+40	−2801	−2733	− 68
1947....	19906	19854	+52	−2753	−2662	− 91
1948....	19926	19857	+69	−2710	−2590	−120
1949....	19944	19861	+83	−2666	−2517	−149
1950....	19966	19864	+102	−2623	−2443	−180

Column 1,4 : Annual mean of the measured component.
Column 2,5 : Adjusted component, computed on the basis of equations 1a, 1b.
Column 3,6 : Difference of the measured and computed components : the superposed wave.

Table III

The secular variation of the Z- and T- component in the observatory Chambon la Forêt

Year	1	2	3	4	5	6
	Z_m	Z_c	ΔZ	T_m	T_c	ΔT
1883....	41930	42204	−274	46296	46564	−268
1884....	41902	42166	−264	46270	46537	−267
1885....	41872	42129	−257	46247	46511	−264
1886....	41866	42092	−226	46247	46485	−238
1887....	41898	42056	−158	46289	46461	−172
1888....	41948	42022	− 74	46345	46436	− 91
1889....	41943	41988	− 45	46352	46413	− 61
1890....	41935	41955	− 20	46354	46390	− 36
1891....	41940	41923	+ 17	46365	46368	− 3
1892....	41968	41892	+ 76	46401	46346	+ 55
1893....	41978	41862	+116	46426	46326	+100
1894....	41938	41832	+106	46394	46305	+ 89
1895....	41937	41804	+133	46407	46286	+121
1896....	41938	41777	+161	46417	46267	+150
1897....	41944	41750	+194	46436	46248	+188
1898....	41958	41724	+234	46460	46231	+229
1899....	41937	41700	+237	46453	46214	+239
1900....	41938	41676	+262	46468	46197	+271
1901....	41889	41653	+236	46438	46182	+256
1902....	41861	41631	+230	46422	46166	+256
1903....	41824	41610	+214	46393	46152	+241
1904....	41770	41590	+180	46348	46138	+210
1905....	41730	41571	+159	46316	46125	+191
1906....	41667	41552	+115	46264	46112	+152
1907....	41622	41535	+ 87	46223	46100	+123
1908....	41553	41518	+ 35	46159	46089	+ 70
1909....	41514	41503	+ 11	46121	46079	+ 42
1910....	41511	41488	+ 23	46122	46069	+ 53
1911....	41480	41474	+ 6	46097	46059	+ 38
1912....	41436	41461	− 25	46059	46051	+ 8
1913....	41395	41449	− 54	46021	46043	− 22
1914....	41353	41438	− 85	45978	46035	− 57
1915....	41329	41428	− 99	45949	46028	− 79
1916....	41345	41419	− 74	45957	46022	− 65
1917....	41351	41410	− 59	45957	46017	− 60

Year	1	2	3	4	5	6
	Z_m	Z_c	ΔZ	T_m	T_c	ΔT
1918....	41391	41403	− 12	45989	46012	− 23
1919....	41365	41396	− 31	45961	46008	− 47
1920....	41313	41391	− 78	45913	46004	− 91
1921....	41270	41386	−116	45876	46002	−126
1922....	41239	41382	−143	45844	45999	−155
1923....	41226	41380	−154	45834	45998	−164
1924....	41223	41378	−155	45831	45997	−166
1925....	41207	41376	−169	45814	45996	−182
1926....	41204	41376	−172	45808	45997	−189
1927....	41236	41377	−141	45840	45998	−158
1928....	41224	41379	−155	45825	45999	−174
1929....	41241	41381	−140	45837	46002	−165
1930....	41251	41385	−134	45842	46004	−162
1931....	41306	41389	− 83	45894	46008	−114
1932....	41318	41395	− 77	45905	46012	−107
1933....	41337	41401	− 64	45923	46017	− 94
1934....	41351	41408	− 57	45937	46023	− 86
1935....	41380	41416	− 36	45963	46029	− 66
1936....	41374	41425	− 51	45959	46036	− 77
1937....	41422	41435	− 13	46002	46043	− 41
1938....	41465	41446	+ 19	46043	46051	− 8
1939....	41484	41457	+ 27	46065	46060	+ 5
1940....	41513	41470	+ 43	46097	46069	+ 28
1941....	41543	41483	+ 60	46128	46079	+ 49
1942....	41548	41498	+ 50	46142	46090	+ 52
1943....	41568	41513	+ 55	46160	46101	+ 59
1944....	41611	41529	+ 82	46205	46113	+ 92
1945....	41633	41546	+ 87	46228	46125	+103
1946....	41658	41564	+ 94	46247	46138	+109
1947....	41682	41583	+ 99	46273	46152	+121
1948....	41695	41603	+ 92	46291	46167	+124
1949....	41715	41624	+ 91	46314	46182	+132
1950....	41714	41646	+ 68	46320	46198	+122

Column 1,4 : Annual mean of the measured component.
Column 2,5 : Adjusted component, computed on the basis of equations 1c, 1d.
Column 3,6 : Difference of the measured and computed components : the superposed wave.

These functions allow to compute for any date the (mathematically) adjusted values at Chambon la Forêt. The results calculated are presented in column 2,5 of table II and III. Forming the differences of the observed and

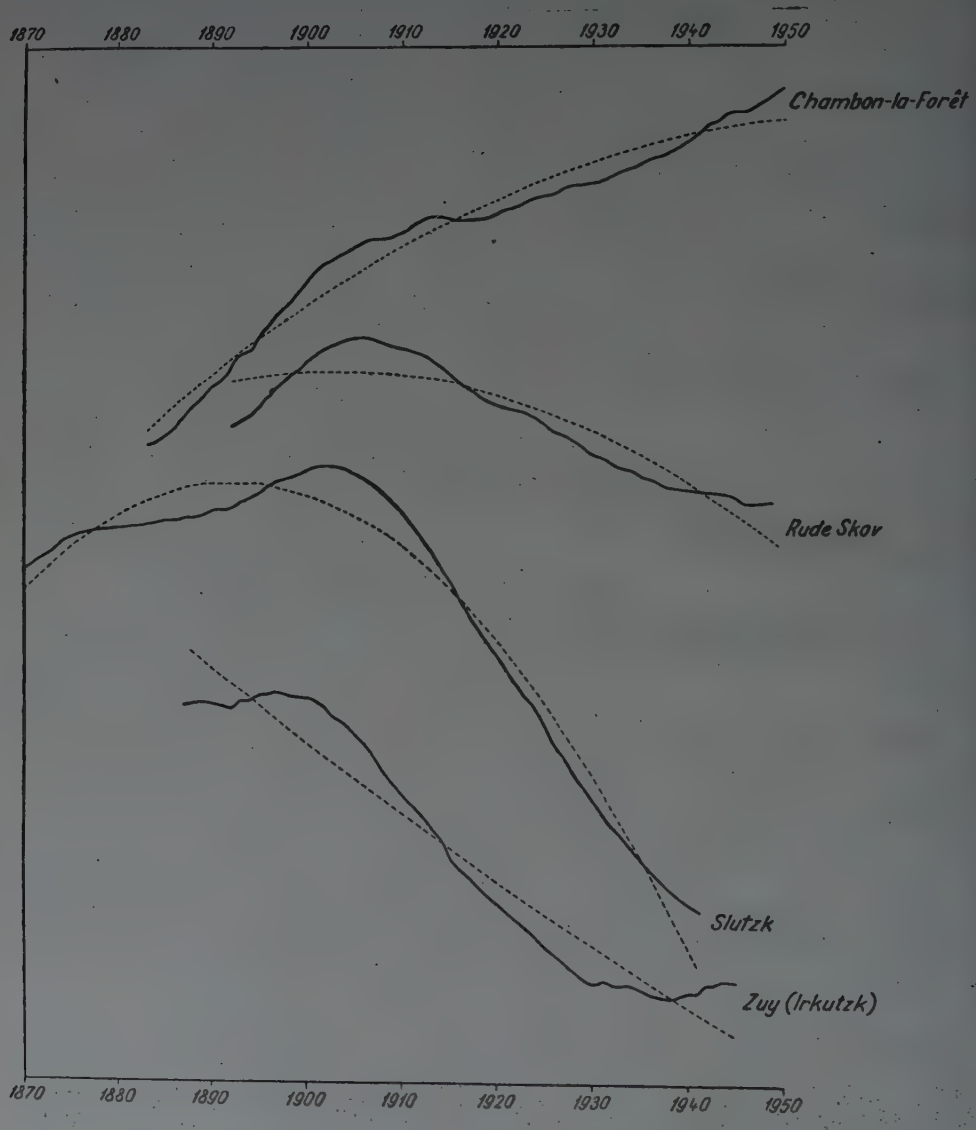

Fig. 1. Measured and mathematically adjusted variation of the north (X) component in the observatories Chambon la Forêt, Rude-Skov, Slutzk, and Zuy

computed values, the differences — characteristic of the superimposed wave — change sign at certain time-intervals. In the regular course of the curve presenting these differences a wave of a period of several decades superimposed on

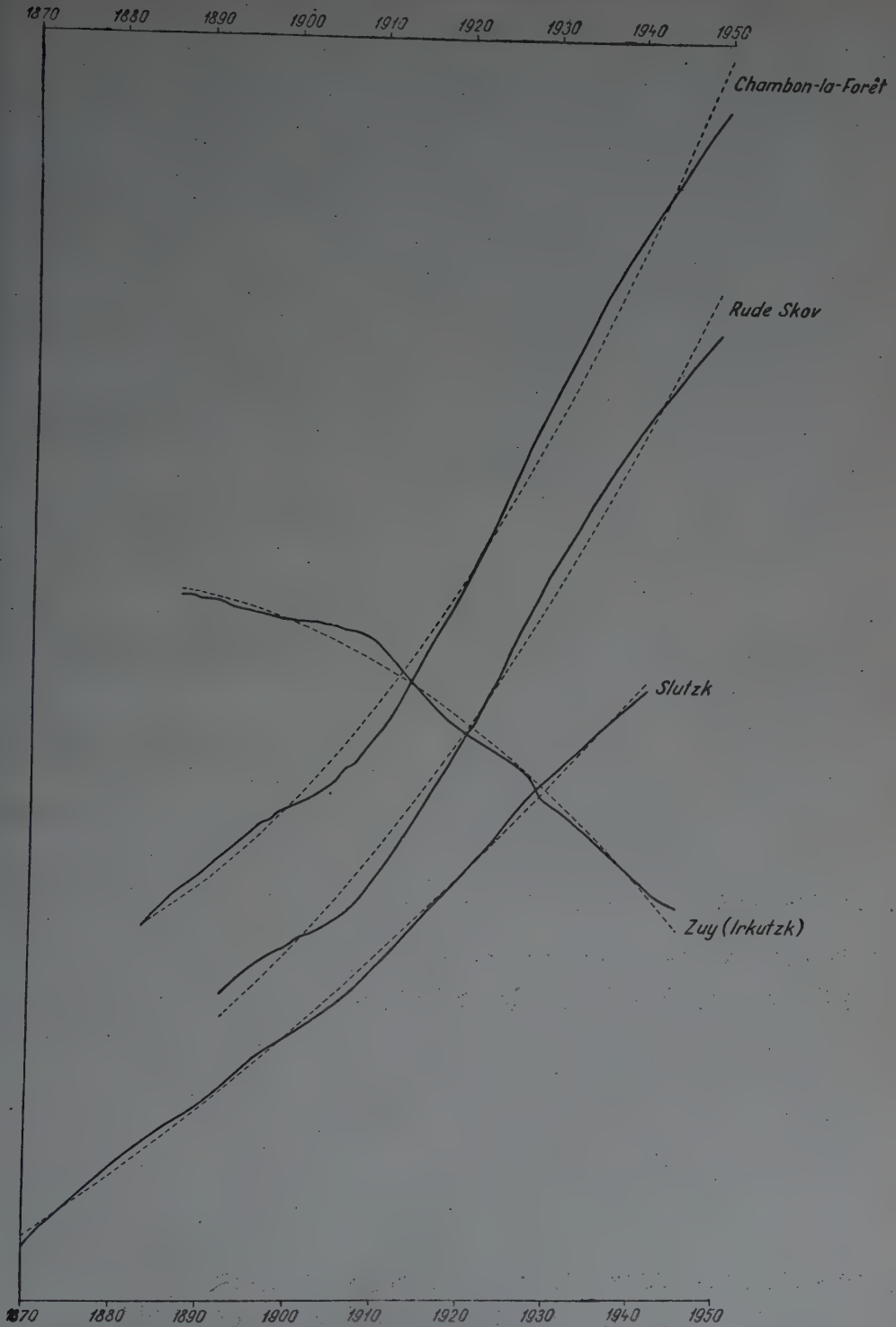

Fig. 2. Measured and mathematically adjusted variation of the east (Y) component in the observatories Chambon la Forêt, Rude-Skov, Slutzk, and Zuy

the main secular wave may be easily recognized. The differences are presented in columns 3 and 6 of Tables II and III. The superimposed wave recorded by some observatories is illustrated in figures 1, 2, 3.

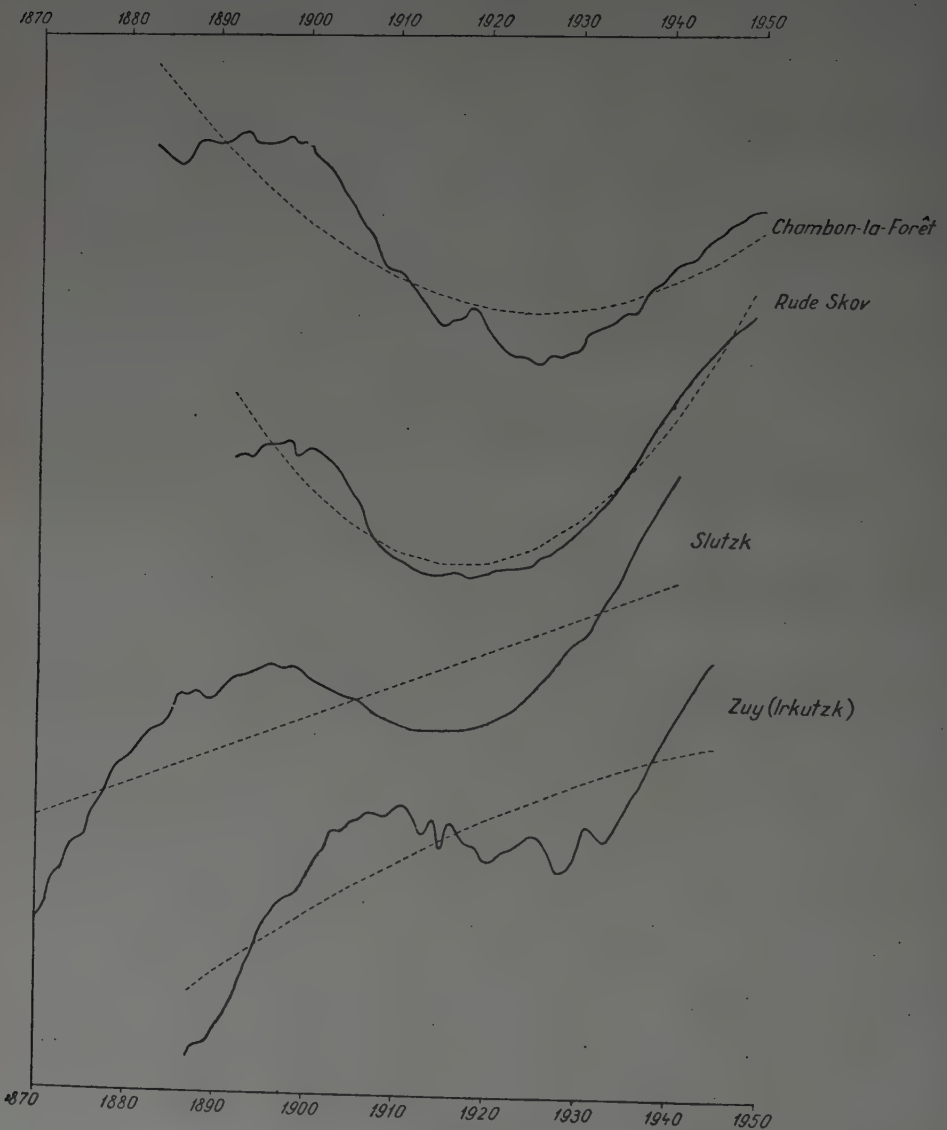

Fig. 3. Measured and mathematically adjusted variation of the vertical (Z) component in the observatories Chambon la Forêt, Rude-Skov, Slutzk and Zuy

Characteristics of the superimposed wave

The sensitivity and reliability of the applied method may be easily stated. The starting values (at about 1850) of the observatories disposing of long observation series reveal the difficulties met in measuring and the instrumental inaccuracies of those times. However, the data clearly reveal a gradual improvement of instrumental techniques. Erratic data sharply distinguish themselves on the wave, allowing a ready establishment of the correct data.

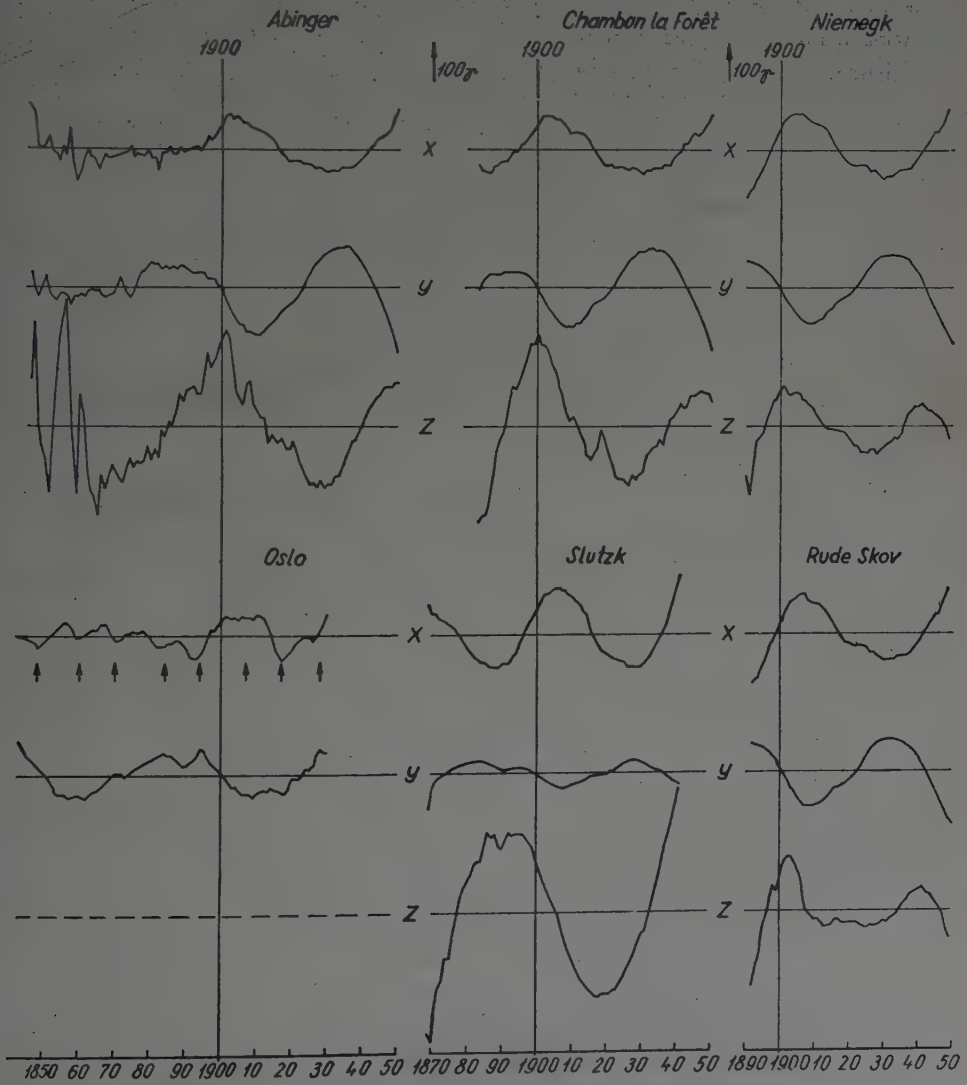

Fig. 4. The superimposed wave in some European observatories (Abinger, Oslo, Chambon la Forêt, Niemegk, Rude-Skov, Slutzk)

A still more important proof to the sensitivity of the method is furnished by the fact that in the superimposed wave we can easily recognize the common traits of the secular variations recorded in observatories situated in close vicinity. This recognition is very significant, for these common traits may be attributed to common reasons yet unknown. These properties are not of discontinuous character, unlike the measuring errors, they rather look like slow wave-folds lasting for many years.

The superimposed waves and their peculiarities are shown in figures 4 and 5, except for those of some of the observatories, where a neighbouring observatory with a longer series recorded a similar wave. Fig. 4 illustrates the wave of a few European observatories. In the short series of Rude Skov and Niemegk the part prior to 1900 is but indicated. In the long series of Chambon la Forêt it is definitely revealed even before 1900. In the Oslo-series, which goes back as far as 1843, two complete wave periods may be traced. We did not represent the Z-wave at Oslo where the inclination series is broken. In the observatory at Abinger the wave is likewise observable in every series since 1846.

At Oslo the trend of the wave essentially differs from that of all others. The cause of this phenomenon may be attributed to the northern situation of the observatory. In the drawing, below the X-wave the dates of the sunspot maxima are indicated by arrows. Apparently, they coincide with the relative minima of the curve. Among the 36 observatories studied, this was the only one where a connection of these values with the simple sunspot-frequency could be established. There exists no other observatory with long observation series in the vicinity of the arctic region, therefore, we did not extend our investigations in this direction. At any rate, we may state, that the amplitude of the wave of sunspot-frequency appearing in Oslo-X is much smaller than the studied superimposed wave.

In the superimposed waves recorded in the European observatories we find many similarities even with different lengths of the investigated series. In the Y-waves characteristic wave formations could be found in about 1915, whilst in the X and Z-waves in about 1910, 1920, 1930, 1938, 1946.

The waves are well discernible also in the data of all the other observatories of the world (Fig. 5).

In the environs of the Pacific Ocean, however, the case is not as plain as that. In observatories situated in the equatorial region the wave shows a period of about 22 years. It is to be regretted that the available series are partly incomplete or broken, partly short. The scarcity of the observatories existing in the enormous area of the Pacific only adds to the difficulties. Nevertheless, some regularities may be established even here. The X-wave at Honolulu and particularly that at Apia clearly show the 22-year Abbot-period of the sunspot — magnetization (sunspot maxima took place in 1907, 1918, 1928, 1938 and 1948, while the extremes of the X-wave at Apia appear in 1908, 1919, 1929, 1939,

and 1950). With these two observatories the curves of the X-wave are like mirror images, relative to one-another. This phenomenon might be interpreted by the almost symmetrical situation of the observatories to the equator. The curves assume extreme values in the years of sunspot maxima (at Honolulu in 1907, 1914, 1929, 1938, and 1948).

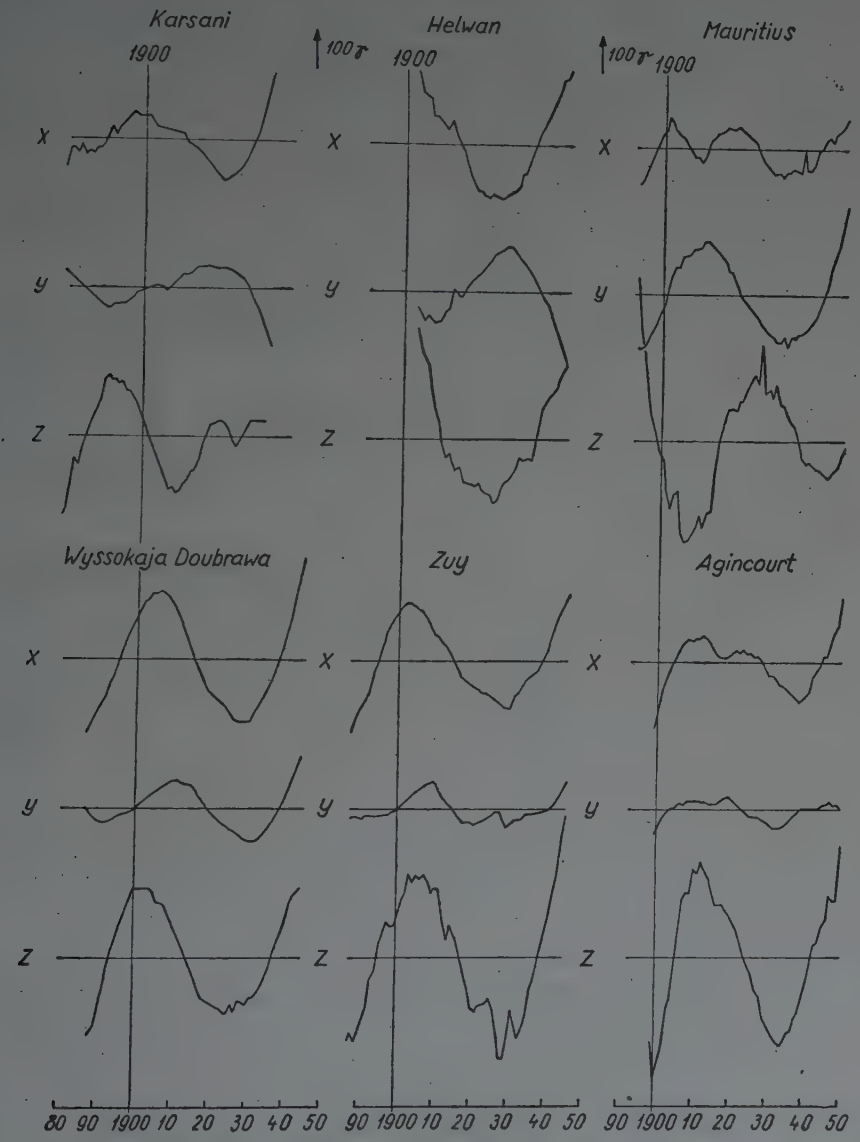

Fig. 15. The superimposed wave in some Asian, African, and American observatories (Karsani, Wyssokaja Doubrawa, Helwan, Zuy, Mauritius, Agincourt)

The interdependence of the waves and the geographical places may be investigated by grouping the waves of the single components according to the geographical longitude. From figure 7 it is evident that the X- and Z-components are in the same phase, in other words, the maxima and the minima of the waves present themselves at the same time over the whole Earth. Their

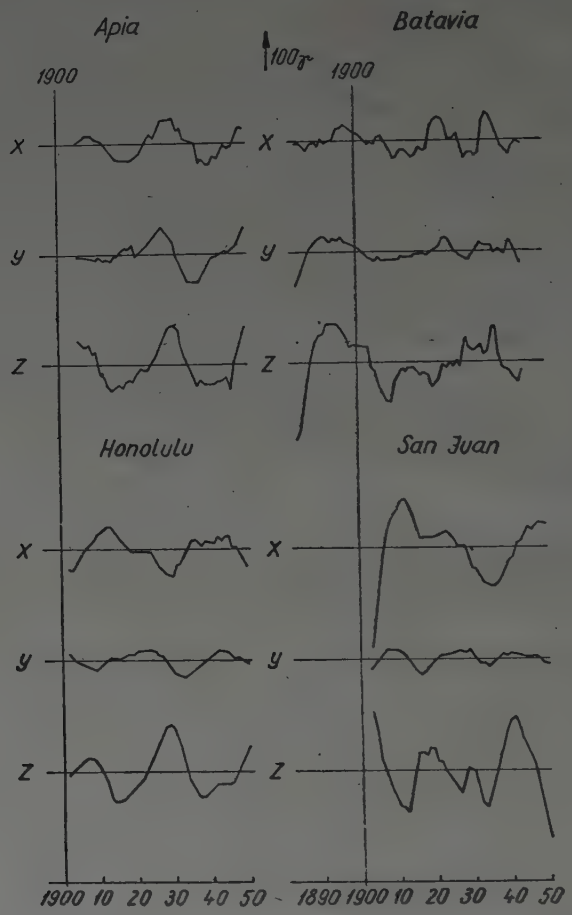

Fig. 6. The superimposed wave in some equatorial observatories

maximum occurs in about 1906 and a minimum in about 1928. Around 1950 the formation of another extreme is already felt. Except for insignificant deviations, this regularity holds throughout. The X-wave at Mauritius shows a wave of the equatorial period of 22 years, it cannot therefore be fitted in the series of the other observatories. In some of the observation series of a few observatories the wave is hardly indicated (Au Tau-Z, Toolangi-Z, Amberley-T). But the observation series recorded at these places are short and the degree of approxi-

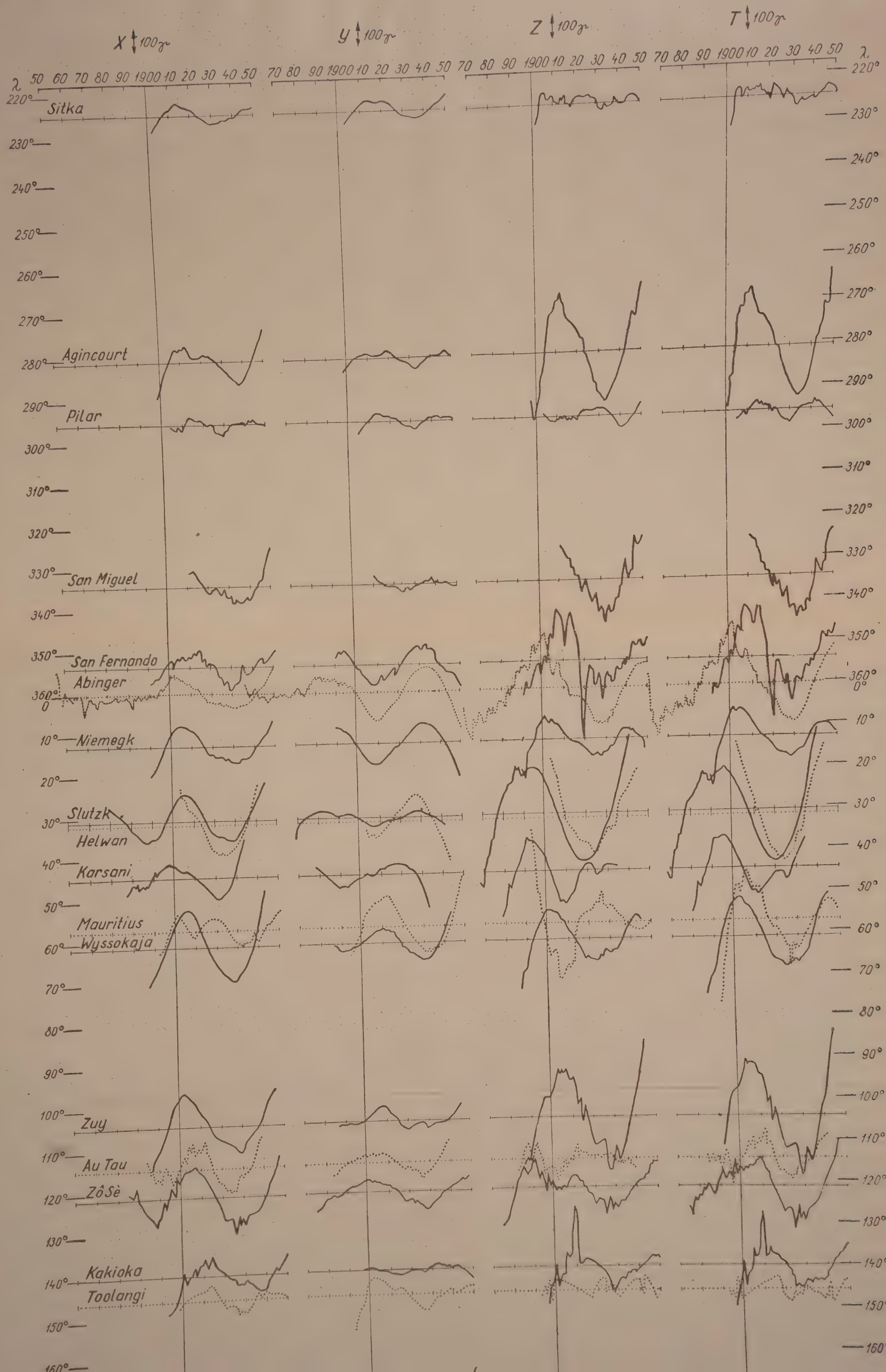
X ↕ 100γ
Y ↕ 100γ
Z ↕ 100γ
T ↕ 100γ
λ
50 60 70 80 90 1900 10 20 30 40 50
220°
230°
240°
250°
260°
270°
280°
290°
300°
310°
320°
330°
340°
350°
360°
0
10°
20°
30°
40°
50°
60°
70°
80°
90°
100°
110°
120°
130°
140°
150°
160°
Sitka
Agincourt
Pilar
San Miguel
San Fernando
Abinger
Niemegk
Slutzk
Helwan
Karsani
Mauritius
Wyssokaja
Zuy
Au Tau
Zô Sè
Kakioka
Toolangi

mation considerably influences the shape of the wave. The superimposed wave at Mauritius has a definitely reverse trend, what is only to be expected, for the observatory is on the southern hemisphere where the increase of the total intensity involves the increase of the negative component. Thus the reverse trend is originated by the orientation of the co-ordinate system.

As against the elements treated so far, the extremes of the superimposed wave in the East-component, in proceeding to the east, appear always earlier. Consequently, the shift of the wave proceeds from east to the west; accordingly, the direction of its procession agrees with that of the great secular trend (remarkably, the tidal shifts have the same direction). This sort of shift of the wave is a general phenomenon, the actually noticeable deviations may be explained by errors in the observations and by the inevitable distortions of our approximations. From the figures it is evident that the shift is so fast that in the observatories lying on opposite meridians, the superimposed waves have the same phase, in other words, the Earth is encircled by two waves. There is no shift in the Y-wave at observatories of the same longitude, even if they are situated at great distances in the north-south

Table IV

The shift in time of the superimposed wave, Y-component

		Y			
	λ	max	min	max	min
Sitka	224°40'	1916	1935	—	—
Agincourt	280°44'	1914	1932	1947	—
Pilar	296° 7'	1914	1932	—	—
San Miguel	334°21'	—	1924	1938	—
San Fernando	353°48'	1894	1910	1933	—
Abinger	359°37'	1885	1910	1934	—
Chambon la Forêt	2°16'	1893	1909	1933	—
Niemegk	12°40'	1892	1908	1933	—
Slutzk	30°29'	1881	1906	1926	—
Helwan	31°20'	—	1908	1927	—
Karsani	44°42'	—	1890	1918	—
Mauritius	57°33'	—	1893	1911	1933
Wyssokaja Doubrawa	61° 4'	—	1891	1910	1931
Zuy	104° 2'	—	1888	1908	1925
Au Tau	114° 3'	—	—	1903	1925
Zo Se	121°11'	—	—	1900	1927
Toolangi	145°28'	—	—	1900	1926
Amberley	172°44'	—	—	1900	1923

direction (Mauritius—Wyssokaja Doubrava, Slutzk—Helwan, Kakioka—Toolangi, Agincourt—Pilar). The shift of the extremes in the Y-wave is given in Table IV. As feasible dates for the extremes we took graphical averages on the basis of the curves, lest their local saddle-backs or salients (originating in the eventual errors of the measurements) may exert an adverse influence on the data. A detailed investigation of the transitions between the 44- and the 22-year periods could not be done because of the small number and the disadvantageous distribution of the observatories.

The vector diagrams of the secular variation

In our computations made so far, the separation of the components and the establishment of their relation to time were arbitrary. The process, namely, does not limit itself to a single co-ordinate, because it does take place in all of the components. For this reason it is more expedient to employ a representation by vector diagrams.

The annual mean values of the observatories determine the annual average position of the end point of the magnetic vector in the three-dimensional astronomical co-ordinate system. In consequence of the secular variation, the position of this point varies from year to year and, consequently, in the course of time, it describes a three-dimensional curve. The vector diagram of the secular variation is a projection of the curve onto the co-ordinate planes. Some of its points are known on the basis of the observations. The vector diagram may be plotted by measuring the observed components on the co-ordinate axes. Each couple of components determines one point in the co-ordinate plane. The vector diagram is obtained by plotting the points referring to different dates and by connecting them with a continuous curve in the order of time. In this plot the distinguished role of the time-parameter dissolves, the components have equal weights, the time runs along the curve and is joined to its single points.

We may draw vector diagrams in every co-ordinate plane by plotting first the observed data, then the data computed by means of the adjusted functions. The relative position of the two curves permits to realize the superimposed wave. Figs. 8, 9, 10 show in the different co-ordinate planes the vector diagrams of the secular variation as recorded in four observatories. From the figures it is evident that in spite of some dissimilarities exhibited in the secular variation, the wave clearly appears in the records of all of the observatories.

The adjusted vector diagrams are very suitable to illustrate the secular variation, since they do not contain any of the minor features of local character and the eventual errors committed in the observations. The vector diagrams of the adjusted secular variation computed from the data of the single observatories are shown in Figs. 11, 12, 13. Each curve indicates the variation in time of the observation series recorded at the single observatories.

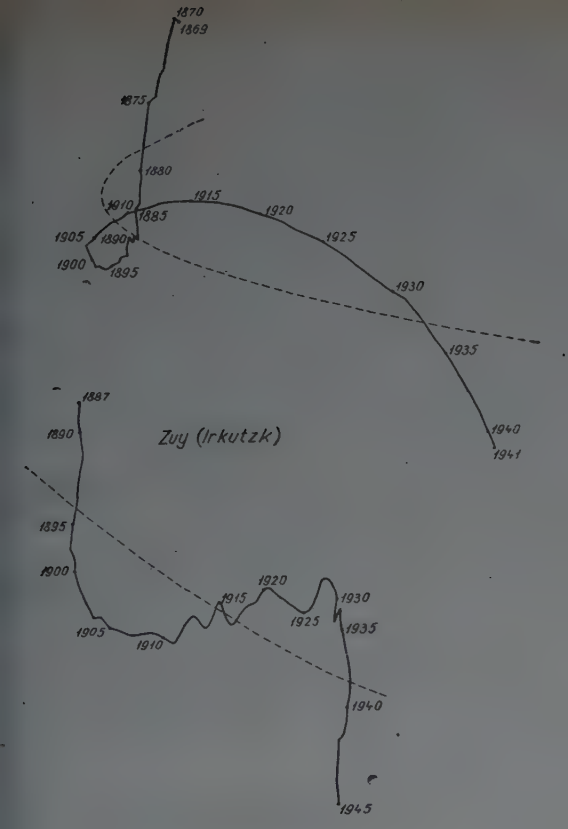

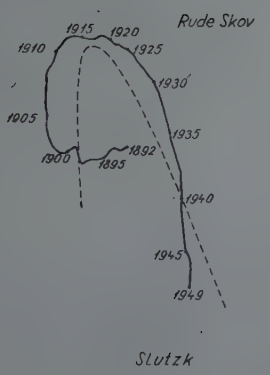

Slutzk

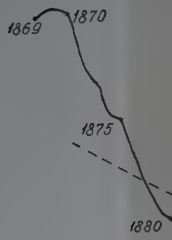

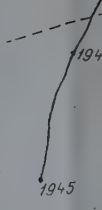

Fig. 8. **Measured and adjusted vector diagram**

Fig. 9

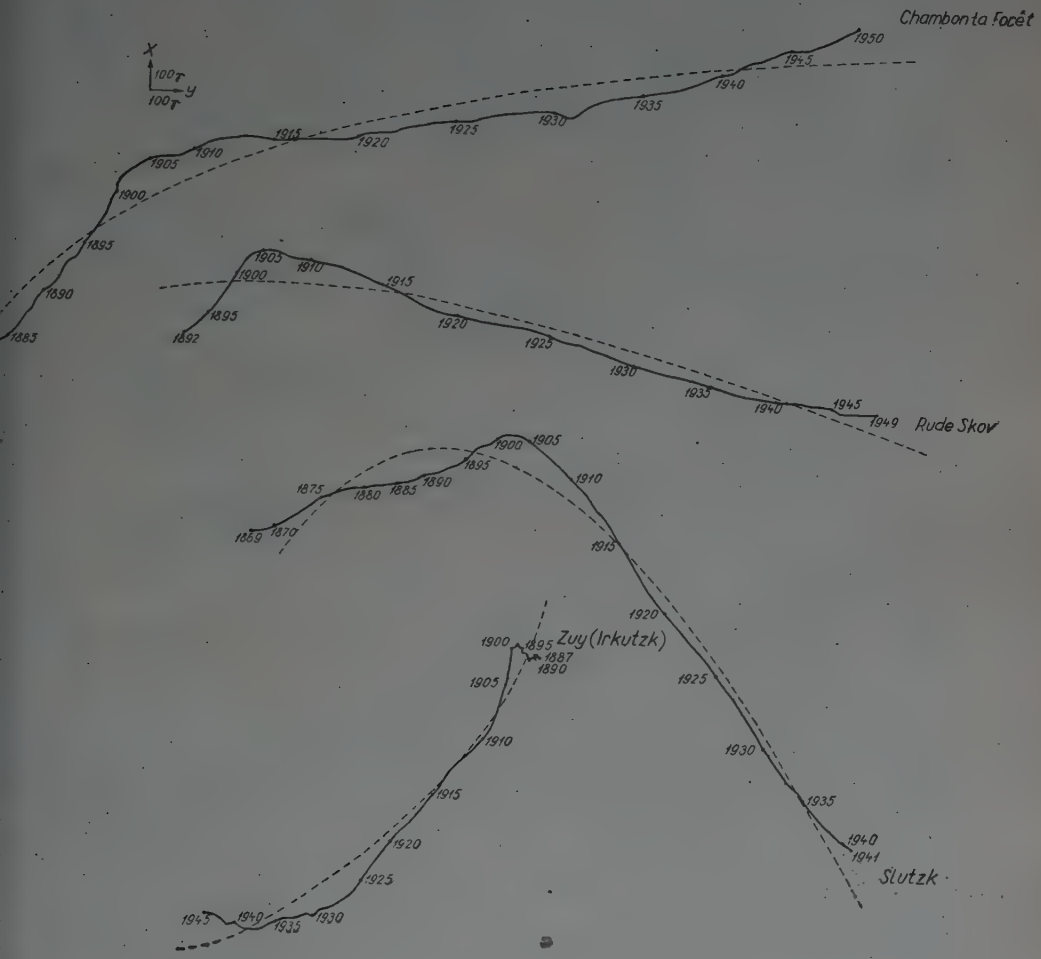

Fig. 10. Measured and adjusted vector diagram in the XY-plane

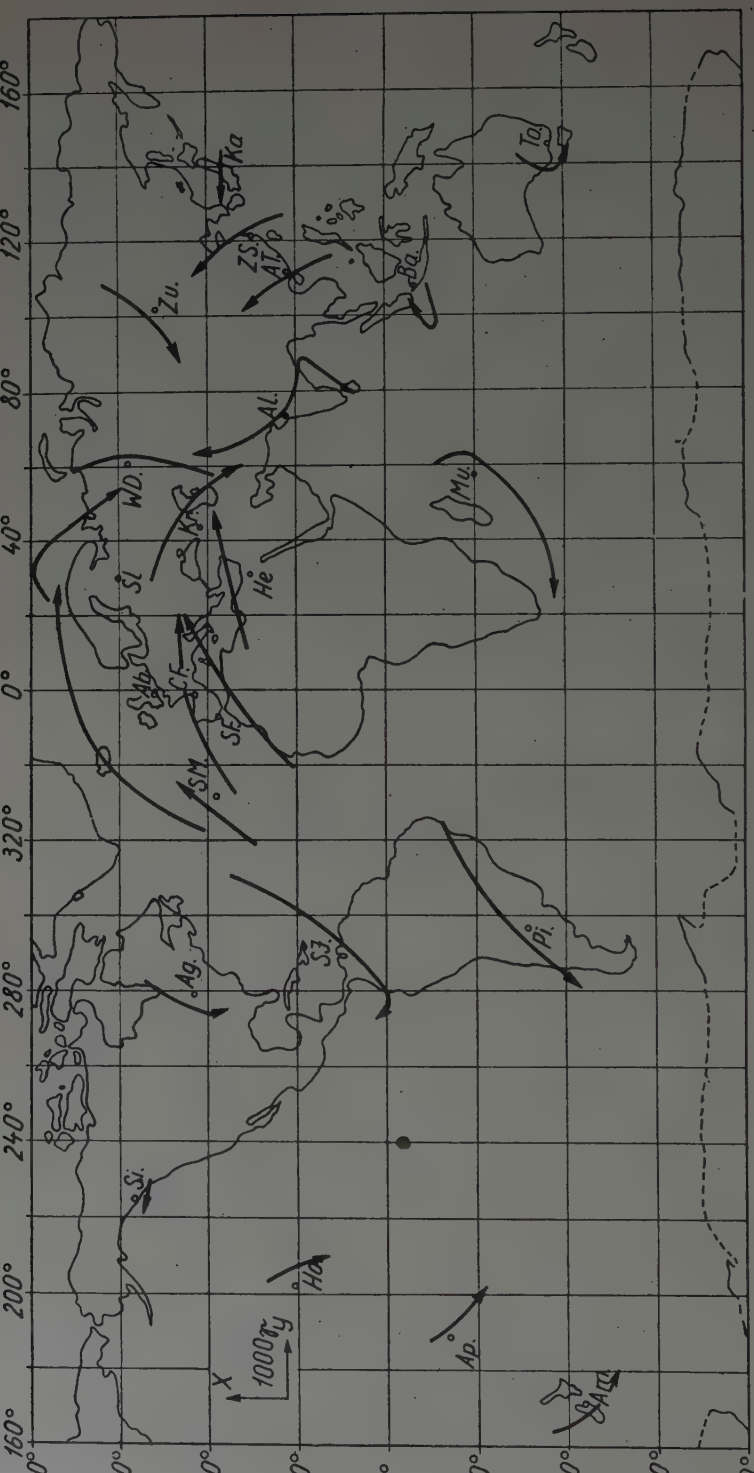

Fig. 11. Vector diagrams of the secular variation in the XY-plane, representation on worldmap

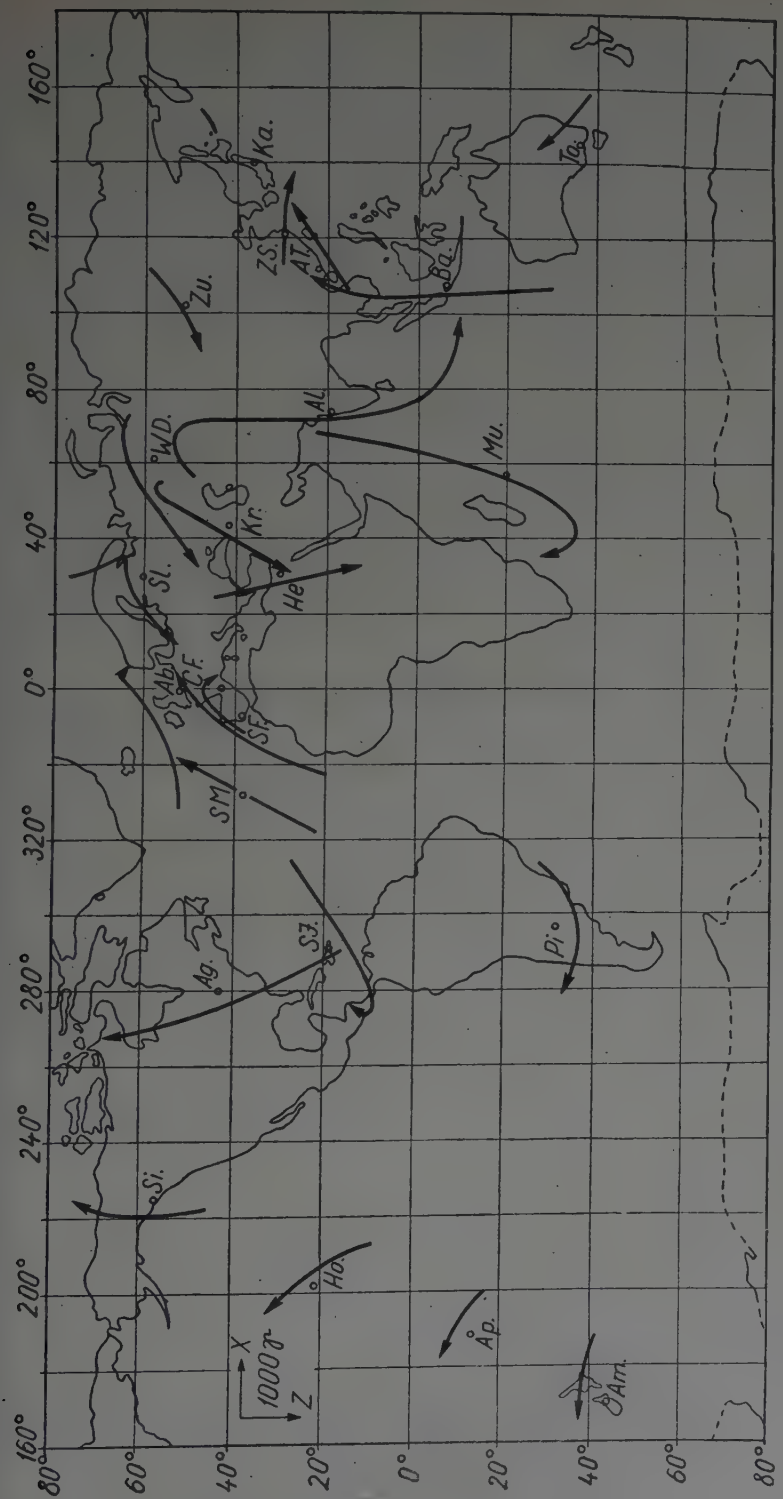

Fig. 12. Vector diagrams of the secular variation in the XZ-plane, representation on worldmap

The vector diagrams plotted in the plane XY systematically turn against each other around the Eurasian Continent. It is apparent that the most intensive increase of the vertical component appears in the center of the Continent, in Iran. On inspecting the drawings one has the impression that the curves in space of the secular variation exhibit some similarity to the magnetic lines of force of an electric circuit which running in clockwise direction in the interior of the Earth encircles the Eurasian Continent. The vector diagrams of the European observatories show in the plane XZ a sharp change in their course in about 1930. The scarcity of the observatories and the relative shortness of their observation series adds to the difficulties of extending investigations over the entire Earth.

In like manner we may draw also the vector diagrams of the superimposed wave, which are likewise projections of the change of the three-dimensional vector onto the co-ordinate-planes. Since the wave character of the superimposed wave is already expressed in the observation series, the vector diagrams in the single co-ordinate planes are closed curves. In Figs. 14, 15, 16 the vector diagrams of the superimposed wave, recorded by the more significant observatories are presented. As the superimposed Y-wave has a shift in time (the phase of the X-, and Z-waves being the same over the whole Earth) the direction of rotation of the vector diagrams in the XY-, and YZ-planes changes four times during one run round the Earth. At the meridians separating the quadrants the curves degenerate to straight lines. In the XZ-plane the curves run round — with the only exception of Zuy — in the negative direction.

The representation by vector diagrams fairly mitigated the prevailing one-sidedness implied by the isolated study of the single components with respect to their direction relative to the astronomical co-ordinates, but the employment of this sort of co-ordinates is considered as arbitrary, conditions maintained further on. This arbitraryness could be greatly lessened by the adoption of an appropriate co-ordinate system given by the secular variation itself.

If the function approximating to the observation series is a second degree power series of the time, it is easy to demonstrate that the adjusted vector diagrams are parabola arcs and the curve in space determined by the vector diagrams falls into its own osculating plane, i. e. the curve is in effect a plane curve (plane parabola).

The vector diagram of the actually measured data runs round the adjusted parabola in a wave-like shape. Considering this phenomenon in the space, we can state that the actual curve in space spirally encircles the adjusted curve (which, when the approximation is of second degree represents a parabola in the osculating plane). The superimposed wave is the projection of this spiral onto the single coordinate planes.

Each point of the actual curve in space is accompanied by a trihedron correlated to it. The three-dimensional co-ordinate system formed by the planes

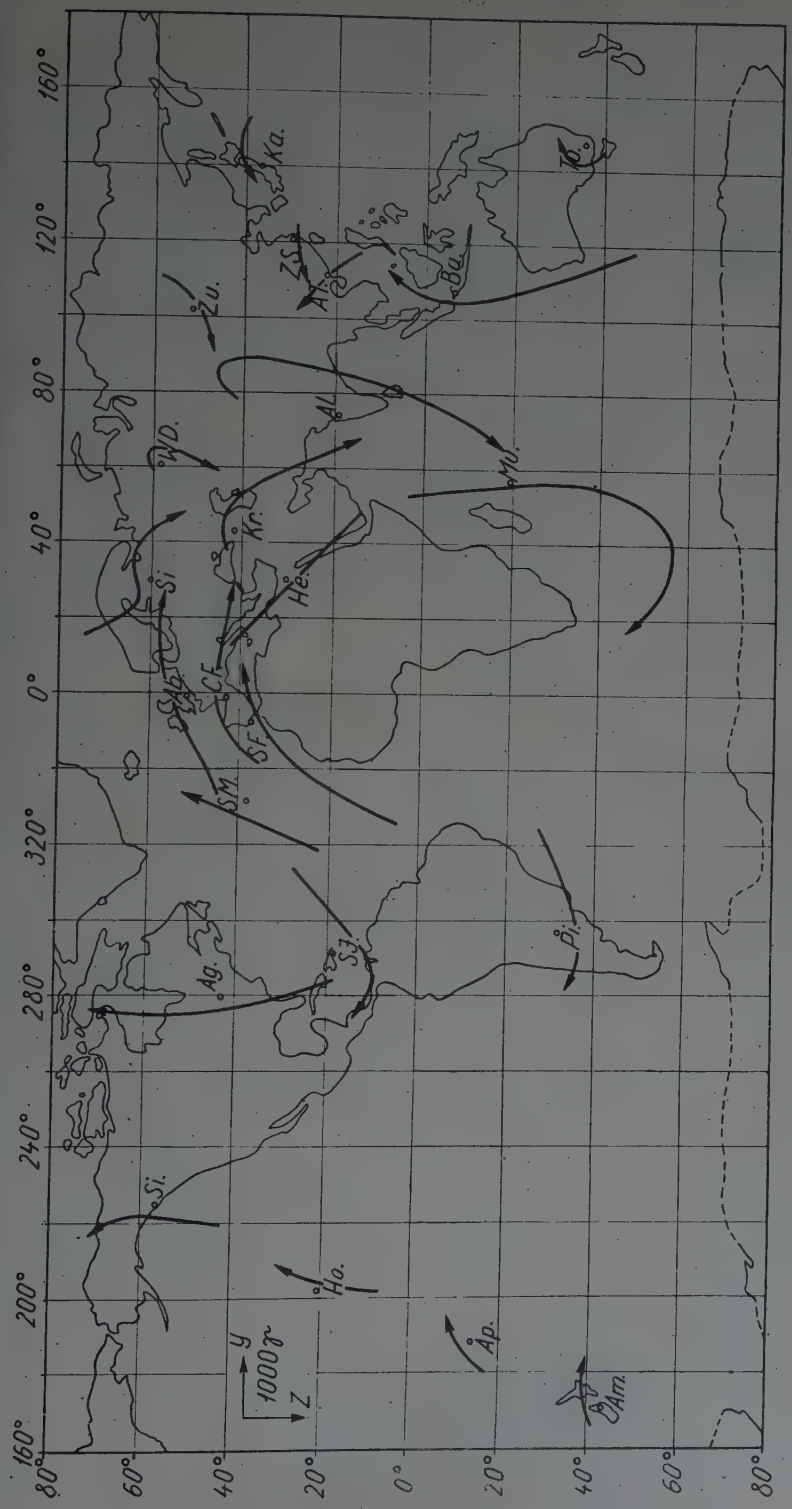

Fig. 13. Vector diagrams of the secular variation in the YZ-plane, representation on worldmap

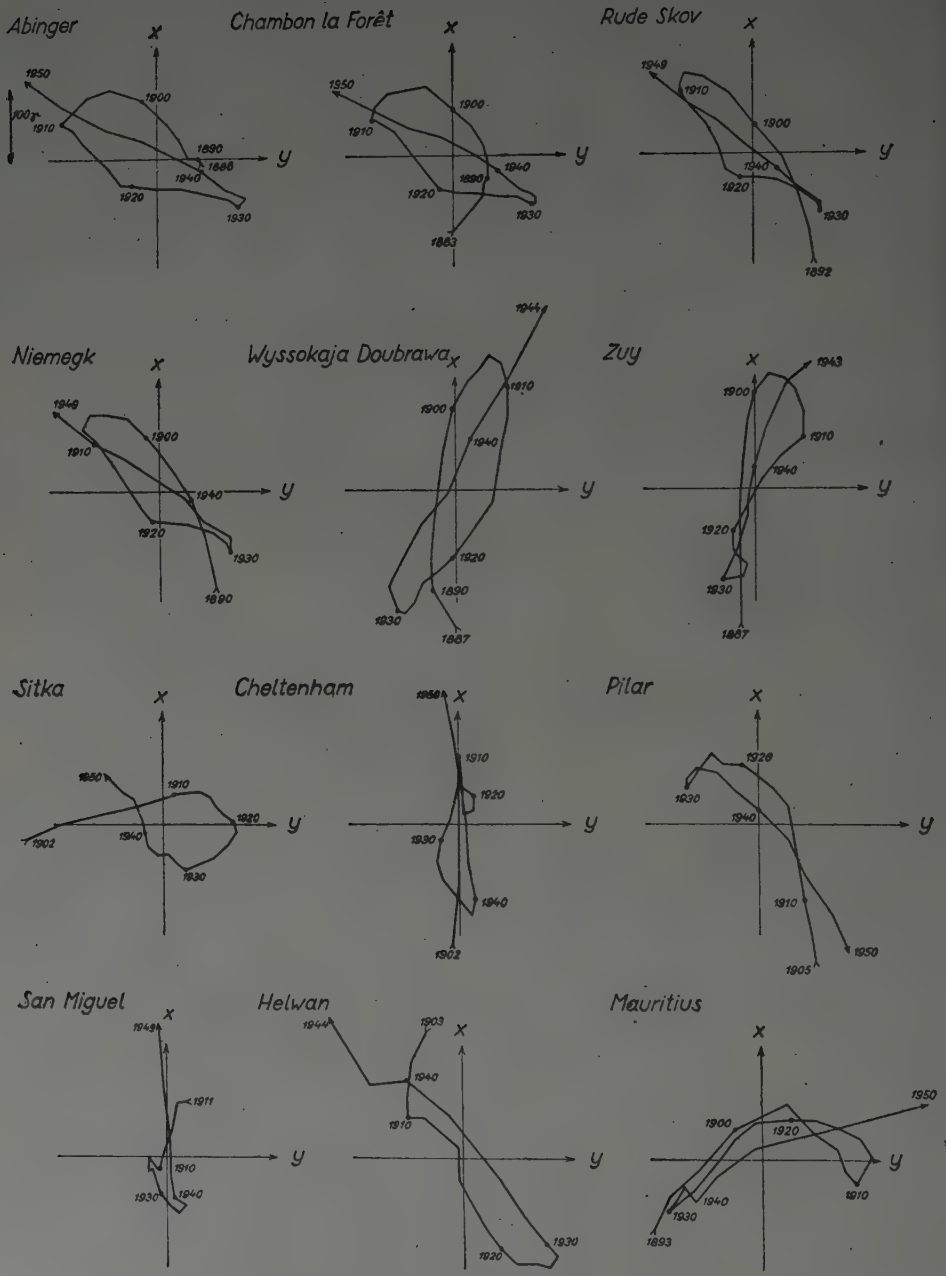

Fig. 14. **Vector diagrams of the superimposed wave in the XY-plane**

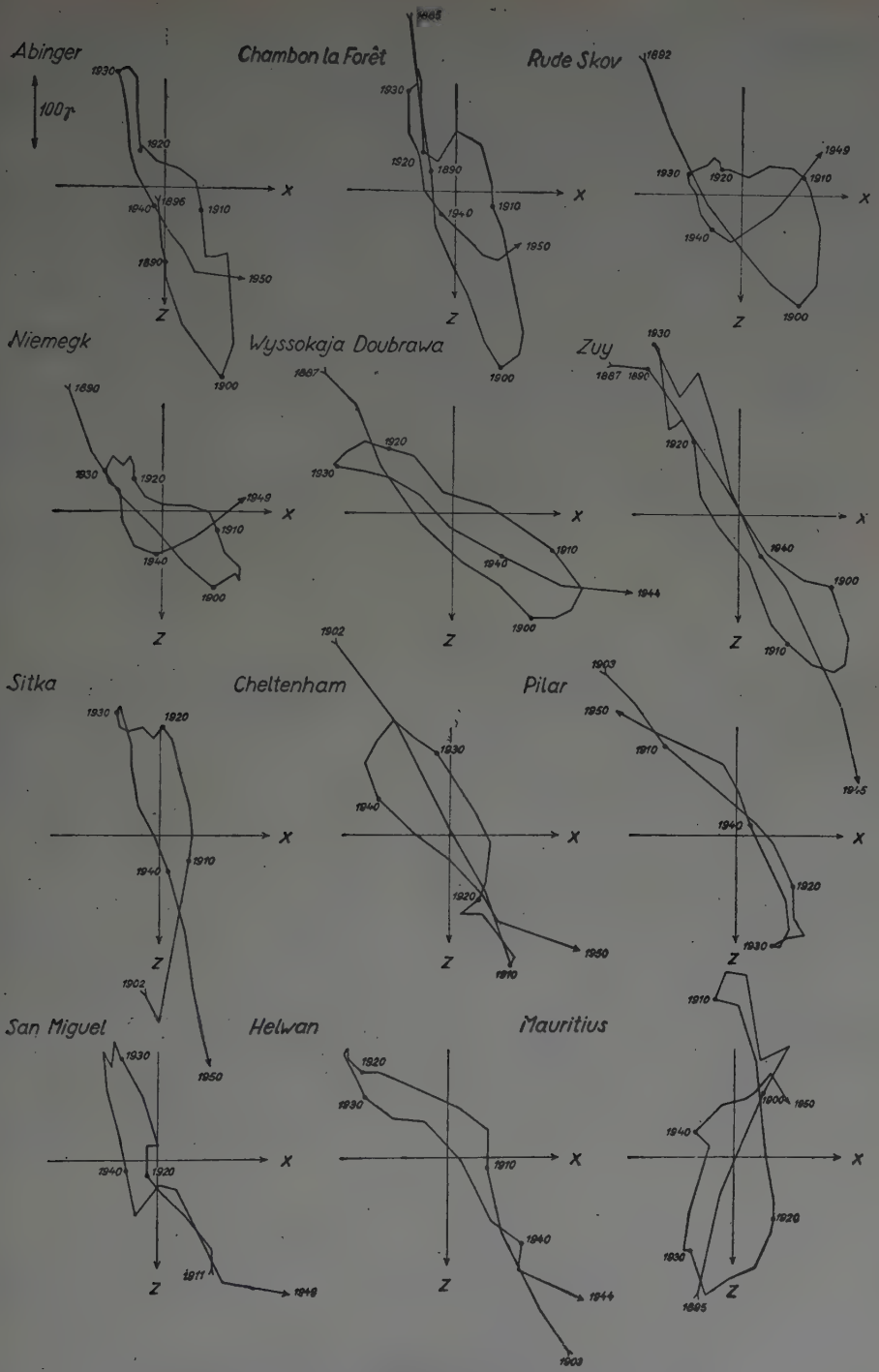

Fig. 15. Vector diagrams of the superimposed wave in the XZ-plane

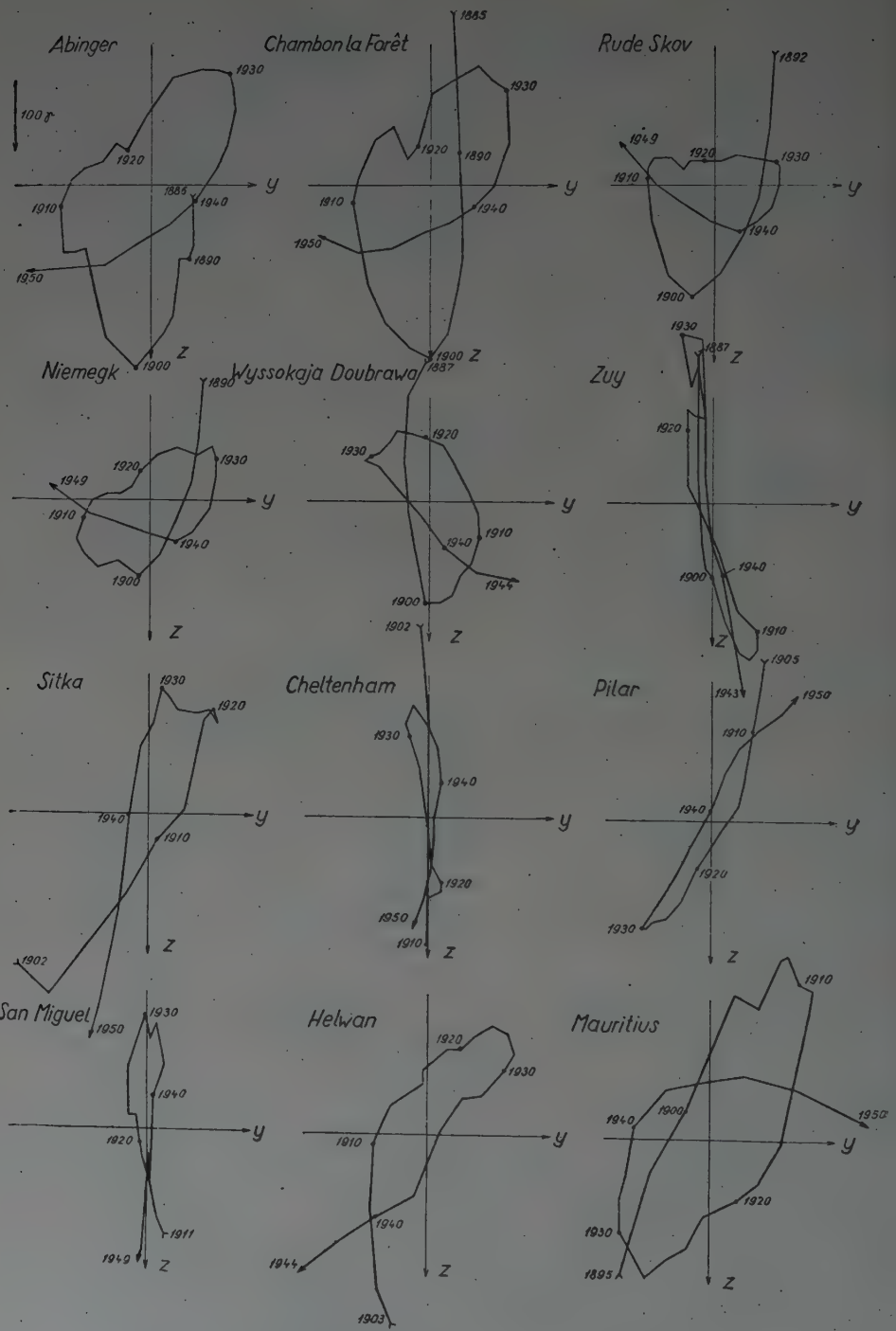

Fig. 16. Vector diagrams of the superimposed wave in the YZ-plane

of the trihedron represents a system properly attached to the secular trend, in which we can determine the reciprocal positions of the measured and the computed points and investigate the superposed trend.

The projection of the superimposed vector onto the tangent of the actual curve is within a certain time-interval positive, later it becomes negative; consequently, the measured point will from time to time run fast, then lag, relative to the adjusted point. The phenomenon corresponds to an acceleration, and respectively, to a slowing down of the secular trend, or in other words, to a wave of longitudinal character. This phenomenon should be called the longitudinal effect of secular variation.

As for the components in the direction of the binormal, and the principal normal, they indicate the projection of the superimposed wave onto the normal plane and represent a spiral motion of the secular variation. We should call this phenomenon the transversal effect of the secular variation.

The further study of these two phenomena is still in progress. The obtained results will be published in a subsequent paper.

SUMMARY

It may be established that in the secular variation of each element of the geomagnetic force a wave of great amplitude, with a period of about 44 years definitely appears. In the longest observation series the wave can be traced back as far as the forties of the last century and it is demonstrable even in series of various length, recorded by observatories situated at different points of the Earth. Consequently, its existence is unquestionable. In the equatorial observatories the wave is halved and shows the 22-year long Abbot-period of sunspot-magnetization. On the H-wave at Oslo we can discern a wave with the sunspot frequency of 11 years. In the data of observatories at different places the corresponding waves show identities and symmetry relations.

The superimposed wave of the declination (D) and that of the east component (Y) proceeds from west to the east, encircling the Earth in two waves. The extreme values of the superimposed wave in the rest of the magnetic elements are synchronous over the entire Earth, (disregarded some minor local features, errors of measurements, and some inevitable displacements caused by approximations to the observation series of various length).

In representations by vector diagrams the wave naturally appears in every co-ordinate plane and by means of these diagrams we can recognize some further regularities.

Considering the phenomenon in space, it is found that the originally measured curve in space surrounds in spiral form the (mathematically) adjusted curve (transversal effect). The superimposed wave is a projection of the spiral onto the single co-ordinate planes.

Referred to the adjusted secular variation, the actual variation is by times fast and late, respectively (longitudinal effect).

The study of the latter two phenomena is in progress, results will be published later.

LITERATURE

1. Barta, Gy.: A földmágnességi értékek változásának törvényszerűségei hazánkban. (Regularities in the variation of the geomagnetic elements in Hungary.) A Magyar Tudományos Akadémia Műszaki Tudományok Osztálya Közleményei, Budapest, vol. 5. no 1—2, 1952.

2. Barta, Gy.: A földmágneses tér évszázados változásainak 44 éves periódusáról. (Előzetes közlemény.) (The 44-year period of the variation of the geomagnetic field. Preliminary note.) Geofizikai Közlemények, Magyar Állami Eötvös Loránd Geofizikai Intézet, Budapest, vol. 3., no 1, 1954.

3. Bock, R.—Schumann, W.: Katalog der Jahresmittel der magnetischen Elemente der Observatorien und der Stationen, an denen eine Zeitlang erdmagnetische Beobachtungen stattfanden. Berlin, 1948.

4. Johnston, H. Freeborn: List of geomagnetic observatories and thesaurus of values. Journ. of Geophys. Research, September, 1951.

5. Kondér, I.: A mágnesség és iránytű története. (The history of magnetism and compass.) Térképészeti Közlöny, no 1—2, 1943—1948.

6. Munroe, E. H.: Tables on sunspot-frequency for 1749—1948. Terr. Magn. 1948.

7. Pramanik, S. K.: Secular variation of the magnetic field at Colaba and Alibag. Journ. of Geophys. Research, September, 1952.

8. Steiner, L.: A Föld mágneses jelenségei. (The magnetic phenomena of the Earth.) Budapest, 1923.

9. Wasserfall, K. F.: Periodic changes in △ D at Oslo, 1843—1930. Terr. Magn. September, 1943.

О ПЕРИОДЕ 40 –50 ЛЕТ ВЕКОВОЙ ВАРИАЦИИ ГЕОМАГНИТНОГО ПОЛЯ

ДЬ. БАРТА

Установлено, что в вековых вариациях всех элементов геомагнитной силы определенно проявляется волна большой амплитуды продолжительностью примерно в 44 года. Волна эта в самых длинных обсерваторийных сериях прослеживается обратно до 1840-вых лет и показывается и в сериях различной длины на наблюдательных пунктах, располагающихся на разных местах Земли, следовательно, ее фактическое существование является несомненным. В экваториальных обсерваториях имеет место полуделение этой волны, и она показывает двадцатидвухлетний Abbot-период намагниченности солнечных пятен. В волне *H* обсерватории г. Осло обнаруживается одиннадцатилетняя волна встречаемости солнечных пятен. В соответствующих волнах обсерваторий, располагающихся на разных местах, обнаруживаются тождества и связи симметрии.

Геомагнитное склонение [*D*] и наложенная волна восточной составляющей [*У*] идут с востока на запад и окружают Землю в двух волнах. Крайние величины наложенной волны других магнитных элементов являются одновременными на всей Земле (не имея ввиду мелких проявляющихся в волне местных свойств, а также погрешностей в измерениях и смещений, являющихся неизбежными при приближении к сериям различной длины).

В изображении векторных диаграмм, конечно, также появляется волна на всех координатных плоскостях, и в этих векторных диаграммах обнаруживаются дальнейшие закономерности.

Рассматривая явление в пространстве, видно, что пространственная математически уравновешенная кривая спирально окружается измеренной в действительности пространственной кривой (поперечный эффект). Наложенная волна является проекцией этой спирали на разные координатные плоскости. Действительные вариации по временам опаздывают или спешат по сравнению с уравновешенными вековыми вариациями (продольный эффект). Исследования двух последних явлений осуществляются и в настоящее время. Результаты будут сообщены.

A NEW THEORY ON THE INTERNAL CONSTITUTION OF THE EARTH AND ITS GEOLOGICAL-GEOPHYSICAL CONSEQUENCES

By

L. EGYED

GEOPHYSICAL INSTITUTE, EÖTVÖS-UNIVERSITY, BUDAPEST

The problem

The main problem of geology and geophysics has always been the nature of the Earth's internal constitution and the cause and mechanism of the phenomena observed on its surface. In the following we endeavour to give a new, dynamic conception of the internal structure of the Earth in good agreement with physical and geological observations. This conception seems to be apt to account for the formation of the Earth's crust, the origin of tectonic forces, some paleogeographic phenomena and, moreover, for the mechanism of mountain building. The present paper is regarded, however, only as an attempt to solve this complex of problems.

The structure of the crust

The problem of the internal constitution of the crust is less difficult near to the surface and becomes more and more difficult with increasing depth. The continental crust, according to seismological data, consists of two layers, below which there is a uniform ultrabasic shell enveloping the whole Earth (Fig. 1).

The following average velocity data are given for the continental crust and the underlying magma [1], [2], [3], [4]:

Upper part of the crust	$\bar{P} = 5{,}6$ km/sec ;	$\bar{S} = 3{,}4$ km/sec
Lower part of the crust	$P^* = 6{,}4$ «	$S^* = 3{,}8$ «
Magma layer	$P_n = 8{,}2$ «	$S_n = 4{,}4$ «

The velocities at different pressures for different types of rocks as calculated from laboratory experiments are shown in Table I [5].

Data calculated from velocities show that the upper part of the crust consists of granites or granodiorites. The rock type corresponding to the lower part of the crust is gabbro or diorite, whereas that of the magma layer : dunite and peridotite. This is also in good agreement with geochemical observations.

Table I

Wave velocities in idealized rock types, as calculated from compressibility and Poisson's ratio according to L. H. ADAMS

Rock Type	5 km (1300 bars)		15 km (4000 bars)		35 km (10 000 bars)	
	V_P	V_S	V_P	V_S	V_P	V_S
Syenite	5,9	3,4	6,1	3,5	6,4	3,6
Granite L.	5,9	3,4	6,0	3,5	6,3	3,7
Granite H.	5,8	3,5	5,9	3,6	6,2	3,7
Granodiorite	5,8	3,4	6,0	3,5	6,2	3,7
Diorite	6,4	3,6	6,5	3,7	6,8	3,8
Gabbro	6,8	3,8	6,9	3,9	7,2	4,0
Olivine gabbro	7,0	3,9	7,1	4,0	7,4	4,2
Peridotite	7,4	4,2	7,5	4,2	7,7	4,3
Dunite B	7,9	4,5	8,1	4,5	8,2	4,6

Seismic investigations carried out in the area of the Atlantic and Pacific oceans, respectively, show that there is an essential difference between the basement of the deep-seas and that of the continental crust. The granitic layer

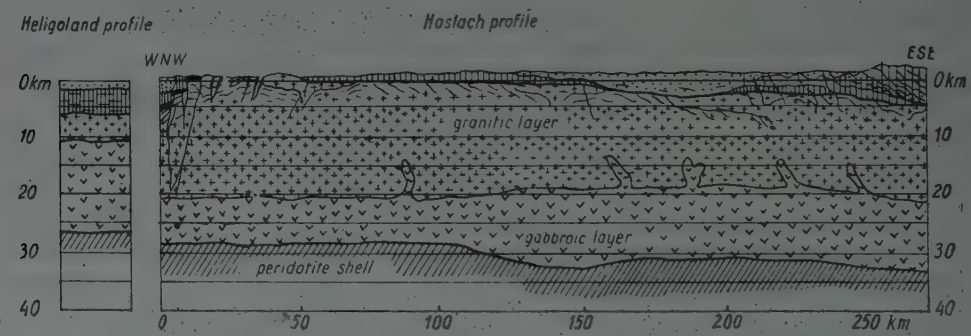

Fig. 1. The profile of the Earth's crust at Heligoland and Haslach

according to the measurements of EWING [6] and RAITT [7] is absent over the oceanic areas, whereas the thickness of the gabbroic layer covering the greatest part of the deep-seas does not exceed 5 km. These data are also in full agreement with the equilibrium of the Earth's crust.

The difference in the character of the oceanic and the continental structures is reflected in morphological data as well. We refer only to the double maxima of the hypsometric frequency curve (Fig. 2). The first maximum occurs at +0,1 km above sea level, whereas the second one lies at — 4,7 km below sea level i. e. there is a most frequent level for continental, and one for oceanic areas

These two distinct levels refer to the fact that the transition from continental to oceanic areas is discontinuous.

It is very interesting to compare the different frequency curves of the Atlantic, Indian and Pacific oceans, respectively, shown in Fig. 3. The curves

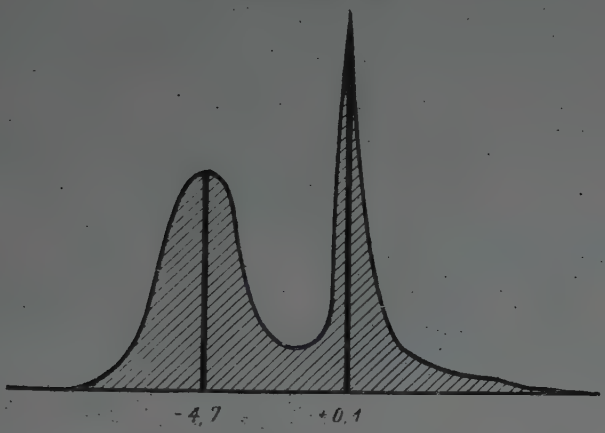

Fig. 2. The hypsometric frequency curve

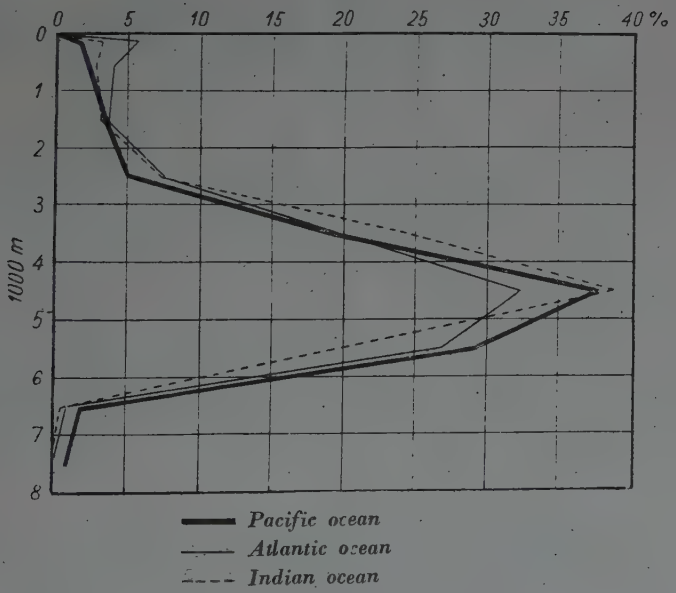

Fig. 3. The depth distribution in the area of the Pacific, Atlantic and Indian oceans

are nearly identical and their coincidence denotes, that the evolution of the three deep-sea areas was brought about by the same mechanism in which the hydrostatic equilibrium played the leading part. On the other hand, also the

density and viscosity of the materials taking part in the evolution were essentially the same.

Discontinuous transition of the continental and oceanic areas is shown also by the morphology of the continental shelves.

The dynamic behaviour of the Earth's surface is reflected also in earthquakes. The most characteristic feature of great ($M > 6$) earthquakes is their occurrence in long belts (Fig. 4) [8]. The most important belts of earthquakes

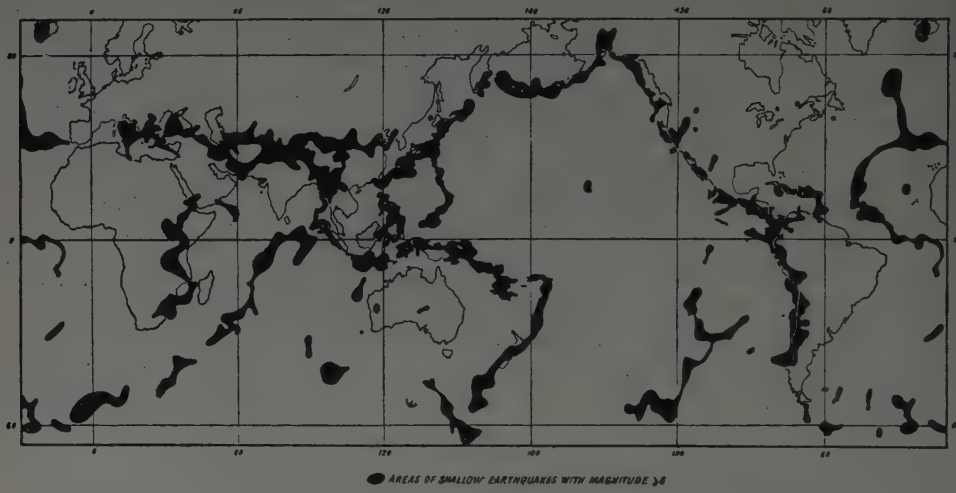

Fig. 4. The distribution of shallow earthquakes (M > 6) according to KONING

take place on the border of the Pacific ocean, in the area of the Alpide orogenic zone, in that of the Atlantic Ridge and the rift zones of Africa. Moreover, these seismically active zones are characteristically associated with arcuate tectonical and morphological forms.

The zonal distribution of the seismic areas shows that the outer part of the Earth's mantle and crust are under stress and that the seismically active areas, characterised by fault systems, are the weakest parts of the crust. This assumption is supported also by the distribution of the hypocenters of deep-focus earthquakes.

Physical data on the interior of the Earth

The most important discontinuities in the Earth's interior, according to seismic data, are the following:

33 km MOHOROVIČIĆ discontinuity
80—150 km Low-velocity layer of GUTENBERG
(413 km BYERLY discontinuity)

986 km REPETTI discontinuity
2900 km GUTENBERG—WIECHERT discontinuity
4980—5120 km Discontinuity layer of LEHMANN

The distribution of the layers:

0— 33 km	layer A
33— 413	B
413— 986	C
986—2900	D
2900—4980	E
4980—5120	F
5120—6370	G

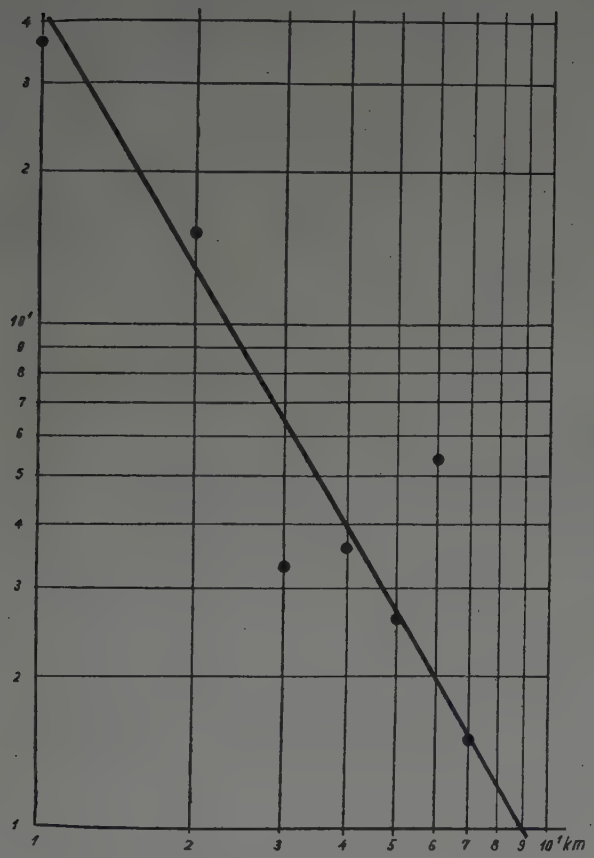

Fig. 5. The sum of the BENIOFF-numbers as a function of depth

Let us plot the values of the BENIOFF-numbers of the earthquakes occurring between 1930 and 1945 at a depth of $h - 50$ and $h + 50$ in function of h in a double logarithmic system (Fig. 5); we see that they are lying on a straight line, whereas the accumulation of deformation energies becomes unnoticeable in the neighbourhood of the REPETTI discontinuity.

On the other hand, the interior of the Earth is characterized by the following data [9]:

1. The velocity distribution of longitudinal and transverse waves is nearly continuous in the mantle (to a depth of 2900 km).

2. At the boundary of the core, i. e. at a depth of 2900 km, the velocity of longitudinal waves decreases discontinuously by about 40 per cent and the transverse waves disappear.

3. The velocity of longitudinal waves in the transition layer to the inner core (4980 to 5120 km) increases by about 10 per cent.

4. The upper limit of error in density determination within the mantle lies at 1 per cent, and within the outer core (2900—5000), at 3 per cent.

5. There is a discontinuous increase in density of about 65 per cent at the boundary of the core.

6. The pressure amounts to 100 000 bar at a depth of 300 km, to 1,37 megabar at the boundary of the core and to 3,64 megabar (1 bar $= 10^6$ din cm^{-2}) in the Earth's center.

7. Variation of gravity in the mantle amounts to less than 5 per cent.

Data concerning the material composition of the upper part of the simatic layer seem to be reliable.

The structure of the mantle

The latest important investigations concerning the structure of the mantle were carried out by F. BIRCH [10], [11]. He has shown that for the Earth's interior the following equation is valid:

$$1 - g^{-1}\frac{d\Phi}{dr} = \left(\frac{\partial K_T}{\partial P}\right)_T + A\alpha\gamma T + B(\alpha\gamma T)^2 + C\alpha\tau\Phi g^{-1}.$$

In this equation g is the value of gravity; $\Phi = \frac{K_s}{\varrho}$ i. e. the ratio of adiabatic compressibility to density; T the absolute temperature; α the volume thermal expansion: $\alpha = \frac{1}{v}\left(\frac{\partial v}{\partial T}\right)_p$; $\gamma =$ GRÜNEISEN's ratio; $\gamma = \frac{\alpha\Phi}{C_P}$, where C_P is the specific heat at constant pressure; τ is the adiabatic gradient, and P the pressure. These quantities are all functions of the radius r. The terms containing the constants A and C are ranging from 0,1 to 0,2. Consequently, the quadratic term characterized by B may be neglected.

Supposing a homogeneous composition of the mantle, BIRCH computed the curve of $\left(\frac{\partial K_T}{\partial P}\right)_T$ as a function of depth on the basis of BRIDGMAN's experiments and MURNAGHAN's finite strain theory.

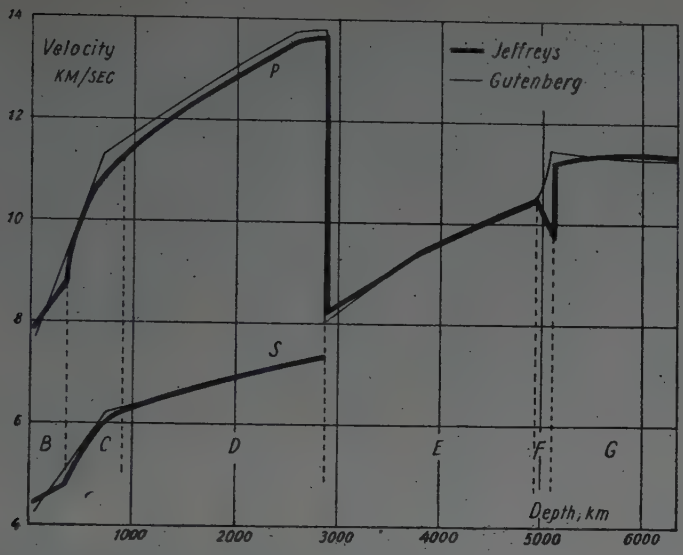

Fig. 6. The velocity of P- and S-waves according to GUTENBERG and JEFFREYS

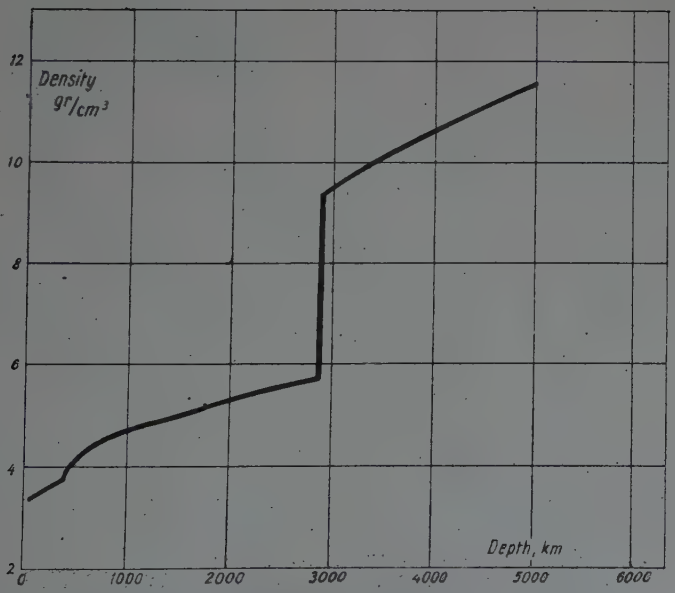

Fig. 7. The density as a function of depth according to BULLEN

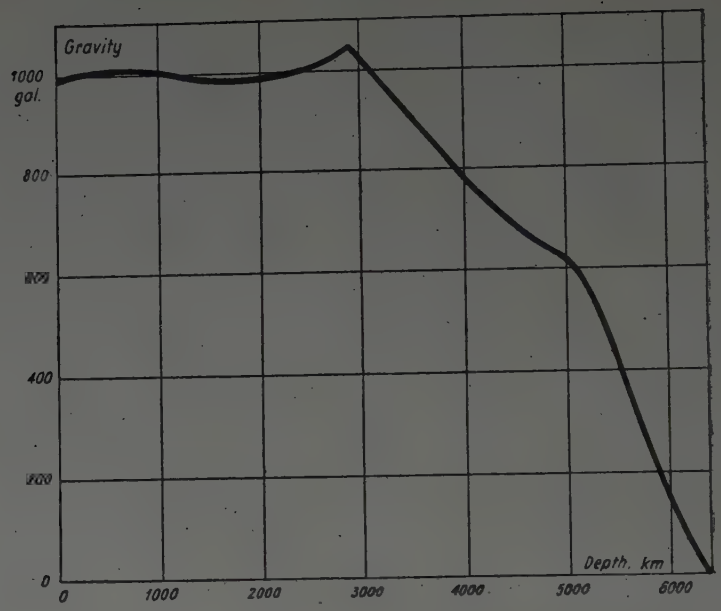

Fig. 8. The gravity within the Earth according to BULLEN

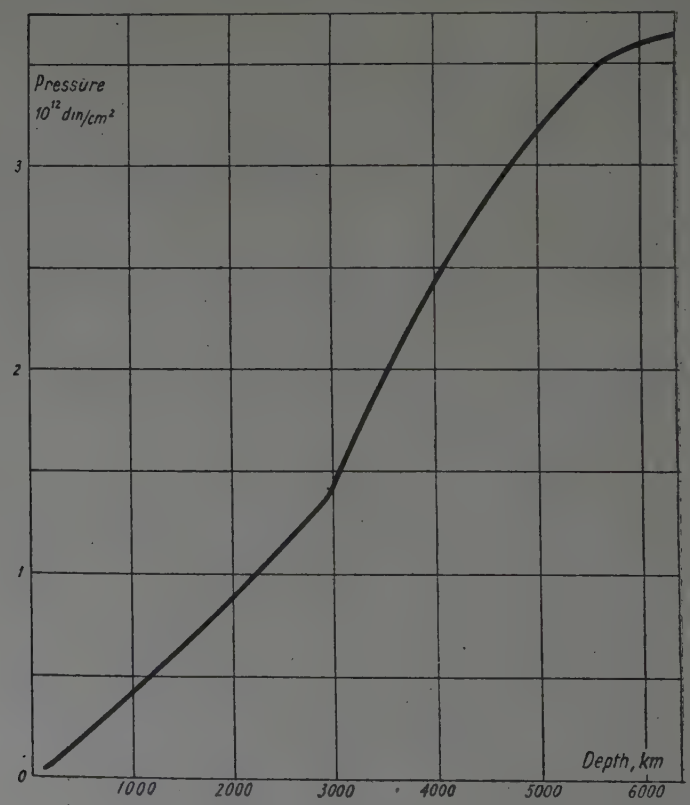

Fig. 9. The pressure distribution within the Earth

The values of $1 - g^{-1}\frac{d\Phi}{dr}$ were computed according to velocity data of JEFFREYS and GUTENBERG, respectively. The result is shown in Fig. 11.

It is remarkable that at a depth ranging to 800 — 900 km there is a great difference between the theoretical values of $\frac{\partial K}{\partial P}$ and the values of $1 - g^{-1}\frac{d\Phi}{dr}$

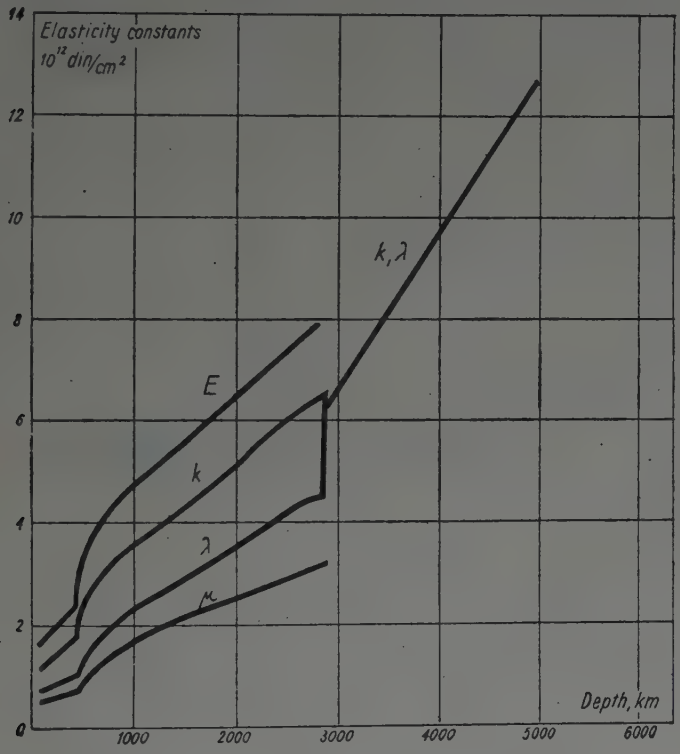

Fig. 10. The elasticity constants within the Earth

calculated from measurements, whereas below 900 km theoretical and measured values show a good agreement. It can be concluded from this fact that between 900 km and 2900 km the composition of the mantle is homogeneous and the values of $\alpha\gamma T$ and τ can be neglected.

The discrepancy observed above 800 km has been interpreted by BIRCH as a deviation from homogeneous composition. Likewise he computed the value of $\frac{K}{\varrho}$ observed at different depths for zero pressure. The result is shown in Fig. 12. According to this diagram the mantle is homogeneous between the depths of 900 km and 2900 km. The computed values show a rapid increase of $\left(\frac{K}{\varrho}\right)_0$

between 300 and 800 km. BIRCH came to the conclusion that this layer, coinciding practically with layer *C*, represents a transition from the familiar silicate minerals of layer *B* to the high-pressure-phase of layer *D*.

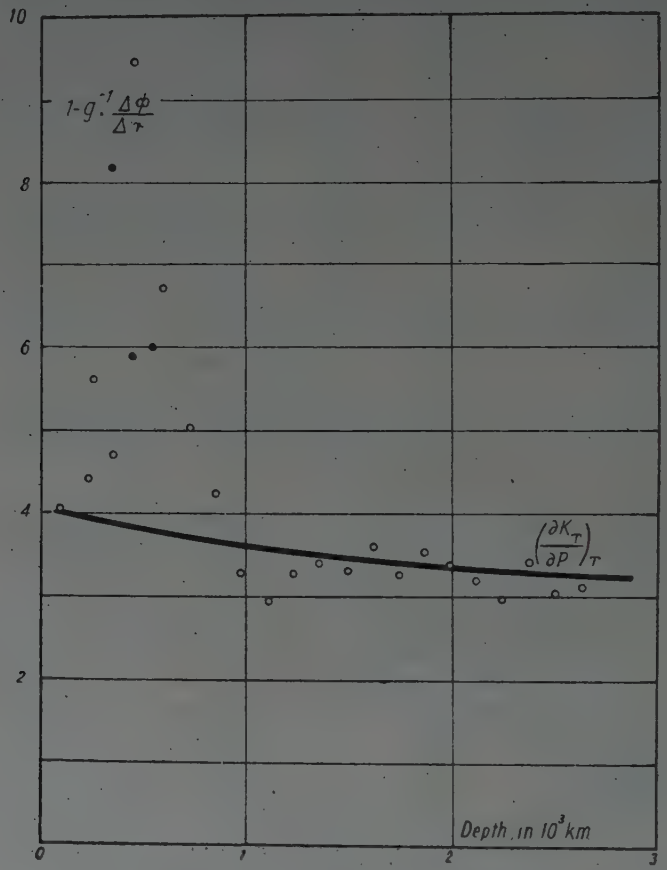

Fig. 11. The value of $1 - g^{-1}\frac{d\Phi}{dr}$ in the mantle on GUTENBERG's and JEFFREYS' data and the theoretical curve of $\left(\frac{\partial K_T}{\partial P}\right)_T$ according to BIRCH

Hypotheses concerning the material constitution of the Earth

There are three types of hypotheses concerning the internal constitution of the Earth : the iron-core hypothesis, the hypothesis of KUHN and RITTMANN and the RAMSEY hypothesis.

One chief characteristic of the different iron-core hypotheses is that the seismic discontinuities are identified with changes in material composition

and the principle is adopted that the internal composition is to be compared with the composition of meteorites.

In this conception the outer part of the mantle corresponds to the stony meteorites and is a mixture of olivine and pyroxene, i. e. it is essentially peridotite-like.

The inner part of the mantle, under the REPETTI discontinuity, is similar to transition meteorites. GOLDSCHMIDT believes that this part of the mantle

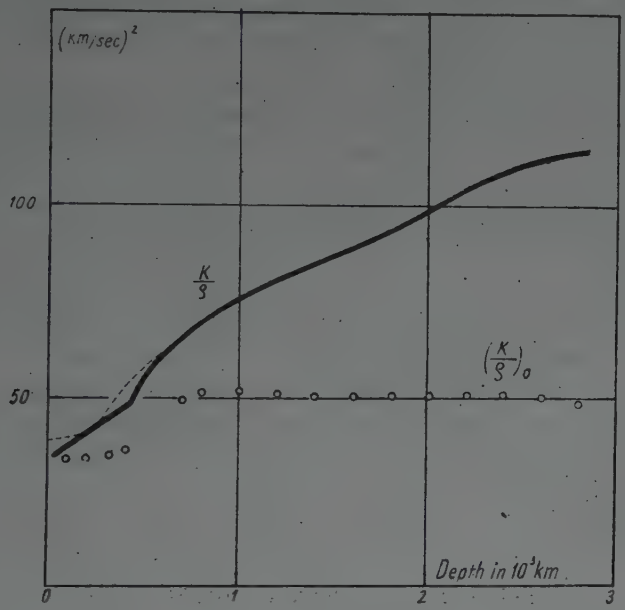

Fig. 12. The values of $\frac{K}{\varrho}$ on JEFFREYS' and GUTENBERG's data and the value of $\left(\frac{K}{\varrho}\right)_0$ at 0-pressure according to BIRCH

is composed of the oxides and sulphides of heavy metals. The Earth's core corresponds to the iron meteorites.

The modern conception of the iron-core hypothesis is developed by F. BIRCH. In his opinion, great changes and phase transitions may be observed only in layers *B* and *C*. Layer *D* is a high-pressure modification of ultrabasic silicate minerals. He believes that the core consists of iron alloying with lighter elements, including also metallic hydrogen. There is no discrepancy between the properties of the inner core and those of crystalline iron. Accordingly, we are dealing with a system, where the crystalline inner core is surrounded by a layer of fluid iron.

Several difficulties arise in connection with the different iron-core hypotheses. We are stating them as follows :

1. The sharp discontinuity at the boundary of the Earth's core as a consequence of differentiation is not accounted for. Chemical differentiation is still less motivated than gravitational differentiation.

2. F. BIRCH's investigations show that the mantle is homogeneous at depths ranging from 900 km to 2900 km. In view of diffusion phenomena the sharp material discontinuity at the boundary of the core is incomprehensible.

3. The GUTENBERG—WIECHERT discontinuity, according to the iron-core hypotheses, is a surface where a change in material composition occurs. At the same time temperature is so high on this surface, that the mass consisting mostly of iron passes into the molten state. The coincidence of both these circumstances is highly improbable.

The internal composition of the Earth, according to the KUHN—RITTMANN hypothesis [12], becomes more and more homogeneous with depth. Beyond a certain limit (at about 2000 km) the inner part of the Earth is represented by a solar mass of a composition resembling to that of the Sun. The seismic discontinuities are only the consequences of a change in physical parameters and not of a different material composition. The GUTENBERG—WIECHERT discontinuity appears in this hypothesis as a consequence of decrease in the relation time of the shearing stresses below the period of seismic waves : consequently, the shearing stresses cannot exist any longer. The velocity of longitudinal waves, therefore, decreases discontinuously and the transverse waves disappear. Density, however, increases continuously through the boundary of the core.

This theory seems to be very attractive but cannot provide a basis for serious discussion. Let us mention the difficulty that, on the ground of KUHN and RITTMANN's conception, no reflection can arise contrary to the observed *PcP* waves, at the boundary of the core. The continuous increase of density represents a further contradiction to the results of various investigations. (The discontinuous transition of density at the boundary of the core is a proved fact [13], [14].)

The third type of hypotheses is represented by the phase-transition theory of RAMSEY [15] based on observed high-pressure phase-transitions and quantummechanical considerations. RAMSEY believes that the composition of the Earth becomes more and more homogeneous with depth and seems to be very similar to that of olivine. He suggests further that the seismic discontinuities are only high-pressure phase transitions corresponding to rearrangements in the electron shells. The GUTENBERG—WIECHERT discontinuity represents a rearrangement in the electron shells as well, but the atoms and molecules obtain in the course of this rearrangement a metallic character.

RAMSEY considers the decrease in velocity of the longitudinal seismic waves at the boundary of the core a consequence of the liquid state caused by high temperature. The inner core, however, appears to be a crystalline modification of metallic olivine.

This attractive hypothesis involves the same difficulties as the iron-core hypothesis. There is very little probability in the coincidence of the phase-transition surface with the surface of melting temperature.

The new model

The correct model of the Earth must explain, besides observed gravitational and seismological facts, the origin of tectonic energies and all phenomena observed on the Earth's surface as well. All Earth models used up to now have been of static character. On the subsequent pages we are trying to give a dynamic model explaining all observed phenomena related to the Earth including mountain building.

In the first place, it has to be elucidated whether or not the seismic discontinuities deep in the Earth represent discontinuities in composition as well?

It has been mentioned above that a sharp discontinuity could hardly be ascribed to differentiation and an original discontinuity due to different composition would have disappeared owing to diffusion phenomena.

BIRCH's investigations show that layer *D* of the mantle, extending to the boundary of the core, is homogeneous. Two possibilities are mentioned as to the homogeneity of the mantle at a depth ranging from 800 to 2900 km.

1. Originally the whole mantle was homogeneous and layer *D* has remained unchanged, differentiation having affected only the layers above, including layer *C*.

2. Differentiation has affected the whole mantle, by settling-out of a uniform aggregate of the highest-melting components as high-pressure phases and by rejecting lower-melting components toward the surface.

In BIRCH's opinion the second alternative must be preferred. The present writer thinks that the first possibility is more plausible than the assumption of a material change beyond a homogeneous layer of 2000 km thickness.

Consequently, it is a plausible supposition that, beyond a certain depth, probably beneath 800 km, the composition of the Earth becomes homogeneous. This homogeneity, however, refers only to the massnumber distribution of atoms and not to molecular composition.

Differentiation phenomena have mainly affected layers *B* and *C*. In layer *D* and in the core, i. e. below 900 km, the material composition of the Earth seems to be homogeneous. In layer *B*, characterized by ultrabasic rocks, the low-velocity zone of GUTENBERG between 80 and 150 km may be explained by a geothermic gradient of 6,6 C°/km. In layers *B* and *C*, at a depth ranging from 200 to 700 km, a high-pressure phase transition, probably, prevails.

Considerations of the phenomena and data referring to the Earth's interior lead to the following conclusions : The pressure in the mantle is carried by the

electron-shells of atoms. The consequence of the pressure is a lattice-like structure where each atom has its fixed position relative to its neighbourhood. The particles displaced by an outer force, e. g. earthquake-waves, return to their original position in consequence of the shearing forces due to the lattice-like structure. This seems to be the cause of the rigidity observed in the mantle. This assumption is supported also by the fact that, in the mantle, rigidity is increasing proportional to pressure.

In the Earth composed of homogeneous material the GUTENBERG—WIECHERT discontinuity, under a depth of 2900 km, is only a physical surface beyond which matter exists in an ultrahigh-pressure phase (= ultraphase). Characteristics of this ultraphase, according to present observations, are the following: *a)* Density is greater than in normal state; *b)* Forces acting between the particles grow to such an extent, that pressures below 3 megabars ($3 \cdot 10^{12}$ din cm^{-2}) do not cause a rearrangement of the particles; *c)* At the pressures existing within the Earth this ultraphase in unstable and a steady and irreversible transition from the ultraphase toward the normal state is going on.

In this conception the rigidity of the mantle is only a consequence of the existing pressure bringing about a lattice-like structure of matter.

The GUTENBERG—WIECHERT discontinuity being the boundary of normal state, pressure beyond this surface is not sufficient to cause a lattice-like structure according to property *b)* of this state, and therefore no transverse waves can be observed in the core where the pressure is less than 3 megabars. The LEHMANN zone, between 4980 and 5120 km represents a transition zone, where the pressure attains the value at which the particles rearrange into a lattice-like structure. In this conception the structure of the inner core is a consequence of pressure: at its boundary shearing stresses, caused by the lattice-like structure, reappear and the velocity of longitudinal waves increases. The necessary reappearance of transverse waves in the inner core is a further consequence of the above said. The discontinuous increase of density at the boundary of the core (at the depth of 2900 km) is a consequence of property *a)* of the ultraphase state.

The origin of matter in the ultraphase state of the Earth must necessarily be in connection with the origin of the solar system. Possibly, the development of the solar system has taken place in the following manner: At the beginning our Sun had a companion (probably a white dwarf, consisting of degenerated matter). This companion, however, became unstable and disrupted so that its greater part flew out of the gravitational field of the Sun. At the same time the center of gravity remained in or near to the original orbit. As a matter of fact some distinct parts of this star remained in the neighbourhood of its own center of gravity. These are the planets, at least the inner planets, and the satellites. In its primeval state the whole mass of the planets and satellites represented an ultra-high pressure modification becoming, at the

essentially lower pressure, unstable, and consequently, a steady transformation toward the normal state has been going on. In all probability, Mercury and the Moon, in their whole mass, are already in normal state, therefore, their density is about 3,3.

Interesting inferences may be deduced from property *c)* of the ultraphase state. Supposing the ultraphase state in the Earth is unstable and a steady and irreversible transformation is going on from the ultraphase toward the normal state of the atoms, then the amount of atoms in the ultraphase will show a continous decrease and the mass of the Earth, composed of matter in the normal state, will be steadily increasing. However, density in the normal state is less than in the ultraphase state, therefore, the volume of matter is increasing.

Property *c)* of the ultraphase state has, therefore, the consequence that the volume of the Earth is steadily increasing.

It will be shown that the most probable, estimated increase of the Earth's radius is 0,5 mm/year.

An attempt will be made in the following to show that, on the basis of this surprising and unusual result all phenomena related to the Earth, among them such problems as were difficult to explain up to now, become familiar, moreover, theoretical inferences are in fair agreement with observations not only qualitatively but also quantitatively.

The formation of the Earth's crust

The following facts relating to the mechanism of the formation of the Earth's crust, are to be explained.

1. The difference in the petrographical constitution of the continental and oceanic areas ;

2. the double maxima of the hypsometric frequency curve ;

3. the coincidence of the depth-frequency curves of the Atlantic, Pacific and Indian oceans, and

4. the discontinuous transition of the continental areas into the oceanic areas.

We have to point out that these facts cannot be explained on the ground of the theories hitherto established. In view of the steady growth of the Earth's volume the mechanism of the formation of oceans and continents may be sketched.

In the primeval state of the Earth a granitic-gabbroic layer has been formed owing to differentiation on top of the undifferentiated ultrabasic matter. This layer has solidified by cooling through heat-radiation. Due to the irreversible transition toward the normal state, the volume of the Earth has been continuously

growing and the solid crust has got under the action of stresses. In the course of this process the volume of the Earth attained a certain limit, beyond which the stresses surpassed the strength of the rocks and the crust disrupted. The ultrabasic magma, along the line of rupture, rose to a level corresponding to hydrostatic equilibrium and, being much denser than the granitic-gabbroic layer, its level remained about 5—6 km lower than the first surface of the Earth i. e. the surface of the continental areas. These areas represent the oceanic basins of to-day.

The above described mechanism accounts for the petrological difference between continental and oceanic areas and the double maxima of the hypso-

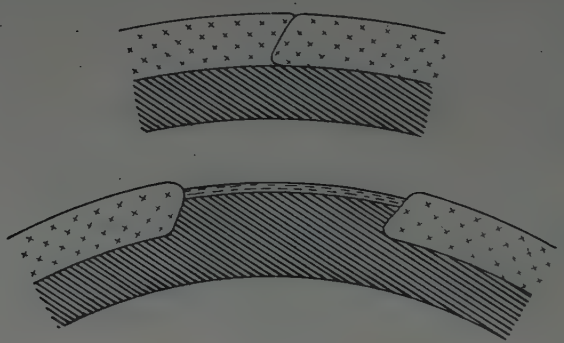

Fig. 13. The mechanism of the formation of oceans

metric frequency curve, as well as for the discontinuous transition of the borders of the continents to oceanic areas.

Probably, the first disrupture of the crust has taken place in the area of the Pacific ocean and the arcuate form of the continental borders is also a consequence of this phenomenon.

The formation of all the oceans, however, did not take place at the same time, but in the course of a progressive evolution, by way of the same mechanism as the formation of the first ocean basin. This fact is supported also by data represented in Fig. 3.

The yearly average increase of the Earth's radius computed from the area of the continents

We may establish the radius of the Earth as it existed at the time of the early crust on the basis of the formation of oceanic basins. The area of the sialic part of the Earth's surface covers about $2 \cdot 10^{18}$ cm^2. This area corresponds to the Earth's surface at the time of the formation of the first crust. From the equation $4\pi R_0^2 = 2 \cdot 10^{18}$ cm^2 the corresponding radius is $R_0 = 4 \cdot 10^8$ cm.

The time elapsed is $4{,}4 \cdot 10^9$ years [16], [17], and the increase of the radius about $2{,}4 \cdot 10^8$ cm. Consequently, the yearly average increase of the radius is 0,55 mm/year.

Variation of the continental areas covered by ocean water and the yearly average increase of the Earth's radius

KUENEN [18] came to the conclusion, that the highest estimate of the increase of the volume of oceanic water since the beginning of the Cambrian amounts to about $50 \cdot 10^{21}$ cm^3 i. e. less than 4 per cent of the whole water

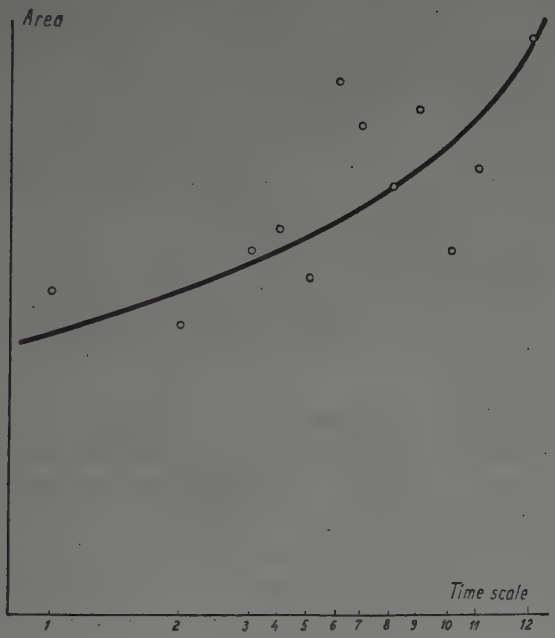

Fig. 14. The variation of continental areas not covered by sea-water according to data of STRAHOW. 1. Middle and Upper Cambrian. 2. Lower Silurian. 3. Upper Devonian. 4. Lower Carbonifereous. 5. Upper Carbonifereous. 6. Upper Permian. 7. Upper Triassic. 8. Upper Jurassic. 9. Lower Cretaceous. 10. Upper Cretaceous. 11. Paleogene. 12. Upper Pliocene

content of all the oceans put together. However, in case of an expanding Earth its surface is continuously growing and, therefore, the sea level is in average steadily decreasing. Juvenile waters have little influence on this process.

It is obvious that, in case the sea-level was higher in the past than now, the average extension of the continental areas covered by oceanic waters was also greater and took a decreasing trend in the course of geological times. From the observed decrease we may conclude the expansion of the Earth, and we

can also establish the rate of the yearly increase of the Earth's radius. To this purpose the paleogeographical maps of STRAHOW [19] were plotted on the surface of a sphere and the continental areas not covered by water determined with the aid of a planimeter. The data obtained are represented in Fig. 14 as a function of time, and are lying mainly on a monotonously increasing line. Scattering of these data is a natural consequence of warpings having happened in the course of the last 500 million years. By way of the above data the rate of increase of the Earth's radius may be established. However, an increase of the Earth's surface (dF) can be observed only in the area (F_s) of the seas, while the whole water content of the oceans ($F_s \cdot m$) remains practically constant. Consequently, the depth (m) of the oceans has decreased by dm while the Earth's surface has increased by dF, following the equation

$$(F_s + dF)(m - dm) = m \cdot F_s$$

From the above follows that the average increase of the Earth's surface is

$$dF = \frac{F_s \cdot dm}{m}$$

At the present time, the surface of the continental areas not covered by water is, according to STRAHOW's data, twice as great as it was 500 million years ago.

It may be assumed that the level-distribution on the Earth was comparatively the same 500 million years ago as it is to-day.

The distribution of the Earth's surface on different levels is the following

Table 2

The area of the Earth's surface	10^6 km^2
above sea level	148,1
« 0,2 km	111,1
« 0,5 km	71,2
« 1,0 km	42,3

According to these data the area lying above 500 m is equal to half of the area of the Earth's surface lying above sea-level.

Consequently, it may be supposed that the sea-level was about 500 m higher in early Paleozoic times (500 million years ago) than it is at present. Indeed, the area of the seas amounts to $361 \cdot 10^{18}$ cm^2 and the average sea-depth to

$3{,}8 \cdot 10^5$ cm. Therefore, the increase of the Earth's surface in the course of the last 500 million years may be expressed in the form

$$dF = \frac{F_s \cdot dm}{m} = 4{,}75 \cdot 10^{17} \text{ cm}^2.$$

On the ground of these data the Earth's radius in early Paleozoic times may be derived. The present surface of the Earth being $51 \cdot 10^{17}$ cm^2, at the beginning of Paleozoic times it was $46{,}25 \cdot 10^{17}$ cm^2. From this figure the Earth's radius may be computed as $6{,}08 \cdot 10^8$ cm. Thus, the increase of the Earth's radius in the course of the last $5 \cdot 10^8$ years amounts to $0{,}29 \cdot 10^8$ and the yearly average increase to 0,58 mm/year. This is in good agreement with the estimated average growth discussed in the last paragraph.

It has been shown that the expansion of the Earth is supported by paleogeographical evidence and that the derived rate of increase of the Earth's radius is in good agreement with values estimated in a different way.

Decrease of the Earth's angular velocity and the average yearly increase of the radius

Observations have shown that the angular velocity of the Earth's rotation has been steadily decreasing. The value of it amounts to approximately $5{,}2 \cdot 10^{-6}$ sec/year, i. e. the decrease in the length of a day yearly to $5{,}2 \cdot 10^{-6}$ sec.

Formerly, the decrease of velocity has been assigned to the effect of tidal phenomena, but the latest investigations have shown that their effect is compensated by the effect of the athmosphere on the whole.

However, the decrease in the velocity of rotation is a natural consequence of the Earth's expansion.

We may state that, in case no external forces are acting, the kinetic energy of the Earth is constant. The kinetic energy may be expressed in the form

$$\frac{2\pi^2}{T^2} \Theta = c$$

where Θ is the moment of inertia, T the period of one rotation ($T = 1$ day), and c is a constant. This equation may be written in the form

$$T^2 = \frac{2\pi^2}{c} \Theta$$

With the expansion of the Earth the moment of inertia is increasing, consequently, together with it the rotation period of the Earth increases simultaneously too. From the above equation the change of the rotation time may be derived :

$$dT = \frac{T}{2} \frac{d\Theta}{\Theta}$$

On the other hand, the moment of inertia may be written in the form :

$$\Theta = \int r^2 \sin^2 \varphi \, dm$$

The increase of the moment of inertia, considering the increase of the radius Δr, is given by the equation

$$d\Theta = 2 \Delta r \int_r^R \int_0^{2\pi} \int_0^{\pi} \sigma r^3 \sin^3 \varphi dr d\vartheta d\varphi$$

or expressed in explicite form by using for σ an average value σ_a

$$d\Theta = \frac{4\pi}{3} (R^4 - r^4) \Delta r \sigma_a$$

A suitable average density value for σ_a is

$$\sigma_a = \frac{\sigma_r r + \sigma_R R}{r + R} = 4{,}15$$

where r = the radius of the core and R = the radius of the Earth), hence

$$d\Theta = 2{,}6 \cdot 10^{36} \Delta r$$

and

$$dT = 1{,}40 \cdot 10^{-4} \Delta r \text{ sec.}$$

The yearly increase of the radius obtained from the above equation is

$$\Delta r = \frac{dT}{1{,}40} \cdot 10^4 = \frac{5{,}2}{1{,}40} \cdot 10^{-2} \text{ cm/year} = 0{,}38 \text{ mm/year.}$$

This value is in very good agreement with the average values, determined previously, of 0,55 and 0,58 mm/year. The average of the three values amounts to 0,5 mm/year, which will be taken as the increase of the radius in the following paragraphs.

The energy of tectonical forces and the energy of earthquakes

A great amount of energy is released by the transition of the ultraphase matter into normal state. Its amount may be estimated from the fact that the whole mass of the mantle must have been uplifted. Indeed, the greatest part of this energy is employed to the increase of gravitational energy only. The yearly release of energy is

$$E_{exp} = M_m \cdot g_m \cdot \Delta r$$

where M_m is the mass of the mantle, g_m the value of gravity in the mantle and $\Delta r = 0{,}5$ mm/year the yearly increase of the radius.

Therefore, the energy yearly released by the transition amounts to

$$E_{exp} = 2 \cdot 10^{29} \text{ erg.}$$

The energy yearly released in earthquakes is, according to data by GUTENBERG and RICHTER [20] about $2{,}5 \cdot 10^{24}$ erg in average, in case it is computed from the equation

$$\log E_t = 11 + 1{,}6\, M$$

where M is the magnitudo of earthquakes. This value seems to be only a fraction of the established yearly value of $2 \cdot 10^{29}$ erg.

However, in the case of an expanding Earth elastic stresses arise and an accumulation of deformational energies take place in the crust and in the upper part of the mantle. These energies represent the source of tectonic forces and only part of them is released in earthquakes.

Let us compute the amount of the strain energies. In case of a stress p, the strain Θ (the relative change of volume) is

$$\Theta = \frac{2\,(1 - 2\,\sigma)}{E} \cdot p = \frac{2\,p}{3\,k}$$

where σ is the Poisson-ratio, E the Young-modulus and k the incompressibility of the upper part of the mantle. If we have a square with an area of 1 cm^2, the increase of radius dR will cause the lengthening of the sides of this square by $\frac{dR}{R}$. The height of the cube, the base of which is formed by this square, is shortening however by $2\sigma \frac{dR}{R}$ as a consequence of the lengthening of the sides by

$\frac{dR}{R}$. Therefore, the relative change of volume is

$$\Theta = 2(1-\sigma)\frac{dR}{R}.$$

For the upper part of the mantle $\sigma = 0{,}27$ approximately, while $dR = 0{,}5$ mm/year and $R = 6{,}37 \cdot 10^8$ cm. The relative change of volume is

$$\Theta = 1{,}15 \cdot 10^{-10}.$$

Considering the equation of the deformational energies [21],

$$w = \frac{1}{2}k\Theta^2 + \mu e_{ij}^2$$

and supposing $e_{ij} = 0$, the above deformation gives an energy-density of

$$w = 0{,}76 \cdot 10^{-8}\ \text{erg/cm}^2$$

for the first year of accumulation, because the value of $k = 1{,}16 \cdot 10^{12}$ din/cm^2.

It has been mentioned above, that the yearly amount of energies released in earthquakes is $2{,}5 \cdot 10^{24}$ erg, From this figure $2{,}15 \cdot 10^{24}$ erg is the energy released in shallow, $0{,}29 \cdot 10^{24}$ erg in intermediate and $0{,}06 \cdot 10^{24}$ erg in deep-focus earthquakes. The greatest part of the elastic energy has accumulated in the upper part of the mantle of 60 km thickness.

In the first year this energy amounts to

$$W = 4\pi R^2 \cdot h \cdot w = 2{,}3 \cdot 10^{17}\ \text{erg},$$

and seems to be only a fraction of the energy yearly released in the earthquakes. At the same time the stress acting in the crust, considering a deformation of $\Theta = 1{,}15 \cdot 10^{-10}$, may be expressed on the ground of the equation $\Theta = \frac{2p}{3k}$ as

$$p = \frac{3}{2}k\Theta = 2 \cdot 10^2\ \text{din/cm}^2.$$

It is known, that the breaking strength of the rocks occurring in the upper part of the mantle amounts to about 10^{10} din/cm^2 [22]. However, earthquake foci are places, where the strength of the rocks is overcome by stresses. 10^{10} din/cm^2 is attained only, when the deformation Θ equals to $5{,}7 \cdot 10^{-3}$. This

deformation takes place only in the course of $5 \cdot 10^7$ years, if an increase of the radius of 0,5 mm/year is considered.

In the course of 10^7 years the strain amounts to

$$\Theta_{10^7\ year} = 1{,}15 \cdot 10^{-3}.$$

Accumulated energy occurring in the upper part of the mantle of 60 km thickness amounts to

$$W = 2{,}3 \cdot 10^{31}\ \text{erg}.$$

Consequently, the yearly average energy amounts to $2{,}3 \cdot 10^{24}$ erg i. e. equals the yearly amount of energy released in shallow earthquakes. The maximum amount of energy accumulated in the upper part of the mantle, considering only the zone of shallow earthquakes ($h < 60$ km), is $5 \cdot 10^{32}$ erg.

The periodicity of geological phenomena may be interpreted from the computed values of elastic energies. If we take into account the state of the Earth's crust after disruption, at least $5 \cdot 10^7$ years have to elapse before stresses accumulate to cause a new rupture in the crust, and the magma basement of the new oceanic areas extending along the previous line of rupture has time enough to solidify. In this solid state stresses are able to accumulate again. The values given above show that the energies released by the rupture of the crust are considerably greater than those released in earthquakes. The forces originating from these energies are very great. They are called tectonical forces and are acting, in the first place, during orogenic periods corresponding to ruptures of the crust. The source of the tectonical forces are the elastic energies accumulated in the upper part of the mantle. The amount of energies released in earthquakes represents only a part of the accumulated energies during non-orogenic periods.

When a rupture takes place, the majority of the accumulated elastic energy will be released and a new process of accumulation will start. From the above we come to the conclusion, that the rupture of the crust is a periodical phenomenon and the period of an orogenic cycle has a duration of at least $5 \cdot 10^7$ years. This estimate is in accordance with geological observations.

The mechanism of deep-focus earthquakes

One of the most interesting problems of geophysics is the origin of deep-focus earthquakes. It is known that in elastic bodies the angle between the surface of rupture and that of tensional stress is greater than 45°. The hypo-

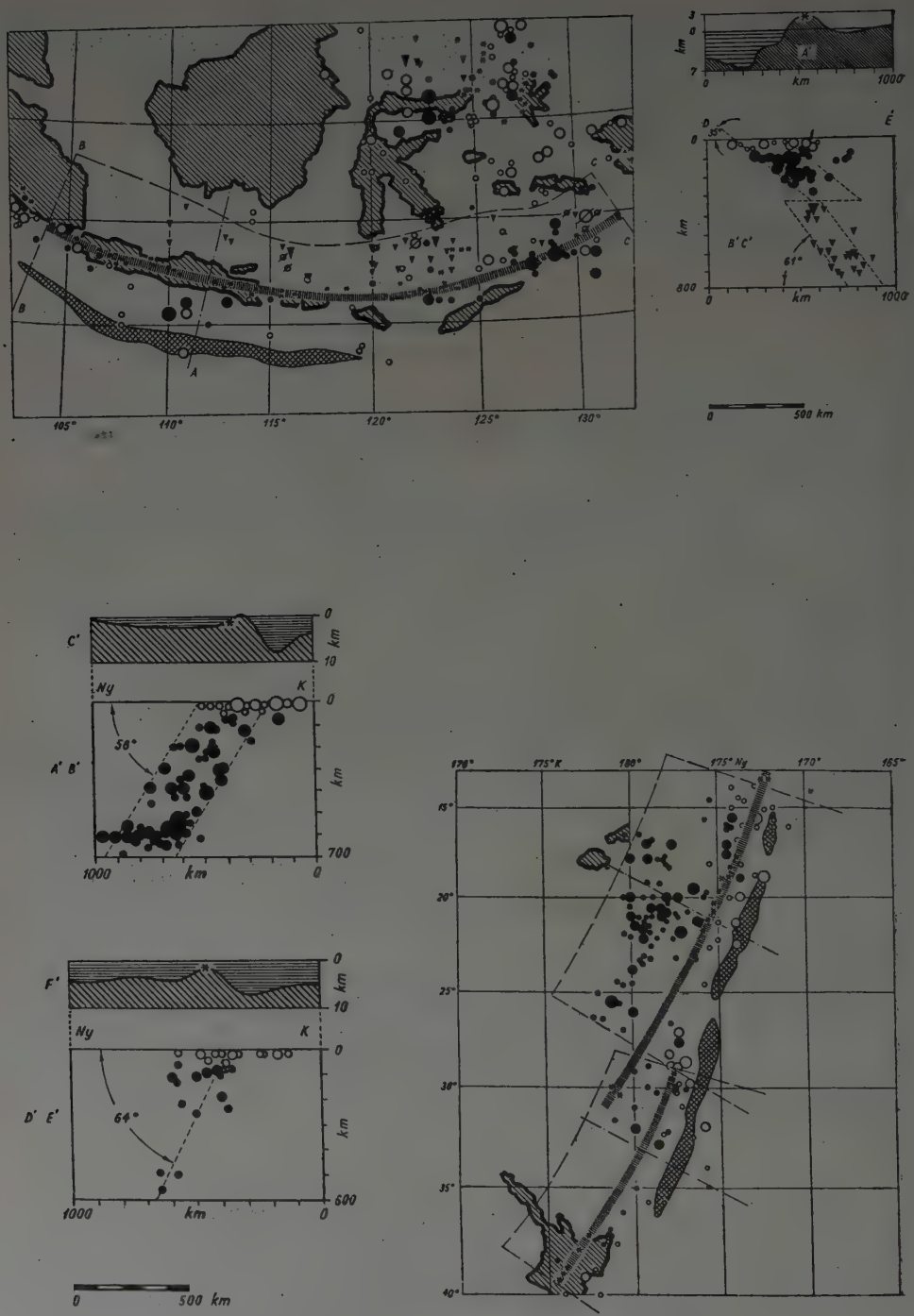

Fig. 15. Distribution of earthquakes foci according to BENIOFF

centers of deep-focus earthquakes, according to investigations of BENIOFF [23] take place along a shear plane forming an angle of about 60° with the Earth's surface (Fig. 15). This may be interpreted as a consequence of tangential tensile stresses, in agreement with the effect of the expansion of the Earth. Laboratory experiments are also supporting this conception.

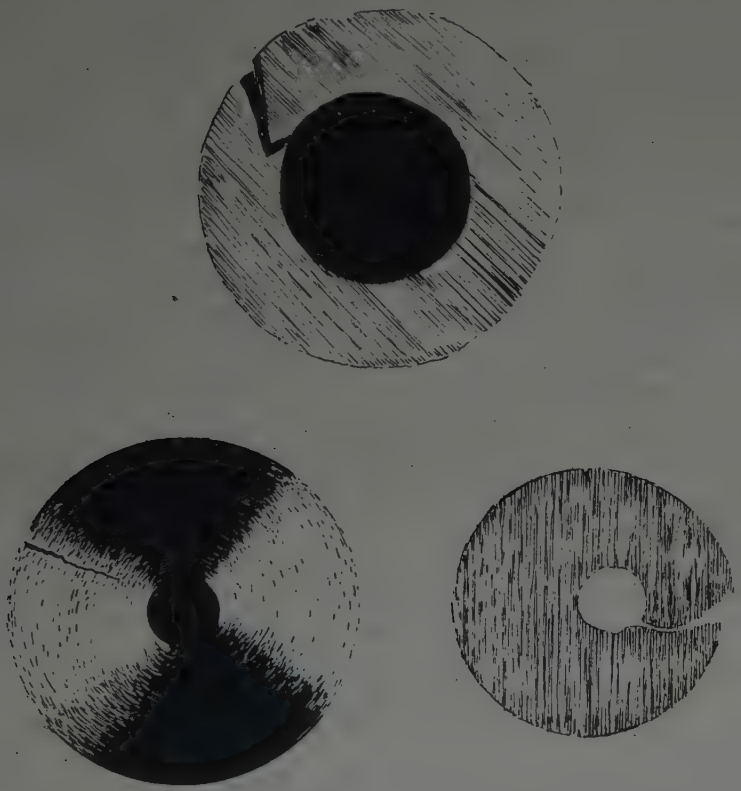

Fig. 16. Cylinders ruptured by internal pressure, according to BRIDGMAN

BRIDGMAN [24] examined in the course of his famous laboratory experiments the problem, whether the theoretical inferences of elasticity are in accordance with experimental data. Thick hollow cylinders were put under great internal pressure. Experiments, however, showed that expectations based on the simple elastic theory were very far indeed from the mark, with respect to both the maximum pressure and the character of rupture. Cylinders stand an internal pressure very much higher than the tensile limit pressure, and the rupture of cylinders made of ordinary grades of steel invariably starts at the outside surface and travels inward, rather than starting at the inside and running out. The developed breaking surfaces were similar to those observed at deep-

focus earthquakes forming mostly an oblique plane (or curved surface) very similar to that of the hypocenters of deep-focus earthquakes (Figs. 15, 16). Deep-focus earthquakes can be considered, therefore, as the consequences of shearing stresses caused by expansion of the Earth's mantle.

The breaking surfaces occur at the weakest areas of the Earth's surface, i. e. at first on the boundary of the oceans and continents, and the breaking lines on the surface are mostly of arcuate structure. This circumstance, however, may be interpreted as a consequence of expansion as well.

The origin of forces producing deep-sea troughs

We have shown in another paper [22], that the origin of deep-sea troughs is connected with a couple of forces acting at the boundary of the continents. It is known, that the elastic properties of continental rocks are different from those constituting the basement of the oceanic areas, i. e. the Young-modulus of the continental rocks is smaller, than the modulus of simatic rocks forming the bottom of the oceans. Consequently, the relative tension originated in the expansion of the Earth is greater on the upper part of the continental, than on the upper part of the oceanic areas. On the other hand, the relative tension at the bottom of the sialic blocks under the continents is of about the same order of magnitude as the relative tension of the simatic rocks, at the same level, under the oceanic areas. Therefore, the effect of stresses acting at the boundary of the continents by an expansion is the same as the effect of a couple of forces corresponding to the deformation observed by deep-sea troughs.

Formation of the fracture systems on the Earth's surface

There are some surprising morphological consequences of an expanding Earth too.

The resistance of the sedimentary layers overlying the elastic crust is very small comparing to the tensile stresses, consequently, by an expansion of the Earth faulting systems are produced in the sedimentary layers. The breaking surfaces of these faulting systems are mostly invisible as the sediments are only quasi-plastic, but they are washed out by surface waters forming the drainage system of the area. A classical example of this conception is represented by the Hungarian drainage system [25] shown in Fig. 17, as well as the linear pattern of the North-American drainage system brought forward by HOBBS (Fig. 18).

The formation of the characteristically arcuate form of the African Rifts is also in good accordance with the expansion of the Earth. A further evidence

is produced in favour of our conception by the formation of the Red Sea by a drift, along a faultline (Fig. 19).

Moreover, there are some morphological features in the area of the deep seas characterising the expansion of the Earth. Fig. 20 represents a trough-system of a length of 5000 km, taking place near to the Equator, West of South America. It shows a rupture caused by tensional stresses.

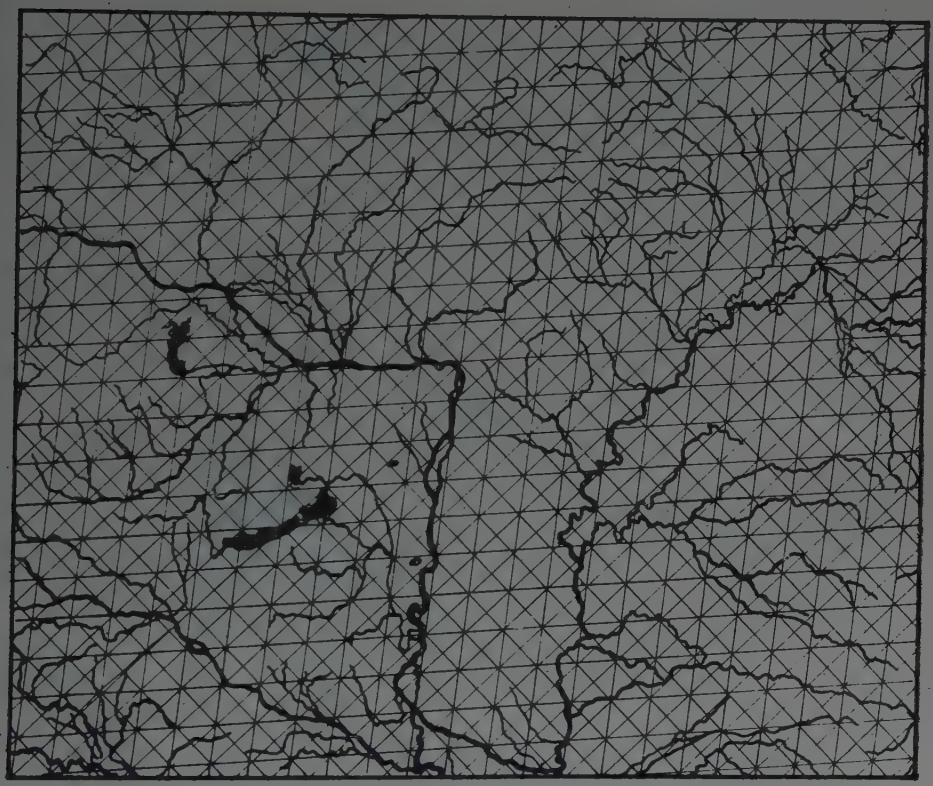

Fig. 17. Drainage map of Hungary as a faulting system

Another figure (Fig. 21) illustrates the morphology of the oceanic bottom East of the Tonga and Kermadec Islands and New Zealand. A third figure (Fig. 22) represents the morphological features near to the Sandwich Islands and Antarctica south of Africa. The two latter are characteristic for a spherical membrane ruptured under the action of tensile stresses.

There are also other evidences concerning the expansion of the Earth's crust [26].

Problem and mechanism of continental drifts

The formation of the ancient parts of the Pacific basin and the present continents forming then a single connected block has been brought about by the first rupture of the crust. This is the starting point of the TAYLOR—WEGENER theory, that claimed to explain the evolution of the present distribution of the oceans and continents.

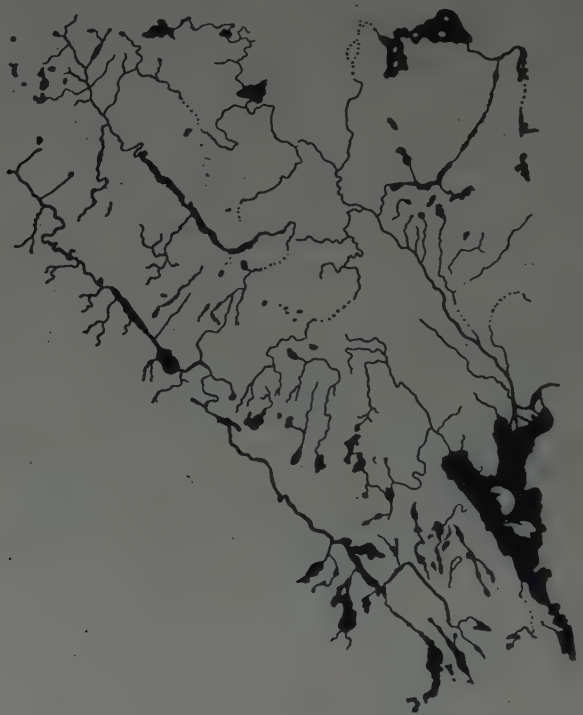

Fig. 18. Drainage map of part of North America according to HOBBS

At the end of the Carboniferous, in WEGENER's theory [28], the connected block of the continents, the so-called Pangaea, disrupted and drifted apart. As a consequence of the breakup the evolution of the Atlantic and Indian oceans began. WEGENER has supported his conception by a series of geodetical, geophysical, paleontological and tectonical arguments.

In view of the fact that the distance between the South-American and the African coasts is about 4000 to 5000 km and the shifting has taken place in the course of a period of 200 million years, the velocity of drifting must be 1—2 cm/year. The disproportion of this slight value compared to the whole distance between the coasts makes observations and measuring impossible.

WEGENER's geodetical arguments are, therefore, inconclusive. The most serious problem of the WEGENER theory is, however, the origin of forces producing rupture and drifting of the continental blocks. From our model these forces are obvious consequences of the expansion of the Earth. On this basis, the explanation for the distribution of continental masses is the following. After the development of Pangaea, in consequence of the expansion of the Earth, stresses were produced in the crust, also bent owing to the growth of radius.

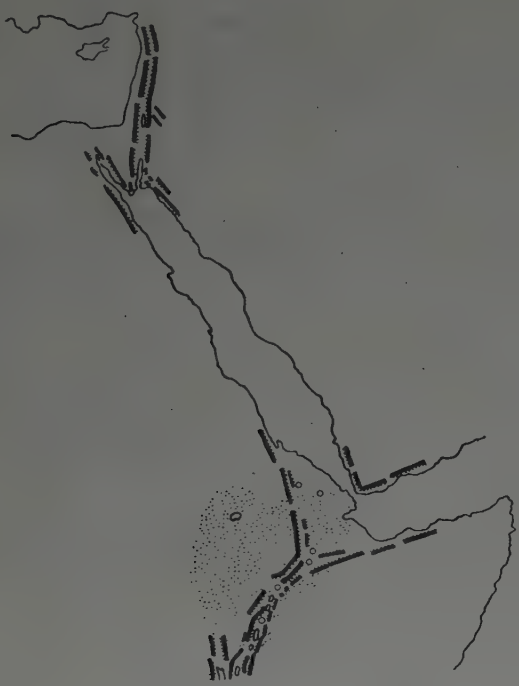

Fig. 19. The faulting system of the Red Sea

Stresses acting in the crust surpassed, at a certain limit, the strength of the rocks and the crust disrupted in the same way as in the case of the formation of the Pacific ocean.

If we take into account the value of the growing velocity of the Earth's radius and the morphology of the Atlantic Ridge, we must conclude that the formation of the Atlantic ocean has taken place at least in two rhythms. During the first basins extending westward from the Atlantic Ridge were formed. There remained, however, a land connection between Europe and North America through Greenland. The connection between Africa and South America was in existence along the coasts of Brazil and another connection in the South,

through New Foundland, the Sandwich Islands and Antarctica as well. This part of the Atlantic ocean is formed in early Pre-Cambrian times.

STILLE has shown [29] that, according to geological data, a northern and a southern basin of the Atlantic ocean existed already in Pre-Cambrian time, in accordance with the above statement.

The basins of the Atlantic ocean East to the Atlantic Ridge were formed as the second rhythm only after Carboniferous, and the former land connections of the western basins ceased to exist.

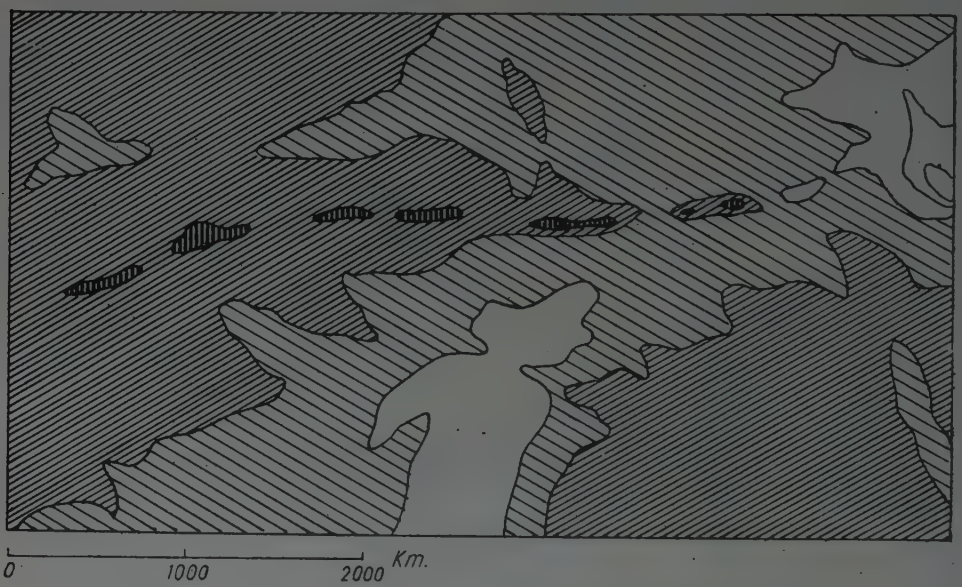

Fig. 20. Morphology of the Pacific ocean, West of South-America

The described mechanism is in agreement with STILLE's geological results [28], and ROTHÉ's conception [29] and seems to be a modification of the WEGENER-theory.

The mechanism of mountain building

Cause and mechanism of mountain building have always been major problems of the Earth Sciences.

The shrinking of the Earth and the magma currents, respectively, are regarded, however, in most theories as the causes of mountain building.

According to observations, for mountain building the followings are characteristic :

1. Mountain building represents a periodical phenomenon.

2. Mountain building has been brought about in the course of a relatively few phases, each of relatively short duration.

3. Mountain formation takes place along the boundary of large belts.

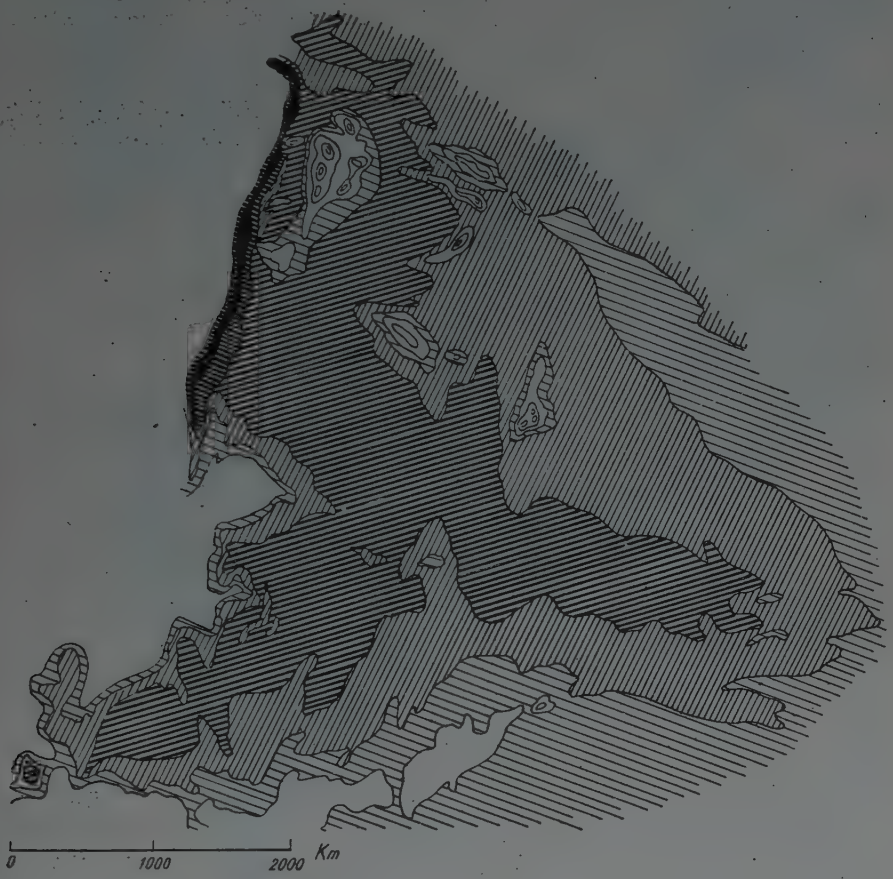

Fig. 21. Rupture-like basin east of New Zealand

4. In the course of each orogenic phase tectonic activity occurs more or less simultaneously in different regions of the Earth.

Three main phases of mountain building are known :

a) The phase of the formation of geosynclines. Large subsiding belts are collecting great masses of sediments.

b) The phase of folding. Subsidence is accelerated and the strata become folded.

c) The phase of uprise. The folded masses of the geosynclines are elevated above sea level.

By aid of geophysical observations two remarkable facts may be illustrated.

1. The seismically active areas occur in the form of large belts (Fig. 4).

2. The distribution of isostatic anomalies along the deep-sea troughs is similar in form to those occurring along the Carpathians, Appenines etc. On the other hand, the position of young volcanic belts in the area of the deep-sea troughs is similar, as to isostatic anomalies, to that of ancient (tertiary) volcanoes in the area of the Carpathians and Appenines.

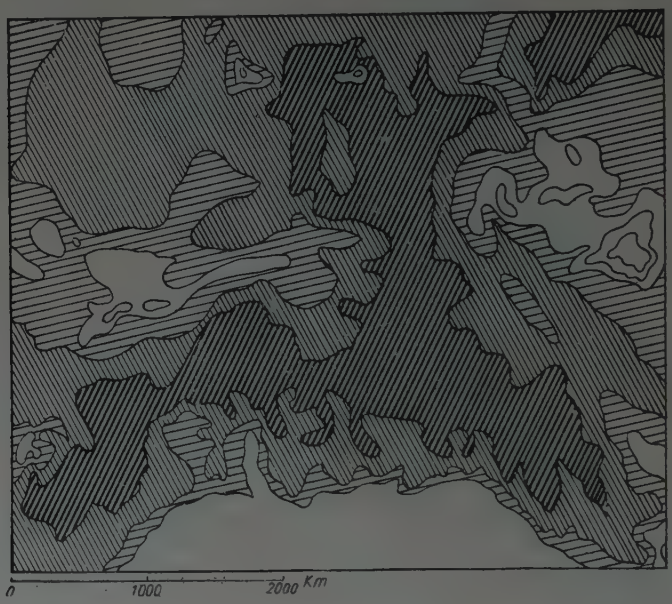

Fig. 22. Rupture-like basin between Africa and Antarctica

In order to explain the mechanism of mountain building it is to be considered that the Young-modulus of the sialic (continental) masses is smaller than the modulus of the simatic (oceanic) areas. Consequently, stresses originating in the expansion of the Earth are resulting in large warpings taking place in the crust. In consequence of these warpings some areas are subsiding others, however, uprising. Subsiding areas have become geosynclines covered by sea-water, while the great masses of material eroded from the elevated parts of the crust have accumulated in them. Naturally, warping takes place mostly in large belts according to the characteristics of solid bodies.

The subsidence of the areas called geosynclines will go on till the crust is able no more to carry the stresses acting from within. Having surpassed the critical stresses, elastic energies are released by rupture of the crust and, finally, warping caused by stresses is ceasing. The area of geosynclines filled up by sediments accumulated, folded and metamorphosed will be uplifted as an effect

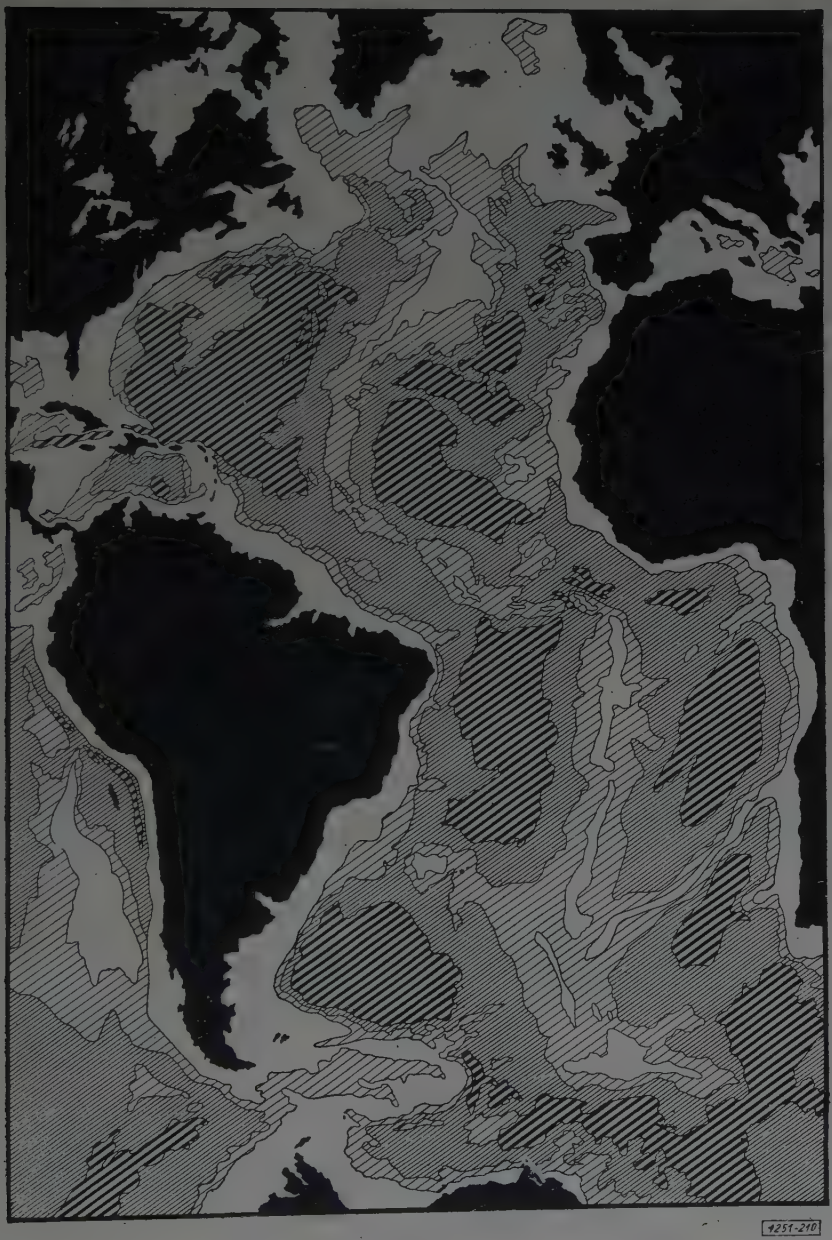

Fig. 23. The Atlantic Ridge

of the elastic forces and, partly, of isostasy. Big layers consisting of folded and metamorphosed rocks emerge high above sea level and form the huge bulks of the mountain chains.

The formation of nappes, in compliance with the «théorie des écoulements» [30], takes place as a consequence of warping of huge dimensions. Big slopes

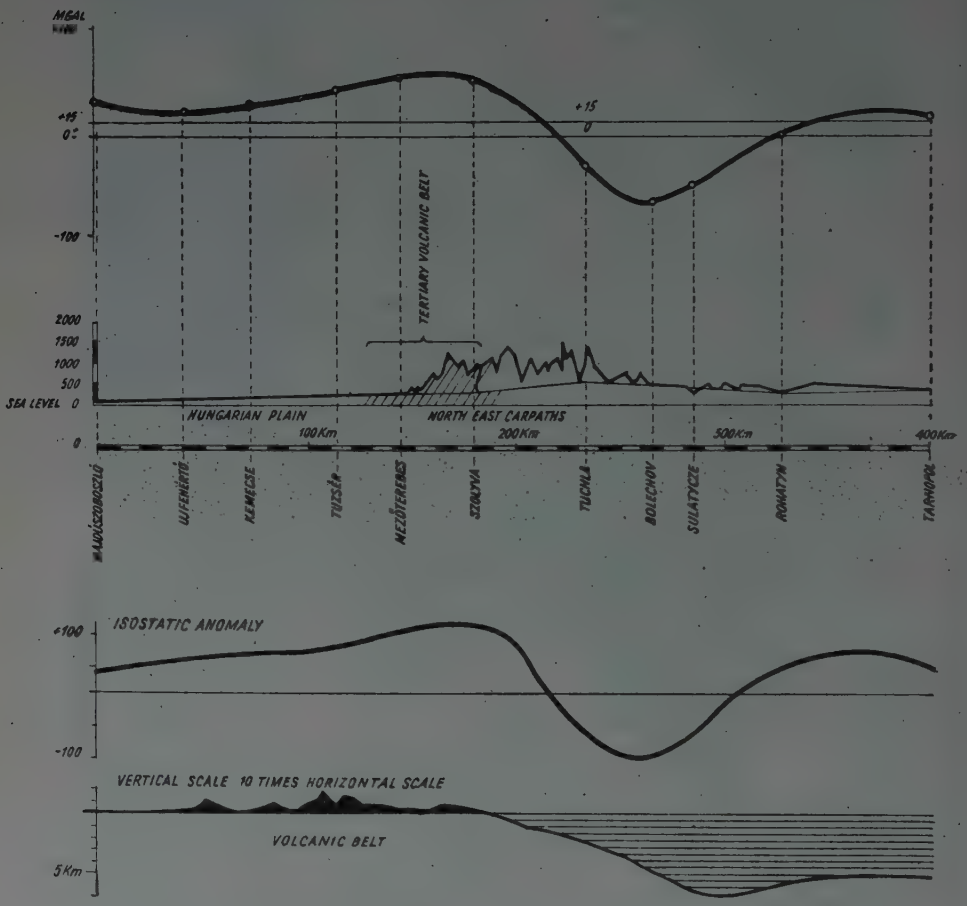

Fig. 24. Profile across the NE Carpathian Mountains and across Japan

(megaslopes) originate from the given mechanism bearing great amounts of material which, by their own weight, begin to slide over several dozens of kilometers.

When the crust ruptures, large amounts of hot magmatic masses are coming into contact with layers of the ocean bottom and, at the same time, the temperature of the sea-water begins to get warmer. Consequently, the external heat energy of the Sun can vaporize large amounts of sea-water. The

climate of the Earth becomes warmer and more humid over large areas and the process of decay gets more intense. Moreover, great climatic changes will take place showing their effect in development of coal-seams, bauxite etc.

The described mechanism not only gives a clue to both the sinking tendency of geosynclines and the uprise following the geosynclinal phase, but to the periodical nature of mountain building as well. The laws, brought forward by STILLE [31] are the natural consequences of this mechanism of mountain building. At the same time the duration of each of these periods may be computed to about 50 million years as a minimum, during which the elastic energy accumulated within the crust will suffice to create a new orogenic phase. Indeed, the amount of energy required by Kainozoic mountain building may be estimated as the work employed at the uplift of a mass of 40 000 km length, 500 km width and 10 km height and of a density of 2,7 g cm^{-3}, the height of the uplift amounting to 5 km. The work achieved by this process equals to $3{,}5 \cdot 10^{32}$ erg. On the other hand, the maximum of elastic energy accumulated in the Earth's crust amounts to $5 \cdot 10^{32}$ erg, i. e. of the same order of magnitude as required for the Kainozoic folding.

Finally, the establishments of H. STILLE [28], i. e. that the area of the deep-seas has greatly extended during geological time, are in very good agreement with the outlined mechanism of the formation of oceanic areas.

SUMMARY

A new conception of dynamic character is given for the internal constitution of the Earth. The main feature of the conception is that the material composition of the Earth becomes more ad more homogeneous within its interior. The Earth's core consists of matter in ultra high-pressure phase. This ultraphase state is, however, unstable and, therefore, a steady expansion of the Earth's volume is going on.

In the second part of the paper it is shown that the conception of the expansion of the Earth is able to account for the formation of the crust and the oceanic basins, the energies of tectonic forces and earthquakes, the origin of deep-focus earthquakes, the morphological features of the Earth's surface (fracture systems, deep-sea troughs, the African Rifts etc.), the continental drift, the periodicity of geological phenomena and mountain building.

LITERATURE

1. REICH, H.—SCHULZE, G.—FÖRTSCH, O.: Das geophysikalische Ergebnis der Sprengung von Haslach im südlichen Schwarzwald. Geol. Rundschau **36**, 85—96, 1948.

2. REICH, H.—FÖRTSCH, O.—SCHULZE, G.: Results of Seismic Observations in Germany on the Heligoland Explosion of April 18, 1947. Journal of Geophys. Research **56**, 147—156, 1951.

3. BIRCH—SCHAIRER—SPICER: Handbook of physical constants. Baltimore 1942.

4. REINHARDT: Steinbruchsprengungen zur Erforschung des tieferen Untergrundes. Berlin, 1954.

5. GUTENBERG, B.: Internal Constitution of the Earth. 1951.

6. EWING—WORZEL et al.: Seismic refraction measurements in the Atlantic Ocean basin. Bull. Seism. Soc. Am. **40**, 233—242, 1950.

7. RAITT, R. W.: Crustal structure of the equatorial Pacific Ocean from seismic refraction observations. Assemblée de Rome, Résumé 107, 1954.

8. KONING, L. P. C.: Summarizing consideration on the distribution of earthquakes in relation to their magnitude and focal depth. Geologisch Instituut Mededeling No. 207, Universiteit van Amsterdam.
9. BULLEN, K. E.: An introduction to the theory of seismology. Cambridge 1947.
10. BIRCH. F.: Elasticity and constitution of the Earth's interior. Journal of Geophys. Research, **57**, 227—289, 1952.
11. BIRCH, F.: Symposium on the Interior of the Earth. The Earth's Mantle. Elasticity and Constitution. Trans. AGU. **35**, 78—85, 1954.
12. KUHN, W.—RITTMANN, A.: Über den Zustand des Erdinnern und seine Entstehung aus einem homogenen Urzustand. Geol. Rundschau, **32**, 215—256, 1941.
13. BULLEN: loc. cit.
14. BÅTH, M.: Le rapport des densités à la limite du noyau de la terre. Assemblée de Rome, Résumé 48, 1954.
15. RAMSEY, W. H.: On the nature of the Earth's core. Monthly Notices, Roy. Astr. Soc. Geoph. Suppl., **5**, 1949.
16. ALLAN, D. W.: L'âge de la terre calculé d'après la méthode du plomb. Assemblée de Rome, Résumé 28, 1954.
17. UREY, H. C.: The temperature of the primitive Earth. Assemblée de Rome, Résumé 69, 1954.
18. KUENEN, P. H.: Marine Geology. New York—London 1950.
19. STRAHOW, N. M.: Основы исторической геологии. (Outlines of Historical Geology, in Russian). Moscow, 1948
20. GUTENBERG, B.—RICHTER, C. F.: Seismicity of the Earth and associated phenomena. Princeton 1949 and 1954.
21. BULLEN, K. E.: An introduction to the theory of seismology. Cambridge 1947.
22. EGYED, L.: The formation of deep-sea troughs and related geophysical phenomena. Acta Geol. II 33—50, 1953.
23. BENIOFF, H.: Orogenesis and deep crustal structure — Additional evidence from seismology. Bull. Geol. Soc. Am., **65**, 385—400, 1954.
24. BRIDGMAN, B. W.: The physics of high pressure. London, 1949.
25. EGYED, L.: The relation of deep-structures and morphology in Transdanubia (Hungary) on the basis of geophysical explorations. (In Hungarian.) A Természettudományi Kar Évkönyve 1952—53.
26. BOGOLEPOV, M.: Die Dehnung der Lithosphäre. Zeitschr. d. D. Geol. Ges., **82**, 206—228, 1930.
27. WEGENER, A.: Die Entstehung der Kontinente und Ozeane. Braunschweig, 1929.
28. STILLE, H.: Ur- und Neuozeane. Abh. d. d. Akad. d. Wiss. zu Berlin, 1948.
29. ROTHÉ, J. P.: La structure de l'Atlantique. Annali di Geofisica IV. 27—41. 1951.
30. GIGNOUX, M.: La notion de temps en géologie et la tectonique d'écoulement par gravité. International Geological Congress Report, 1948. Part XIII, 90—96. 1952.
31. STILLE, H.: Grundfragen der vergleichenden Tektonik. Berlin 1925.

НОВАЯ ТЕОРИЯ ВНУТРЕННЕГО СТРОЕНИЯ ЗЕМЛИ И ЕЕ ГЕОЛОГИЧЕСКИЕ И ГЕОФИЗИЧЕСКИЕ РЕЗУЛЬТАТЫ

Л. ЭДЬЕД

Резюме

Одной из важнейших задач геофизики является выявление строения внутренней части Земли и земной коры.

О земной коре и о зоне, лежащей непосредственно под ней, геофизика имеет довольно ясные представления.

Поверхность Земли разделяется на континентальные и океанические территории. Это разделение обосновывается не только на морфологических, но и на петрографических расхождениях. Верхние части континентальных блоков состоят из кислых гранитоподобных пород, а нижние части их — из основных габброподобных. Континентальные массы располагаются над ультраосновной магмой согласно закономерностям плавающих тел. Средняя мощность их — 30 км-ов. На океанических территориях, наоборот, имеется только тонкий слой габброподобных пород, непосредственно под которым лежат ультра-

основные массы. Согласно гидростатическому или изостатическому равновесию самый частый уровень континентов — 100 м над уровнем моря — находится 4800 м выше, чем наиболее частый уровень океанских площадей. Континентальные и океанические территории имеют резкие границы.

Теории о строении Земли расходятся только относительно части под поверхностью преломления Репетти.

Гипотезы о внутренней структуре Земли разделяются на три типы: геохимическо—метеоритовая теория, теория Кун — Риттмена и теория Ремзи.

Геохимическо-метеоритовая теория считает строение Земли сходной со строением метеоритов. По этой теории сейсмические поверхности раздела являются одновременно границами вещественного состава. Согласно этой теории внешняя зона Земли — до поверхности преломления Репетти — сходна со строением каменных метеоритов. Между этой зоной и ядром Земли находится зона, состоящая из окислов и сульфидов тяжелых металлов. Эта зона сходна со строением переходных метеоритов. Наконец ядро, состоящее из сплава железа и никкеля сходно со строением металлических метеоритов.

Это маловерное представление значит, что ядро Земли имеет поверхность определенной температуры, внутри которой вещество находится в расплавленном состоянии. Эта критическая термическая поверхность раздела является одновременно границей вещественного состава.

По теории Куна и Ритмена состав внутренней части Земли становится все более равномерным. Внутри одной данной границы находится только так называемая солярная масса, соответствующая составу Солнца.

Сейсмические поверхности преломления обозначают только изменения физических свойств, а не изменения вещественного состава. По мнению этих исследователей поверхность преломления Гутенберга и Вихерта появится вследствии того, что здесь время релаксации накопления упругой энергии падает под уровень периода сейсмических волн. Таким образом срезывающие напряжения не могут действовать, следовательно, скорость лонгитудинальных волн скачкообразно уменьшается, а трансверсальные волны полностью исчезают. Но удельный вес вещества до середины Земли все время изменяется. Против этой теории отмечается только то, что поверхность преломления Гутенберга и Вихерта не могла бы появляться как рефлексионная поверхность, если только время релаксации уменьшилось бы здесь.

С другой стороны, как видно будет в дальнейшем, непрерывное распределение удельного веса не соответствует этим предположениям.

Третя теория была разработана Ремзи и обосновывается на лабораторных исследованиях Бриджмена и связанных с ними квантуммеханических предположениях.

По мнению Ремзи вещественный состав Земли, двигаясь в направлении центра, становится равномерной. Сейсмические поверхности преломления соответствуют скачкообразному перестроению электронной оболочки вследствие увеличения давления. Внутри поверхности Гутенберга и Вихерта вследствие этого перестроения вещества получают металлический характер.

Новый модель Земли

Изложенные выше модели Земли обяснили только одни части физических наблюдений. Правильный модель Земли должен обяснить все явления единодушно. На основе правильного моделя Земли мы должны отвечать с одной стороны на вопрос внутреннего строения Земли, а этот ответ должен соответствовать данным сейсмических, гравитационных и прочих наблюдений. С другой стороны, мы должны дать ответ о происхождении сейсмических и вообще тектонических энергий, о происхождении земной коры и об изменениях, совершающихся в нее.

В дальнейшем дадим краткий очерк такого моделя.

Прежде всего мы должны разработать ясное представление о внутреннем строении Земли. Обозначают-ли сейсмические поверхности преломления различия во вещественном составе или нет?

Если отождествлять сейсмические поверхности преломления с изменением вещественного состава, выступает вопрос, как могли получиться такие яркие вещественные обособления? Из теорий происхождения Земли такие обособления нельзя отводить.

По исследованиям Ф. Берча, начиная с глубины 800 км-ов до поверхности Гутенберга и Вихерта, Землю можно считать гомогенной. Под такой гомоген-

ной зоной, мощностью 2000 км-ов, кажется маловероятным предполагать вещественное изменение у поверхности Гутенберга и Вихерта. Эта поверхность преломления внутри ее имеют иные причины физического характера.

Считается естественным предположением, что во внутренней части Земли вещественный состав становится гомогенным. Это гомогенное состояние относится не на молекулярное строение, но на массовое распределение атомных ядер.

Вероятно, что дифференциационных явлений не достигают глубину 800 км-ов.

Ниже приводится перечень важнейших наблюдений, относящихся на внутренние части Земли :

1. Скорость лонгитудинальных и трансверсальных волн до ядра Земли (2900 км) непрерывно изменяется.

2. В глубине 2900 км-ов скорость волн P уменьшается в среднем 40%-ами, а трансверсальные волны полностью исчезают.

3. В гранитной зоне внутреннего ядра (4980 – 5120 км) скорость волн P увеличивается 10%-ами.

4. По данным Буллена точность определения удельного веса до границы ядра представляет собой 1%, а в скорлупе ядра (2900 – 5000 км) 3%-ы.

5. Величина удельного веса на границе ядра Земли дисконтинуально увеличивается около 65%-ами.

6. Величина давления в глубине 300 км-ов достигает 100.000 бар, на границе ядра 1,37 мегабар, в центре 364 мегабар (1 бар $= 10^6$ дин см$^{-2}$ около 1 атмосфера ; 1 мегабар $= 10^6$ бар $= 10^{12}$ дин см$^{-2}$).

7. Колебания гравитационного ускорения во внешних оболочках не превышают 5%-ов.

Имея ввиду вышеизложенные данные, следующая картина рисуется по внутренней структуре Земли :

1. Вещественный состав Земли вследствие дифференциации изменяется в крайнем случае до глубины 800 км-ов, нижележащие части до центра Земли являются гомогенными.

2. Слой гомогенной скорости, выявленный Гутенбергом в ультраосновной зоне объясняется термическим градиентом не превосходящим 6,6 C°/км. Между глубинами 200 и 700 км с большей вероятностью имеется переход фаз, выступающий вследствие большого давления.

Объяснение этих явлений представляется следующим образом :

3. Во внешних частях Земли атомы воздержают давление с помощью их электронной оболочки. Большое давление заставляет атомы в решетковую структуру. Таким образом местоположение каждого атома строго определяется. Если какое-нибудь воздействие сил, например, сейсмическая волна их сдвигает из этого положения, тогда силы решетки заставляют их снова принять первичное положение. Вследствие этого наблюдается во внешних зонах большая негибкость, которая увеличивается пропорционально с увеличением давления.

4. Поверхность преломления Гутенберга и Вихерта является критической поверхностью, внутри которой вещество находится в «дегенерированном» состоянии.

Дегенерированное состояние характеризуется следующими признаками : а) удельный вес материалов есть больше чем в нормальном состоянии; б) если давление не превосходит определенную величину, тогда между частицами действуют только силы Куломба ; в) во внутренних частях Земли, вследствие большого давления вещество ирреверсибильным способом переходит из дегенерированного состояния в нормальное состояние.

На основе дегенерированного состояния легко понять исчезание срезывающих напряжений и дисконтинуальное возрастание удельного веса.

Параллельно с возрастанием давления в направление центра Земли дальше увеличивается и удельный вес. Частицы приближаются друг к другу в такой мере, что несмотря на их дегенерированного состояния, они принимают снова решеткообразное распределение.

Вследствие решеткообразного распределения снова появляются срезывающие силы.

Граница внутреннего ядра обозначает достижение этого критического давления, где дегенерированное вещество принимает решеткообразное распределение. Выступление срезывающих напряжений объяснит возрастание скорости лонгитудинальных сейсмических волн на границе внутреннего ядра. Отсюда следует и необходимость наличия трансверсальных волн.

Предположим о дегенерированном состоянии, что при господствующих давлениях центра Земли оно не является стабильным состоянием. При данных давлениях только

нормальное состояние вещества можно считать стабильным. Вследствие этого имеется постоянный процесс перехода из дегенерированного состояния в нормальное состояние. В функции времени запасы дегенерированного вещества Земли постоянно уменьшаются за счет нормального вещественного состояния. Удельный вес нормального вещества значительно меньше чем в дегенерированном состоянии. Отсюда следует, что при переходе в нормальное состояние объем вещества увеличивается. Таким образом вышеизложенный модель Земли имеет то интересное свойство, что объем Земли находится в постоянном возрастании. Предполагается наиболее вероятной мерой этого возрастания 0,05 см/год. Этот порядок величины значит 1 мм/год.

Это неожиданное представление может дать очень простое и ясное объяснение на важнейшие явления Земли.

Прежде всего становится ясным разделение земной коры на континентальные и океанские части, их петрографические различия, расхождения высот наиболее частых уровней континентов и океанов и резкие границы этих двух площадей.

В первичном примитивном состоянии Земли более — менее гомогенная магма дифференцировалась, во-первых, на поверхностных частях Земли.

Таким образом формировалась гранитообразная и под ней габброобразная магма. Обе находились над ультраосновной магмой. В течении охлаждения уплотнилась, во-первых, гранитообразная магма и вслед за тем габброобразная и образовалась земная кора мощностью в среднем 30 км-ов.

Параллельно с дальнейшим охлаждением уменьшилось количество дегенерированного вещества и объем Земли стал увеличиваться. Вследствие увеличения объема выступали напряжения, которые оторвали первичную земную кору. Ультраосновная магма поднималась в оторванных частях до уровня соответствующего его равновесия. Так как удельный вес ультраосновного вещества значительно превосходит удельный вес кислой и основной части коры, уровень поверхности ультраосновной коры остался значительно ниже, чем уровень континентальной поверхности. Из этой картины просто получается, что на поверхности Земли должны находится две наиболее частые уровни и что континентальные и океанические площади должны отличаться и во вещественном отношении. Станет ясным и то, что континентальные площади имеют единое строение и что между континентальными и океанскими площадями нет постепенного перехода. Из вышеизложенного механизма получается необходимым аркообразное строение краевых частей континентов, так как при оторвании шарообразной массы всегда образуются аркообразные линии оторвания.

По общеизвестной теории Вегенера и Телора нынешние континенты до конца карбона образовали одну единую массу. Они оторвались в это время, отдалились друг от друга и в течении 200 миллионов лет постепенно занимали их теперешное местоположения.

Самая большая проблема теории Вегенера суммируется в том, что вызвало те чрезвычайно большие силы, которые могли раздробить континенты и вслед за тем могли передвигать их в огромные расстояния?

Вышеизложенный новый модель Земли вследствие его расширения просто объясняет теорию Вегенера, хотя бы необходимо было изменить некоторые части первоначальных представлений Вегенера.

Если после образования Тихого-океана земная кора представила собой одну единую массу, то при дальнейшем расширении Земли она раздробилась. Вдоль линий оторвания поднималась ультраосновная магма. Этот процесс приводил к образовании Атлантического и Индийского океана. Подтверждает эти предположения тот факт, что диаграммы частот глубины Тихого, Атлантического и Индийского океанов имеют почти одинаковый характер.

Особое внимание заслуживает Атлантическая возвышенность. Полное совпадение этой возвышенности с африканскими и югоамериканскими береговыми линиями вызывает смысл, что это было первичная линия оторвания.

Прекращение дегенерации вызывает и определенное освобождение энергий, ведь при расширении поднимаются огромные массы Земли. Допуская мерой увеличения радиуса 0,1 см/год получается достижение $4 \cdot 10^{29}$ эрг/год. Величина освобожденной энергии землетрясений считается $2{,}5 \cdot 10^{27}$ эрг/год. Это не больше чем одна стотысячная доля вышеупомянутой энергии.

Но дело в том, что при увеличении объема верхние зоны Земли расширяются аналогично надутым мячом, а напряжения накопляются в них в форме упругой энергии. Землетрясения появляются за счет освобождения упругой энергии. Во верхней части Земли, до глубины 60 км-ов это накопление упругой энергии докажется подсчетом использованных при землетрясении энергий.

Увелнчение объема Земли дает ответ на причинах глубинных землетрясений, появляющихся в глубинах нескольких сотень километров.

Бридж мен в началах своих исследований при больших давлениях изучал тот вопрос, как совпадают теоретические выводы теории упругости с данными фактических опытов? Он применял большое внутреннее давление в цилиндрических трубах и увеличил давление до оторвания труб. Он наблюдал, что оторвание начинается напротив теоретических ожиданий всегда с внешней поверхности трубы.

Поверхность разлома всегда образует наклонные плоскости или поверхности. Это очень сходно к тому, что гнезда глубинных землетрясений расположены всегда на наклонных плоскостях. Поверхностная линия этого разлома совпадает с зонами глубокоморских грабенов.

Поверхность плоскости образует 60°-овый угол с поверхностью Земли. Это соответствует растягивательным силам, образующимся при увеличении объема Земли.

Астрономические наблюдения говорят об уменьшении скорости вращения Земли. Величина этого уменьшения определилась в $5 \cdot 10^{-6}$ сек/год.

Причиной этого явления первоначально считали прилив Земли, но современные исследования доказали, что атмосфера уравнивает эффект прилива.

Но уменьшение скорости вращения Земли полностью объясняется предположением увеличения объема Земли. Теоретические подсчеты показали, что увеличением радиуса 1 мм/год соответствует $12 \cdot 10^{-6}$ сек/год уменьшение скорости вращения.

Эта величина хорошо совпадает с вышеупомянутой величиной фактических наблюдений.

Увеличение объема Земли подтверждается и палеогеографическими наблюдениями.

Количество воды, находящееся на поверхности Земли не может увеличиваться в значительной мере. В крайнем случае ювенильные воды, происходящие из магмы могут прибавлять количество воды.

Если принимаем в основу вероятное расширение Земли, тогда в палеозое уровень моря должен был находиться 5–700 метров выше, чем в наших днях. Более высокий уровень моря приводил к тому, что в геологическом прошлом большие части континентов находились под водой.

Эти покрытые водой площади являлись мелководными морями. Параллельно с увеличением объема Земли площади этих мелководных морей все более уменьшились и территории суши постепенно возрастали.

На приложенном чертеже видно изменение величины суши в последних 500 миллионов лет. График составлен на основе планиметрового измерения площадей суши палеогеографических карт Н. М. Страхова.

Полученные таким образом 12 данных убедительно доказывают, что площадь суши во время постоянно увеличивается.

Этими данными возможно и определить годовую скорость увеличения радиуса Земли. В результате подсчета получается среднее число за последних 500 миллионов лет : 0,58 мм/год. Если увеличение радиуса определяется из уменьшения скорости вращения Земли, то получается 0,38 мм/год. Эта цифра относится только на последние 2000 лет, но все-таки хорошо совпадает с другой цифрой, полученной в результате совсем других исходных данных.

Имеется еще одна возможность для определения среднего числа годового увеличения радиуса Земли. Если имеем ввиду суммарную площадь сиаллических территорий, тогда получается 2400 км-овое увеличение радиуса Земли со времени образования земной коры. Земная кора по наиболее современным данным образовалась 4,4 миллиардов лет назад. Делением суммарной цифры с этой цифрой получаем 0,55 мм/год среднее годовое увеличение радиуса Земли. Видно, что этот результат хорошо совпадает с вышеизложенными двумя цифрами.

Новый модель Земли дает объяснение и на происхождение тектонических сил. Для обеспечения 1 мм-ового годового увеличения радиуса переход вещества ядра Земли должен обеспечить минимально $4{,}1 \cdot 10^{29}$ эрг. в год. Большая часть этого служит для увеличения гравитационной энергии, но одна небольшая часть ее накапливается в форме упругой энергии. Во верхней оболочке Земли, до глубины 60 км-ов может накапливаться $5{,}8 \cdot 10^{32}$ эрг. энергия до разрушения и оторвания коры.

Минимальное время, необходимое для такого накопления представляет собой 25–50 миллионов лет.

Наиболее важным эффектом тектонических сил является образование цепных гор. Размеры этой работы также возможно определить. Например альпийское горообразование равно той работе, если плиту 40.000 км длиной, 500 км шириной, 10 км мощности и 2,7 гр/см^3 удельного веса поднимим на высоту 5 км-ов.

Эта работа равна $3{,}5 \cdot 10^{32}$ эгр. Накопленная упругая энергия эту работу легко обеспечит.

Самым сложным является вопрос горообразования. Наши новые представления об увеличении радиуса Земли объясняют и этот вопрос.

Известно, что коэффициенты упругости сильно различаются. Увеличение объема Земли вызывает во верхней части ее коробления. Таким явлением считается образование глубоководных грабенов. Вследствие короблений некоторые площади понижаются в сравнении к их первоначального положения, другие площади поднимаются. Понижающиеся площади стали геосинклиналями, так как они покрывались морем и служили местом осадконакопления.

Понижение этих площадей продолжается пока кора перетерпевает возникшие в ней напряженности.

Сверх определенной напряженности кора разрушается и в связи с этим накопленные энергии высвобождаются. Вслед за тем выравнивается, то есть поднимается до достигания изостатического равновесия.

В течении подъема возникают изгибающие усилия, которые оказывают складкообразование отложенных в геосинклинале осадочных свит. Эти осадочные свиты после окончания подъема находятся в приподнятом положении и с тектонической точки зрения являются складчатыми горными цепами.

Этот вышеизложенный механизм объясняет не только образование геосинклинальных областей и их поднятие, но и периодичность горообразования и закономерности установленные Штиллем по одновременности горообразующих явлений.

SUR LES POSSIBILITÉS DE L'ANALYSE THERMIQUE DIFFÉRENTIELLE DES MINÉRAUX DE MANGANÈSE

Par

M. Földvári-Vogl et V. Koblencz

INSTITUT GÉOLOGIQUE DE HONGRIE, BUDAPEST

Le décèlement des minéraux de manganèse dans la présence de certains autres minéraux entraîne quelques difficultés ; c'est pourquoi, en connexion avec l'analyse thermique différentielle de beaucoup d'échantillons des gisements de manganèse à Urkut et Eplény, nous avons examiné en principe, d'une part, quels minéraux de manganèse sont décelables avec une certitude absolue par l'analyse thermique différentielle, et, d'autre part, quels sont les minéraux dont le décèlement devient incertain dans la présence troublante d'autres matières.

Quant à l'appareillage et la méthode employés, nous renvoyons à notre travail antérieur [1]. Les examens ont été exécutés à partir de la température ambiante jusqu'à 1000° C (quelques fois à 1050° C).

Minéraux des minerais de manganèse carbonatés

Nous connaissons le comportement thermique des minerais de manganèse carbonatés depuis le travail détaillé de Kulp, Wright et Holmes [2]. Nous savons que la courbe thermique typique de la *rhodochrosite* pure montre un crochet endothermique net à 615° C (à notre appareil, par suite de notre méthode modifiée, à 595°), et — si l'accès de l'air n'est pas exclu — ce crochet endothermique marquant la dissociation de carbonate est immédiatement suivi d'un crochet exothermique net (avec un maximum de 720 à 730° C, à nos mesurages) qui est le résultat de l'oxydation du manganèse bivalent. Si, dans la rhodochrosite, une partie du manganèse est substituée par le magnésium ou par le calcium, ces ions substituants augmentent les forces de liaison dans le réseau de carbonate et ils élèvent le crochet endothermique marquant la température de dissociation à une température proportionnelle à la quantité des ions de substitution de Mg et Ca. Si, dans la rhodochrosite, une partie des manganoions est substituée par des ferro-ions, ceux-ci diminuent les forces de liaison et déplacent le crochet un peu vers les températures plus basses. En résumant les observations des auteurs précités, en cas de substitutions d'ions, la dissociation du carbonate de manganèse contenant plusieures sortes de kations est marquée

par un seul crochet sur la courbe thermique, la température duquel dépend de la qualité et de la quantité des ions substituants. Au contraire, dans la présence commune de plusieurs minéraux carbonatés différents, la dissociation de chaque minéral est représentée par un crochet endothermique distinct ; ainsi le crochet de la sidérite se présente, à nos déterminations, entre 490 et 570° C, selon les mesures des cristaux, celui de la magnésite de 650 à 670° C, celui de la calcite de 900 à 920° C.

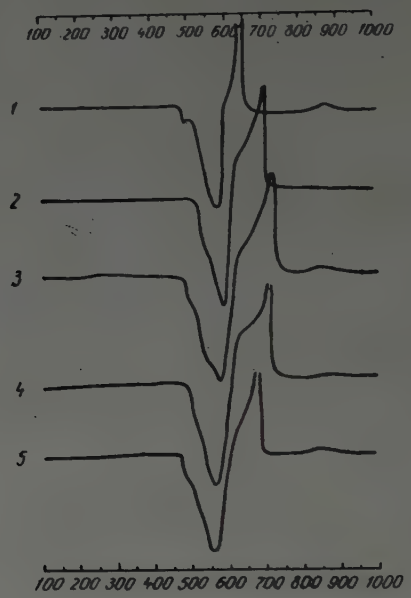

Fig. 1. 1. Sidérite (Roznava [Rozsnyó], Tchécoslovaquie), 2. Rhodochrosite (Alma, Lake Co., Colorado), 3. Mélange dans la proportion de 1 à 1 de rhodochrosite et sidérite, 4. Mélange dans la proportion de 3 à 1 de rhodochrosite et sidérite 5. Mélange dans la proportion de 1 à 3 de rhodochrosite et sidérite

Nos observations s'accordaient aussi avec les constatations de KULP et ses collaborateurs et l'essai des minerais de manganèse carbonatés par l'analyse thermique différentielle — qui est considéré d'ailleurs comme un problème résolu en général après avoir élucidé les détails de la question — n'est troublé particulièrement que par un seul fait, notamment qu'il y a une différence de 30 à 50° C environ entre le crochet de la sidérite et celui de la rhodochrosite, d'où il résulte souvent qu'en cas d'une présence commune des deux minéraux, les deux crochets ne se voient pas séparément, mais c'est seulement le crochet endothermique qui s'élargit. En outre, la figure du crochet de la sidérite ressemble bien à celui de la rhodochrosite, et dans le cas de la sidérite le crochet endothermique est également suivi d'un crochet exothermique, résultant de l'oxydation.

Nous avons donc examiné tout d'abord le problème de la possibilité de la distinction entre le rhodochrosite et la sidérite, sous le rapport de l'analyse thermique différentielle des minerais de manganèse carbonatés.

Nous sommes partis de deux échantillons fondamentaux relativement purs, notamment d'un échantillon de sidérite de Rožňava (Rozsnyó) dont la courbe thermique est représenté à la courbe N° 1 de la fig. 1, et d'un échantillon de rhodochrosite provenant de Colorado, d'une collection de Musée, dont la courbe thermique se voit à la courbe N° 2 de la fig. 1. D'après l'analyse chimique, la teneur en ferrocarbonate de notre échantillon de sidérite est presque 90%, la teneur en carbonate de manganèse de notre échantillon de rhodochrosite est de 98%. La présence de quelques pour-cent des matières accessoires

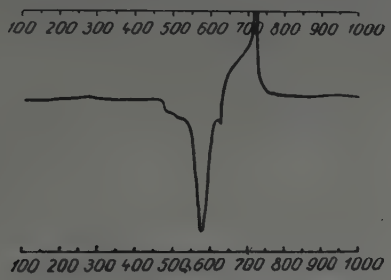

Fig. 2. Décèlement de la rhodochrosite dans la présence de sidérite, par la méthode à compensation

ne se présente pas sur la courbe thermique et ainsi elles n'ont pas troublé nos essais ultérieurs. En partant de ces échantillons-là, nous avons préparé des mélanges à divers pourcentages (courbes N^{os} 3, 4 et 5 de la fig. 1). Aux courbes thermiques différentielles de ces mélanges, on voit bien qu'elles montrent un seul crochet élargi entre 500 et 600° C, au lieu de deux crochets. Ce n'est qu'en quelques cas que la présence commune des deux minéraux est marquée, outre l'élargissement du crochet, par une courbure échelonnée qui se dessine sur la branche descendante. Mais même cet échelonnement peut être mépris ou ramené à des causes tout à fait différentes. P. e. une courbure échelonnée se présente très souvent sur la branche descendante du crochet endothermique au cours de l'analyse thermique différentielle des échantillons purs de sidérite. Nous avons observé pareil phénomène, dans beaucoup de cas, aux échantillons de sidérite de Rudabánya. V. I. Kaourkovsky [3] explique ce phénomène par le fait que ces échantillons de sidérite ont une texture cristalline à mesures hétérogènes. On peut observer même optiquement une texture à grains fins et une texture à grains grossiers dans leur microstructure ; c'est la différence des températures de dissociation de ces deux variétés qui produit l'échelonnement.

Il résulte de tout ce que nous venons de dire que la présence commune de la rhodochrosite et de la sidérite n'est rendue que probable à l'aide de l'analyse

thermique différientielle, par l'élargissement du crochet endothermique et, éventuellement, par la courbure échelonnée du crochet, mais on n'en saurait décider avec une certitude absolue. Par conséquent, l'exactitude de la diagnose doit être augmentée par l'analyse chimique.

Nous avons essayé de rendre plus sûr le décèlement DTA de la présence simultanée de la rhodochrosite et de la sidérite par l'emploi de notre méthode à compensation qui s'est déjà vérifiée dans d'autres cas [1]. Dans l'une des forures nous avons placé notre mélange contenant 50% de rhodochrosite et 50% de sidérite dont la courbe thermique est représentée sur la courbe N° 3 de la fig. 1, dans l'autre nous avons placé autant de l'échantillon de sidérite de Rožňava que la teneur en sidérite du mélange, mais ici elle fut mêlée à une matière inerte. La courbe thermique qui en résulte se voit à la fig. 2. Nous avons réussi à compenser le crochet de sidérite par les effets thermiques opposés des deux forures et c'est seulement le crochet de la rhodochrosite qui apparaît. Mais après le crochet de la rhodochrosite, il se présente un petit crochet troublant qui s'explique par le fait qu'une certaine asymétrie se produit dans les deux forures à cause d'une différence de teneur totale en carbonate, d'où il résulte que la pression partielle du dioxyde de carbon devient différente dans les deux forures au cours de la dissociation. Cet effet troublant s'est particulièrement manifesté quand nous avons essayé de faire disparaître le crochet de la rhodochrosite à l'aide de la compensation. En ce cas-ci, on ne peut pas attendre que la compensation soit efficace, sauf pour le cas où nous aurons la possibilité de travailler sous un vacuum, ce qui sera réalisé bientôt, au cours de nos essais ultérieurs.

La présence d'une quantité considérable de pyrolusite à côté de la rhodochrosite peut aussi nous troubler dans la reconnaissance du crochet caractéristique de la rhodochrosite. Notamment, le premier crochet endothermique de la pyrolusite tombe au domaine de température où se trouve le crochet exothermique d'oxydation de la rhodochrosite et les deux effets opposés peuvent empêcher le développement de tous les deux crochets ; tout comme cela se voit bien aux courbes thermiques des mélanges minéraux artificiels de KULP et PERFETTI [5].

Nous mentionnons encore la constatation de J. KONTA [4] selon laquelle le crochet de la rhodochrosite abaisse considérablement dans la présence de la pyrite et de la melnikovite.

Minéraux oxydés du manganèse

Sur la courbe DTA de la *pyrolusite* et de la *polianite* se présentent deux crochets endothermiques, l'un avec un maximum entre 640 et 670° C, l'autre entre 960 et 1050° C. Au premier crochet, le MnO_2 se transforme en β Mn_2O_3,

au deuxième crochet le Mn_2O_3 se transforme en Mn_3O_4 (hausmannite). Tous les deux processus de transformation sont irréversibles. Bien que la pyrolusite et la polianite ne diffèrent que par le degré de développement des grains cristallins, nous avons examiné la question de savoir s'il y ait une différence observable sur leurs courbes DTA. La courbe N° 1 de la fig. 3 représente un échantillon de pyrolusite du Musée National Hongrois, provenant de la Nouvelle Écosse, la courbe N° 2 montrant un échantillon de polianite de Platten (Tchécoslovaquie). En comparant les deux courbes, il apparaît que tous les deux crochets thermiques de la polianite à cristaux plus développés précèdent ceux de la pyrolusite. Nous avons fait pareilles constatations sur les autres échantillons essayés, sauf

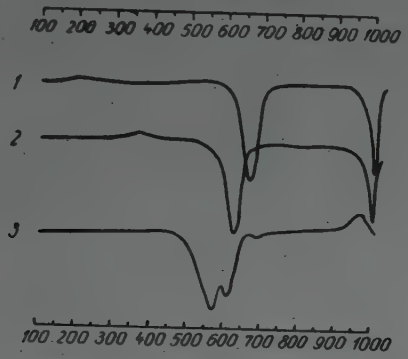

Fig. 3. 1. Pyrolusite (Nouvelle-Écosse), 2. Polianite (Platten, Bohême), 3. Mélange dans la proportion de 1 à 1 de kaolinite et polianite

pour une exception : notamment un échantillon qualifié de pyrolusite s'est transformé à une température extrêmement basse ce qui a rendu incertaines nos observations sur quelque 8 échantillons.

Récemment, on connaît une modification cristalline rhombique de la pyrolusite, appelée *ramsdellite*. D'après la constatation de KULP et PERFETTI [5] la courbe thermique de la ramsdellite montre un crochet exothermique qui marque la transformation de la ramsdellite en pyrolusite à 500° C environ, puis la figure de la courbe est tout à fait identique à celle de la pyrolusite.

Parmi les facteurs qui troublent la diagnose de la pyrolusite, nous avons déjà mentionné le fait que le crochet d'oxydation de la rhodochrosite éventuellement présente peut contre-balancer le premier crochet endothermique de la pyrolusite. Mais dans le cas d'un essai en gaz inerte, si la possibilité de l'oxydation est exclue, cet effet troublant est éliminable.

En outre, la diagnose de la pyrolusite ou de la polianite peut être troublée par la présence de la kaolinite ou d'un minéral argileux appartenant au groupe de kaoline. La courbe N° 3 de la fig. 3 représente l'analyse thermique différentielle d'un de nos mélanges artificiels que nous avons produit par le mélange dans la proportion de 1 à 1 de polianite et kaolinite de Zettlitz. Bien que la

polianite se soit transformée à une température relativement basse, son crochet se distingue nettement du crochet endothermique de la kaolinite. Mais le crochet exothermique, inférieur à 1000° C, de la kaolinite et le second crochet endothermique qui apparaît à la même température à peu près et qui provient de la polianite, se troublent l'un l'autre à tel point que le crochet de la polianite disparaît presque entièrement et le crochet exothermique de la kaolinite s'abaisse considérablement.

D'après KULP et PERFETTI [5], la *hausmannite* ne montre aucun processus causé par la variation thermique, dans l'intervalle de température

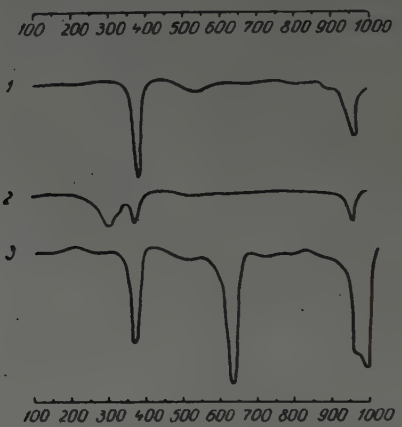

Fig. 4. 1. Manganite (Ilfeld), 2. Mélange dans la proportion de 1 à 1 de manganite (Ilfeld) et lépidocrocite (Rudabánya, Hongrie), 3. Manganite (Ilfeld), échantillon désagrégé

qu'ils ont examiné, c'est-à-dire de 50 à 1000° C. Dans son livre sur les combinaisons oxygénifères du manganèse [6], RODE décrit trois modifications cristallines de la hausmannite notamment : la hausmannite naturelle ou α qui, pendant l'échauffement, se transforme en hausmannite β entre 890 et 960° C par un processus endothermique irréversible ; en continuant l'échauffement, celle-ci se transforme en modification γ entre 1180 et 1220° C, par un processus également endothermique, mais réversible.

Vu que l'échantillon qualifié de hausmannite qui était à notre disposition, contient beaucoup d'impuretés d'autres minéraux d'après notre analyse thermique, nous projetons d'étudier un échantillon artificiel de hausmannite.

Pour étudier la dissociation thermique de la manganite, nous avons choisi des échantillons aussi intacts que possible des collections minéralogiques de l'Université de Budapest et du Musée National. Sur la base des courbes DTA, c'est un échantillon d'Ilfeld qui s'est prouvé le plus intact parmi les échantillons essayés ; sa courbe thermique est représentée sur la courbe N° 1 de la fig. 4. Sur la courbe thermique de la manganite, il se présente un crochet endother-

mique avec un maximum de 350 à 400° C où la manganite se transforme en Mn_2O_3. Le second crochet endothermique avec son maximum de 950 à 980° C marque la transformation du Mn_2O_3 en hausmannite (Mn_3O_4). Les autres échantillons essayés de manganite ont été désagrégés en partie et ils contenaient de quantités considérables de pyrolusite, selon les courbes thermiques. Puisque vers 980° C la pyrolusite montre également un crochet endothermique et vu que la manganite se trouve en général avec la pyrolusite dans les gisements naturels, il faut absolument reconnaître le premier crochet pour la diagnose de la manganite. Nous avons donc examiné le problème des minéraux qui peuvent troubler la reconnaissance du premier crochet de la manganite. Naturellement ici, comme partout, nous ne tenons compte que des minéraux troublants qui se présentent en association naturelle avec le minéral de manganèse en question. Quant à la diagnose de la manganite, il faut surtout prendre en considération l'effet troublant des minéraux de l'hydroxyde de fer.

Le crochet endothermique dû à la déhydratation de la goethite tombe à peu près au même domaine de température que celui de la manganite, par conséquent la présence simultanée de ces deux minéraux doit avoir pour résultat que les deux crochets voisins se présentent en un seul crochet élargi. On peut vraiment observer ce phénomène aux essais de KULP et PERFETTI [5] sur des mélanges minéraux artificiels. La dissociation thermique de la lépidocrocite précède de 50 à 80° C environ celle de la goethite, on a donc espéré de pouvoir déceler la manganite dans la présence de lépidocrocite. La courbe N° 2 de la fig. 4 représente un mélange de lépidocrocite et manganite, préparé en mêlant l'échantillon de manganite d'Ilfeld et de lépidocrocite de Rudabánya, dans la proportion de 1 à 1. Les deux crochets sont tout à fait distincts, bien que dans ce cas-là nous ayons eu la chance d'avoir un échantillon de lépidocrocite dissociable à une température extrêmement basse, évidemment à grains fins.

De tout cela, on peut conclure qu'il est possible de déceler la manganite à côté de la lépidocrocite, mais on ne saurait la distinguer de la goethite par l'analyse thermique différentielle uniquement.

Nous avons déjà mentionné que par le second crochet de la manganite on ne saurait caractériser ce minéral, car la pyrolusite a un crochet semblable dans le même domaine de température. En connexion avec ces deux crochets il a apparu un phénomène qui vaut la peine de s'en occuper à fond. Au cours de l'essai des échantillons de manganite de Musée, nous avons exécuté l'analyse thermique différentielle d'un autre échantillon de manganite d'Ilfeld qui était beaucoup plus désagrégé que l'échantillon pris comme type que nous avons mentionné à propos de nos essais précédents. Ce second échantillon contenait beaucoup de pyrolusite. Comme on le voit bien sur la courbe N° 3 de la fig. 4, le crochet entre 950 et 1020° C est double, comme si le crochet endothermique de la manganite et celui de la pyrolusite se présentaient séparément. Ce phénomène peut être expliqué par les constatations de RODE que l'on lit dans son

livre cité [6]. RODE a démontré que le trioxyde de manganèse — qu'il appela *kurnakite* — avait des modifications α et β, et que la modification α se transformait en hausmannite à une température considérablement plus basse que la modification β. Il a également démontré que dans le cas de la dissociation de la manganite (MnO.OH) la formation de la modification α était beaucoup plus probable que dans le cas de la dissociation thermique de la pyrolusite où se formait du Mn_2O_3 β. C'est la présence des deux modifications du trioxyde de manganèse qui peut expliquer le doublement du crochet à 1000° C environ.

La *braunite* est considérée comme trioxyde de manganèse par les uns [6] et silicate oxydée ($3\ Mn_2O_3\ MnSiO_3$) par les autres [8]. Selon RODE elle diffère de la kurnakite parce que celle-ci contient des ions de manganèse bivalents et

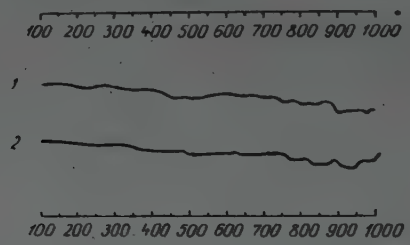

Fig. 5. 1. Rhodonite (échantillon de Musée, d'un gisement américain), 2. Rhodonite (Csucsom, Tchécoslovaquie)

trivalents aussi. D'après KULP et PERFETTI et même selon RODE, jusqu'à 1000° C la braunite n'a pas de processus thermique caractéristique, mais RODE est d'avis qu'entre 1030 et 1100° C un crochet endothermique marque la transformation de la braunite α en braunite β.

Nos essais sur les échantillons de braunite des collections de Musée s'accordent bien avec ce que nous venons de dire.

Pour être complet, nous présentons les courbes thermiques de deux échantillons de *rhodonite* (courbes N° 1 et 2 de la fig. 5), qui — répondant à l'attente — ne montrent pas d'effet thermique caractéristique.

Oxydes et hydroxydes de manganèse composés

Contrairement à la conception antérieure, la *psilomélane* doit être considérée comme un mélange, RAMDOHR (1954) considère aussi le terme psilomélane comme un nom collectif [7]. Vraiment, les minéraux de manganèse, qualifiés de psilomélane dans les collections de Musée, produisent des courbes DTA très différentes selon que la partie prépondérante du mélange est la braunite ou la pyrolusite ou autre minéral de manganèse. D'après RODE, la psilomélane consiste en MnO_2 et en polypermanganites qui contiennent des ions métaux

étranger. Il en résulte évidemment que l'analyse thermique différentielle des psilomélanes ne peut aboutir à un résultat sans équivoque.

Le cas des minéraux à hydroxyde et oxyde, qu'on résume du nom collectif *wad*, est semblable. On ne peut pas attendre de courbes DTA sans équivoque, là non plus.

*

Nous ne considérons pas encore nos essais comme finis. Avec le concours de nouveaux collaborateurs et par l'analyse DTA, minéralogique et au moyen des rayons X des oxydes de manganèse artificiels préparés dans le laboratoire, nous avons le projet de chercher la réponse aux questions demeurées obscures.

RÉSUMÉ

En connexion avec l'analyse thermique différentielle de quantité d'échantillons des gisements de manganèse d'Urkut et Eplény, nous avons étudié les possibilités et les limites de principe de l'emploi de la méthode DTA à l'essai des associations des minéraux des gisements sédimentaires de manganèse. Nous avons examiné quels étaient les minéraux dont la présence commune pourrait troubler les diagnoses par DTA. Le décèlement simultané de la rhodochrosite et de la sidérite sera possible par la compensation du crochet de la sidérite. La diagnose de la rhodochrosite est aussi troublée, mais non considérablement, par la présence de la pyrolusite, de la pyrite et de la melnikovite. Selon nos essais, la pyrolusite est décelable dans la présence de la kaolinite. La diagnose de la manganite est troublé par la présence de la goethite, mais la manganite est bien décelable dans la présence de la lépidocrocite. Nous avons encore étudié le comportement thermique de la braunite, la rhodonite, de la psilomélane et du wad. Nous avons l'intention de continuer nos essais sur des oxydes de manganèse artificiels, préparés dans le laboratoire.

BIBLIOGRAPHIE

1. Földvári-Vogl, M. et Kliburszky, B. : Acta Geologica, Tom, II, fasc. 3—4, 215—230, 1954.
2. Kulp, J. L., Wright, H. D. and Holmes, R. J. : Am. Mineral. **34**, Nos. 3—4, 195—219, 1949
3. Kaourkovsky, V. I. : Journal Prikladnoï Khimii, 1954, N° 2, 136—141
4. Konta, J. : Sbornik III. UUG. XVIII, 601—632, 1951
5. Kulp, J. L. and Perfetti, J. N. : Miner, Magazine, XXIX, 239—251, 1950
6. Rode : Les combinaisons oxygénifères du manganèse. Moscou, 1952
7. Ramdohr, P. : Die Erzmineralien und ihre Verwachsungen, Berlin, 1950
8. Machatschki, F. : Spezielle Mineralogie auf geochemischer Grundlage, Wien, 1953

ВОЗМОЖНОСТИ ПРИМЕНЕНИЯ ДИФФЕРЕНЦИАЛЬНО-ТЕРМИЧЕСКОГО АНАЛИЗА ПРИ ИЗУЧЕНИИ МАРГАНЦОВЫХ МИНЕРАЛОВ

М. ФЁЛЬДВАРИ-ФОГЛЬ—В. КОБЛЕНЦ

Резюме

В связи с дифференциально-термическим анализом многочисленных образцов, взятых из марганцовых залежей сс. Уркут и Эплень, были изучены возможности применения дифференциально-термического анализа для исследования минеральных ассоциаций марганцовых залежей осадочного происхождения, а также принципиальные ограничения применения этого метода. Был изучен вопрос о том, совместное наличие каких минералов может препятствовать определениям, проведенным при помощи дифференциально-термического анализа. Выявление родохрозита и сидерита при их совместном наличии становится возможным посредством компенсации сидеритового пика. Определению родохрозита в меньшей мере мешает также присутствие пиролюзита, пирита и мельниковита. Согласно проведенным исследованиям при наличии каолинита пиролюзит может быть выявлен. Определению манганита мешает присутствие гетита, однако при наличии лепидокрокита манганит оказывается хорошо определимым. Термическое поведение браунита, родонита, псиломелана и вада также было изучено. Исследования будут продолжены на окисях марганца, изготовленных искусственно в лаборатории.

BAYERITE IN HUNGARIAN BAUXITE

By

T. G. Gedeon

RESEARCH INSTITUTE OF METALS, BUDAPEST

In 1928 R. Fricke [1] described a variety of the alumina trihydrate [$Al(OH)_3$] that had precipitated when sodium aluminate liquor was treated with carbonic acid and which he called bayerite. Since then bayerite has been considered as an artificial product unknown in the world of minerals.

Investigating the processes of thermal decomposition in Hungarian bauxites, I have established the curves of the thermal decomposition of alumina hydrates. The initial points of the thermal decomposition of hydrargillite and bayerite showed considerable divergence. In the case of the hydrargillite, the decomposition by heat proceeds in two characteristic steps. At a temperature of about 300° C two moles of water out of the three bound to alumina separate and the substance is converted into boehmite. The one molecule of water left disappears at about 520—530° C. In the case of bayerite, the water bound to alumina begins to depart at a much lower temperature, i. e., at about 190° C and it comes to a close at 300° C. In this range of temperature, all three molecules of water bound to alumina pass off and as a consequence of it, the decomposition peak of the boehmite otherwise appearing in the temperature range of 530° C will also fail to show up (Fig. 2). Bayerite produced in different ways offers two different decomposition curves. Bayerite obtained from sodium aluminate liquor by a hot process (at 50 to 60° C) with CO_2 undergoes thermal decomposition in an even process at steady periods whereas with that obtained by a cold process of thermal decomposition (at 20° C), there are two sharp peaks present close to each other. This two-fold process is likewise characterized by the fact that thermal decomposition comes to an end by 300° C.

Brown, Clark, Elliott [2] had in a paper discussed the thermal decomposition of the hydrargillite. On the curve obtained by the measurement of the difference in heat, there is a small peak occurring at 190° C followed by one at 305° C indicating the decomposition of hydrargillite and then, above 500° C a peak characteristic of the decomposition of boehmite. Similar records have been published by Erdey and Paulik (see Fig. 3—1) in their paper in Hungarian and English [4] and further by Sasvári and Hegedüs [5]. All the hydrargillites examined contained some bayerite, a fact proved by the peak

appearing between 200 and 230° C. Whatever the process pursued may be, the preparation of the curves of thermal decomposition proved more sensitive than that obtained with X-rays according to Debye-Scherrer. In the knowledge of a sufficient amount of data recorded, no difficulty will be met in determining small quantities of the concomitant minerals, provided that they exhibit well defined points of decomposition by heat. If an X-ray examination is made, the quantity

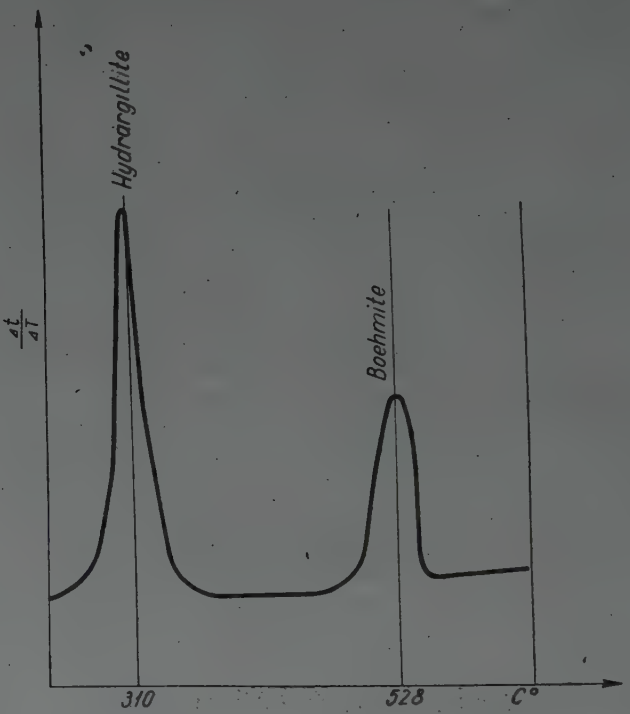

Fig. 1. Heating curve of hydrargillite registered by a Habicht-apparatus

of minerals which affords intensive lines appearing in a measurable degree in the spectrum, amounts in general to 5—6 per cent.

As the thermal decomposition of bayerite begins at 230° C, I have determined the loss of water occurring at both 230° C and 300° C in bayerites produced by the two different methods.

1. In aluminium hydrate obtained from a sodium aluminate solution by cold process and slow CO_2, the loss at 230° C amounts to 10,22 p. c.

2. The loss of water in bayerite at 230° C developed in water, on the surface of aluminium of a high degree of purity and amalgamated according to the MARICSICS—TERZSÁK process [6] amounts to 10,20 p. c.

I have further examined the extent to which the loss of water had increased during the period of drying. The drying examination mentioned before and

lasting an hour proved that the quantity of water removed was nearly the same as 1 mole of H_2O. (1 mole of water is equal to a loss in weight of 11,5 per cent.)

Result of the drying experiment

Method of the precipitation of bayerite	Drying at 230° C			At 300° C
	1 hour	2 hours	3 hours	1 hour
20° C, with CO_2	10,15	11,57	12,88	28,91
60° C, with CO_2	9,66	11,04	12,85	31,44
Industrial product	7,96	8,04	10,55	28,13

It has been proved by the experiment that the drying period lasting about two hours, is sufficient for the removal of 1 molecule of water in the bayerite.

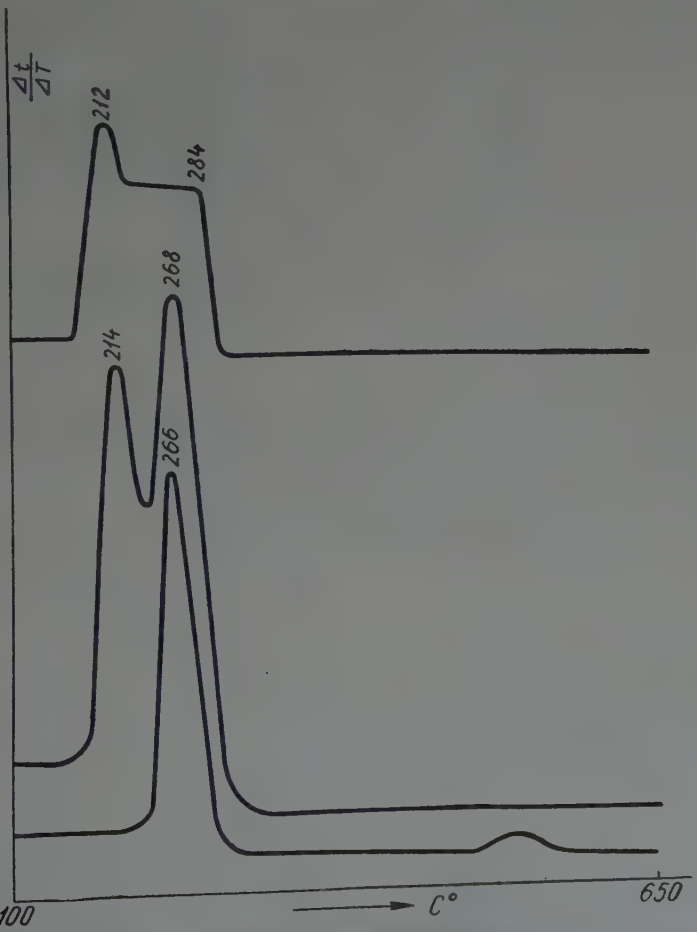

Fig. 2. The upper curve represents a precipitation by CO_2 at 60° C of bayerite
The middle curve represents a cold precipitation by CO_2 at 20° C of bayerite
The lower curve represents the preceeding sample dried at 230° C of bayerite

In the drying period the decomposition slowly goes on and increases up to 300° C when 85 to 90 per cent of the water bound (2,7 moles) leaves. This is at variance with the decomposition process of hydrargillite, considering the fact that calcination at 300° C can remove only 2 moles of water from hydrargillite and the rest is converted into boehmite. This process does not take place with bayerite. In the course of the drying and calcination, respectively, also hydrargillite develops and, consequently, the removal of the three moles of water is not complete. (Three moles of water mean 34,6 per cent of loss in weight.) The curve of thermal decomposition of the substance dried for two hours at 230° C presents at a temperature as low as 540° C a small bend characteristic of boehmite. (See the lowest curve in Fig. 2 yielded by bayerite which had been precipitated at 20° C and then dried for 2 hr. at 230° C ; thus the first peak of the middle curve is already missing there.)

In the course of a close physical examination made on Hungarian bauxites, attention was drawn to the fact that a peak consuming little heat was sometimes observable in the range of temperature around 200° C. According to examinations made and the data available from literature, the first peak of decomposition by heat falls within this range. Further examination has shown that bayerite is present in nearly all kinds of hydrargillite bauxites. Up to now we have found a boehmite bauxite also at Nyirád, which, as proved by its curve of thermal decomposition, exhibits a content of bayerite. The following is a list of bauxites examined :

1. Bauxite violet-coloured found at Iszkaszentgyörgy in the mining area at Kincses.
2. Whitish, pisolithic bauxite from Iszkaszentgyörgy.
3. Variagated, spotted bauxite from Iszkaszentgyörgy.
4. The same bauxite, iron content reduced by tartaric acid solution.
5. Brown bauxite from Iszkaszentgyörgy.
6. Reddish-brown bauxite from Iszkaszentgyörgy.
7. Argillaceous bed-bauxite from Iszkaszentgyörgy. (Above the dolomite-layer.)
8. Yellowish-brown bauxite from Gánt, Bagolyhegy.
9. Dark brown bauxite of Gánt, Harasztos mines.
10. Deep-red-brown bauxite from Nyirád, Izamajor, lens 2.
11. Reddish-brown bauxite from Szöcz, Határvölgy.
12. Brownish-red bauxite from Szöcz, Határvölgy.

Figure 3 shows the curves of thermal decomposition in respect of each of the bauxites, in the sequence of the previous numeration. As a rule, the peak of the bayerite appears but as a wave of small height. It will stand out, however, characteristically, if the bauxite is almost wholly freed from its iron oxide by boiling it for two hours with a quantity of tartaric acid, in excess as referred to the amount of iron-oxide present (Fig. 3, curve 4 on thermal decomposition).

The hydrargillite peaks appear within the usual temperature limits and boehmite (formed from hydrargillite in the course of decomposition due to the action of heat) also shows its peak at the known place. There are one or two

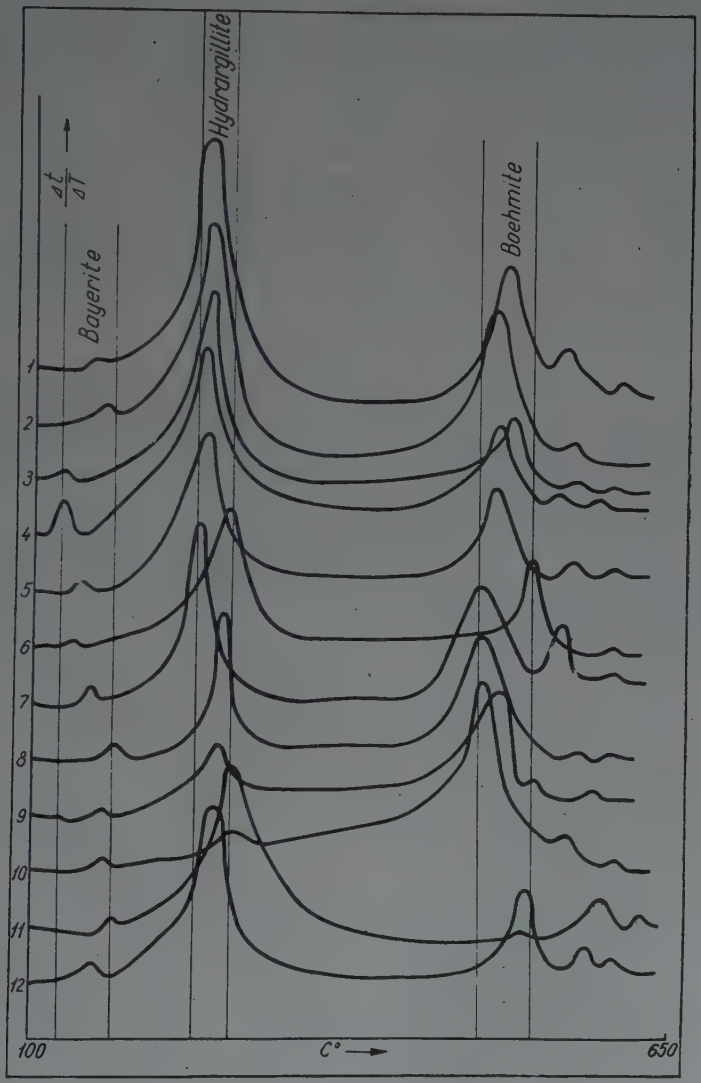

Fig. 3. Thermal decomposition of bauxites

smaller peaks we may notice after that of boehmite which indicate the presence of kaolinite and chlorite in the bauxite.

Having prepared the curves of thermal decomposition, I evaluated the mineral components contained in the bauxite. The value of the bayerite was

	Al_2O_3	SiO_2	Fe_2O_3	TiO_2	CaO	MgO	MnO_2	Loss of ignition
1.	50,32	7,00	16,46	2,95	0,45	0,12	0,06	22,52
2.	54,12	5,85	13,41	2,70	0,65	0,14	0,10	22,26
3.	52,40	1,50	16,30	2,83	0,87	0,23	0,11	24,61
5.	49,90	2,90	19,74	2,84	0,55	0,13	0,19	22,47
6.	47,56	3,36	21,87	2,72	0,75	0,08	0,31	22,08
7.	35,93	12,77	29,92	2,20	0,17	0,09	0,34	18,41
8.	55,02	3,40	20,47	2,83	0,50	0,21	0,17	16,61
9.	56,56	1,97	20,01	2,70	0,45	0,18	0,26	17,84
10.	54,58	5,65	22,28	2,69	0,43	0,09	0,15	12,84
11.	45,52	4,50	22,81	2,51	0,45	0,07	0,09	24,02
12.	49,70	2,76	22,91	2,70	0,40	0,06	0,09	22,50

obtained by multiplying the drying loss suffered at 230° C by the factor 8,657. The quantity of the hydrargillite was computed in the known manner [7]. The amount of kaolinite was computed from the silica contained [8] and the amount of chlorite from MgO by multiplying it with 2,756, in the assumption that the green chlorite scales in the bauxite are present in the form of a clinochloric mineral.

The following is a mineralogical evaluation of the bauxites under examination.

	Temperature of drying °C 230	300	Bayerite	Hydrargillite	Boehmite	Kaolinite	Chlorite
1.	0,99	14,07	8,57	52,40	5,30	15,05	0,33
2.	1,41	13,70	12,20	47,16	12,44	12,57	0,38
3.	1,13	16,86	9,78	63,31	4,29	3,22	0,63
5.	0,94	11,84	8,13	43,16	16,88	6,23	0,35
6.	1,53	14,82	13,24	50,98	3,25	7,22	0,22
7.	1,02	9,11	8,83	30,60	0,50	27,45	0,24
8.	0,75	5,31	6,49	16,44	45,47	7,31	0,57
9.	0,83	6,83	7,18	22,36	44,13	4,23	0,49
10.	0,51	1,33	4,41	12,51	54,13	12,14	0,24
11.	1,01	16,36	8,74	62,10	0	9,67	0,19
12.	0,97	14,41	8,39	54,05	5,29	6,02	0,27

The curves of thermal decomposition were prepared with the Swiss-made Habicht apparatus. The following tabular statement contains the figures showing the values of the respective decomposition peaks and the temperatures observed.

No. of bauxite	Bayerite	Hydrargillite	Boehmite	Kaolinite	Chlorite
	Values of thermal decomposition peaks in °C				
1.	218	300	546	594	648
2.	220	310	534	600	—
3.	186	300	550	598	628
4.	188	304	536	584	616
5.	202	306	538	598	634
6.	200	314	568	—	634
7.	206	296	526	578	632
8.	220	310	526	604	628
9.	216	312	550	582	630
10.	220	322	532	590	632
11.	208	308	534	600	630
12.	210	306	556	592	616

As it may be seen from the table, bayerite has its decomposition peaks varying within the range of 34° C; hydrargillite within 26° C; boehmite within 42° C; kaolinite within 26° C and chlorite within 32° C. The varying amounts of the components in bauxite also have an influence on the values of the different peaks. An interesting example of this is furnished by the variegated spotty bauxite No 3 from Iszkaszentgyörgy which exhibited, after a reduction of its iron content the decomposition peaks of boehmite, kaolinite and chlorite at a temperature lower by 14° C, on an average. Those of bayerite and hydrargillite occurred at temperatures higher by 2 and 4° C, respectively. The great extent to which the admixture of mineral components, alien to the substance under examination, may accelerate or retard the formation of thermal decomposition peaks is known from the literature and also from the research work carried on by Mrs. FÖLDVÁRI [10].

When prospecting for bauxite in the Transdanubian region of the country, in the shaft No VII lowered in the outskirts of the village of Fenyőfő, a bauxite with white nodes was found, at depths of 1,95 to 2,20 meters. The substance of the nodes was examined by K. NAGY at Veszprém and B. KLIBURSZKY in Budapest, observing it by differential thermal analysis (D. T. A.) and its thermal decomposition curve has been prepared also by myself with the use of a Habicht-apparatus (Fig. 4). It applies to all three curves that the decomposition starts at 250° C but the formation of the peaks was recorded at different temperatures by each of the three measuring instruments. To wit: at Veszprém 365° C, in Budapest 315° C and it amounted to 296° C with the Habicht instrument. It further applies to all three curves that the second peak formed by hydrargillite was entirely missing in the heat range around 530° C. The curves,

therefore, confirm the presence of pure bayerite. The composition of the substance is as follows:

Al_2O_3	SiO_2	Fe_2O_3	TiO_2	CaO	MgO	Loss of ignition
65,30	0,36	0,50	0	0,28	0,19	33,30

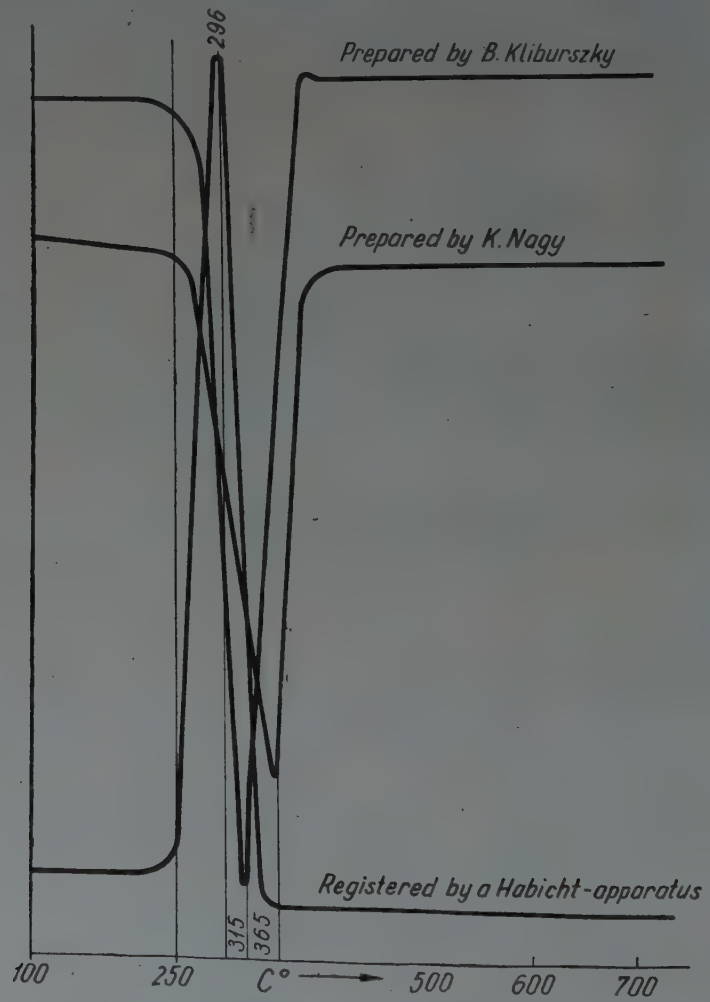

Fig. 4. Records of thermal decomposition. Bayerite in white nodes. Location: Fenyőfő, shaft No VII, at 1,95—2,20 m

When examining Hungarian alunite and aluminite, I have always found the derivatives of alumina separated from the solution to be free from titanium. Likewise, the bayerite at Fenyőfő may be regarded as a titanium-free product

separated from a solution containing sulphate. As such it is a rather pure product and the first mineral recognized in Hungary as bayerite. It contains no sulphuric compound in any measurable quantity. SO_3 in a muriatic acid solution with $BaCl_2$ appears but after a very long time, with a hardly visible turbidity.

In 1930, T. KORMOS gave a description [11] of hydrargillite in Istria. In view of the latest results, the «hydrargillite» at Portole is to be regarded

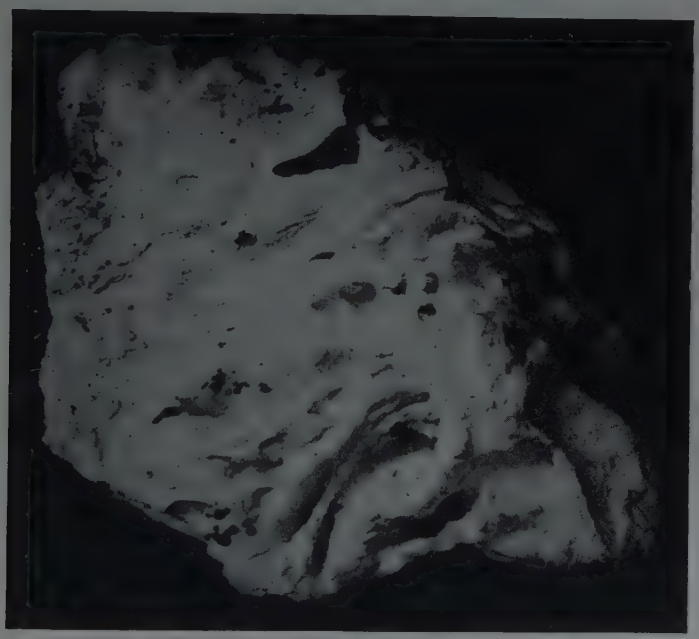

Fig. 5

as bayerite. Its curve of thermal decomposition obtained by measuring the difference in temperature is of the same nature as that of the bayerite at Fenyőfő. The peak of thermal decomposition is at 290° C. Exactly the same value was obtained by SASVÁRI and HEGEDÜS [5] when examining the Istrian substance.

An account of the results of investigation into the formation of aluminium hydrates was given by L. ERDEY at the Annual Meeting of the Hungarian Academy of Sciences held in 1955. In his account, he defined the pH limits within which the various derivatives of aluminium hydrates form : boehmite between pH 8 and 10 ; bayerite between 10,5 and 12.3 and hydrargillite between 12,3 and 13,2. According to his verbal communication, it has been found that bayerite could be detected also in alumina hydrates obtained from an acidic medium.

This is a very important statement for it proves the possibility of the formation of bayerite from a medium containing sulphuric acid.

In literature we often find reference made to the aging of bayerite, a process meant to indicate its conversion into hydrargillite. Aging is considered to be a process going on by itself but in laboratory work it is attained by maturing at a high temperature — 60 to 90° — for several days or weeks. The bayerite recognized in the prospect-shaft at Fenyőfő is of secondary formation as this has already been confirmed in the case of the aluminite. At any rate, its formation goes back to a considerably earlier period than actually indicated by certain laboratory examinations. The depth below surface at which bayerite was found is still a zone exposed to great variations in temperature. Thus, the possibility for the bayerite to be converted into hydrargillite appears to be given.

The bayerite at Portole is a fibrous, travertine-like formation (Fig. 5), deposited free from titanium, from sulphurous springs. It is a hard substance (and that makes it different from the bayerite at Fenyőfő) and, while its formation also dates back to an age preceding the recent epoch, it still has not changed into hydrargillite. The bayerite examined three years ago has been now re-examined with the result that no change had occurred in it either. On the basis of the foregoing it may be stated that the aging of bayerite is to be attributed to conditions other than normal ones.

On the basis of the examinations performed at earlier dates, bayerite had been held to crystallize on the hexagonal system, whilst hydrargillite was classed in the monoclinic system. Two kinds of bayerite have already been described by Fricke [1] who distinguished them by the denotations (a) and (b). He employed a laboratory method to separate them by shaking 20 gr of the substance for three days at 30° C with a 100 ml, 3,75 N solution of NaOH (specific weight 1,15, about 19° Bé). In that bayerite (a) dissolves much easier than bayerite (b) whilst hydrargillite dissolves the least.

Literature on alumina makes no distinction between the two qualities of bayerite. The structure of the bayerite, particularly from a crystallochemical point of view, has only quite recently been made the subject of investigations (Sasvári). These permit the assumption that the bayerite to be found in nature belongs to variety (a).

SUMMARY

It may be stated that the process of the thermal decomposition of bayerite differs from that of the hydrargillite to a considerable extent. When dried for two hours at 230° C, 1 mole of water departs from 3 moles of water. Drying at 300° C can remove the whole quantity of water contained. Bayerite occurs in our hydrargillite type of bauxites but it can be also found in a pure state (Fenyőfő, Portole).

The recognition of the bayerite means a further step in the way leading to a more thorough knowledge of the origin of the bauxites.

LITERATURE

1. Fricke, R.: Zeitschr. f. anorg. allg. Chemie, **175**, 249, 1928.
Fricke, R.: Zeitschr. f. anorg. allg. Chemie, **179**, 287, 1929.
Fricke, R.: Zeitschr. f. anorg. allg. Chemie, **285**, 21, 41, 1951
2. Brown, J. F.—Clark, D.—Elliott, W. W.: Journ. Chem. Soc., p. 84, January, 1953.
3. Erdey, L.—Paulik, F.: Magyar Tudományos Akadémia Kémiai Osztály Közleményei, **5**, 477, 1955.
4. Erdey, L.—Paulik, F.—Paulik, J.: Nature, **174**, 885, 1954.
5. Sasvári, K.—Hegedüs, A.: Magyar Kémiai Folyóirat, **60**, 333, 1954.
Sasvári, K.—Hegedüs, A.: Die Naturwissenschaften, **42**, 254, 1955.
6. Maricsics, S.—Terzsák, S.: Kolloid Zeitschr., **140**, 170, 1955.
7. Gedeon, T.: Földtani Közlöny, **84**, 201, 1954.
8. Gedeon, T.: Magyar Kémiai Folyóirat, **38**, 134, 1932.
9. Gedeon, T.: Földtani Közlöny, **83**, 151, 1953.
10. Földvári-Vogl, M.—Koblenz, V.: Acta Geologica. III, 15, 1955.
11. Kormos, T.: Bányászati és Kohászati Lapok, **63**, 269, 1930.

БАЙЕРИТ В ВЕНГЕРСКОМ БОКСИТЕ

Т. Г. ГЕДЕОН

Резюме

В качестве заключения можно установить, что процесс термического разложения байерита существенно отличается от гидраргиллита. При высушивании в течение двух часов на 230°С из 3 молей воды удаляется 1 моль. При высушивании на 300°С удаляется все количество воды. Байерит встречается в гидраргиллитовых бокситах Венгрии и иногда обнаруживается даже в чистом виде (Феньёфё, Портоле). Благодаря распознаванию байерита опять удалось расширить наши знания о происхождении боксита.

THERMISCHE SCHNELLANALYSE

EIN DTA-APPARAT FÜR INDUSTRIELLE SERIENPRÜFUNGEN

Von

B. KLIBURSZKY

INSTITUT FÜR MINERALOGIE UND PETROGRAFIE DER EÖTVÖS LORÁND UNIVERSITÄT, BUDAPEST

Die DT-Analyse findet in der Mineralogie eine immer weitergreifende Anwendung. Dieser Umstand schuf die Notwendigkeit, einen Apparat für schnelle und serienmässige industrielle DT-Prüfung zu entwerfen.

Die bisher üblichen Apparaturen arbeiten alle mit der bewährten und allgemein angewandten Erwärmungsgeschwindigkeit von 10—15° C/min. Für wissenschaftliche Untersuchungen und genauere quantitative Bestimmungen hat sich diese Geschwindigkeit am zweckmässigsten erwiesen, und sie wird von den Forschern auch an Hand von theoretischen Erwägungen als empfehlenswert betrachtet [1]. Bei einer solchen Erwärmungsgeschwindigkeit dauert eine vollständige Analyse mit einer Erhitzung auf 1000—1100° C ungefähr 100 Minuten. Rechnet man die notwendige Zeit für Vorbereitungen, sowie für die zur Abkühlung der allgemein angewandten Apparate mit grosser Wärmekapazität mit, so beträgt die Dauer einer einzelnen Bestimmung ungefähr drei Arbeitsstunden.

Will man die Anwendbarkeit der DTA-Methoden auch auf das Gebiet der schnellen industriellen mineralogischen Prüfungen ausbreiten, so muss man notwendigerweise die Dauer einer einzelnen Untersuchung wesentlich vermindern. Ausserdem muss beachtet werden, dass der Apparat für solche massenhafte und schnelle Analysen möglichst einfach, leicht zu handhaben und billig sein muss.

Auf Grund der oben genannten Voraussetzungen erstreckte sich unsere Aufgabe in zwei Richtungen: erstens musste ein Apparat entworfen und gebaut werden, dank dessen kleiner Wärmekapazität und anderen Eigenschaften ungefähr das Zehnfache der allgemein angewandten Erwärmungsgeschwindigkeit erreichbar ist; zweitens war es notwendig, die Güte und Reproduzibilität der durch derart schnelles Erwärmen gewonnenen DT-Kurven innerhalb der gestellten Forderungen zu prüfen.

1. Beschreibung der angewandten Apparatur

Die grosse Erwärmungsgeschwindigkeit konnte neben kleiner elektrischer Leistung offenbar nur erzielt werden, wenn man Ofen und Probehälter mit

möglichst geringer Wärmekapazität konstruierte. Man musste daher von der Konstruktion der bisher angewandten Apparate mit einem Probehälter von ungefähr 70—80 g Gewicht und einem Ofen von 500—600 W Verbrauch abweichen. Weiterhin musste man bei der Konstruktion des Ofens für den neuen Apparat berücksichtigen, dass dieser auch für Geländezwecke anwendbar, also auch mit Autoakku heizbar sein musste. Die Konstruktion des Probehälters wurde weitgehend dadurch erleichtert, dass unsere schon seit einiger Zeit angewandte Schaltung mit zwei Thermoelementen [2] nur zwei statt der üblichen drei Bohrungen im Block des Probehälters notwedig macht. Ein Block mit drei Bohrungen hätte vor allem die Wärmekapazität erhöht und auch die Konstruktion und die Bedienung umständlicher gestaltet. Ein weiterer Vorteil

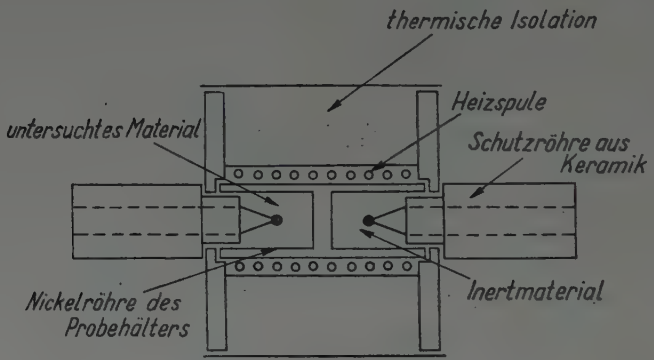

Abb. 1. Ofen und Probehälter

besteht darin, dass die für zwei Bohrungen benötigten zwei Thermoelemente gegenüber den bisherigen drei eine schaltungstechnische Vereinfachung bedeuten und durch die Verkürzung der Pt/PtRh-Thermoelemente eine Verminderung der Selbstkosten erlauben. Wir haben bei unserem bisher benutzten DT-Apparat die Anwendung eines Probehälterblocks mit nur zwei Bohrungen und Thermoelementen bereits früher eingeführt und die Vorzüge dieser Anordnung auch theoretisch begründet [2].

Nach Erwägung dieser Vorbedingungen und Erfordernisse erwies sich folgende Konstruktion des Ofens bzw. Probehälters am zweckmässigsten: der Probehälter besteht aus einer Nickelröhre von ungefähr 40 mm Länge, mit einem äusseren Durchmesser von 10 mm und einem inneren von 6 mm. Diese wird von einer 2 mm dicken Scheidewand in zwei gleich dicke Hälften geteilt. Eine Hälfte enthält die Probe, die andere das Inertmaterial. Die Lötstellen der Thermoelemente liegen in der Probe bzw. im Inertmaterial. Die Drähte der Thermoelemente laufen durch eine Schutzröhre aus Keramik mit geändertem Hals. Durch die Randung der Keramikröhre wird gesichert, dass die Lötstellen der beiden Thermoelemente immer an den gleichen Punkt in der Nickelröhre

geraten. Die Schaltung der Thermoelemente wurde bereits in unserer angeführten Abhandlung [2] mitgeteilt.

Die als Probehälter benutzte Nickelröhre ist von aussen mit einer dünnen Isolierschicht aus erhitztem Kaolin überzogen und mit einem dicken Heizdraht von «Kantál A»-Qualität umwunden. Die Heizspule ist nach aussen durch Asbestwatte isoliert und die ganze Einrichtung in Eternitplatten eingefasst (Ofen und Probehälter sind in Abb. 1 dargestellt). Die aufgenommene elektrische Leistung betrug bei 1100° C, die in 11 Minuten erreicht wurde, ungefähr 100 W.

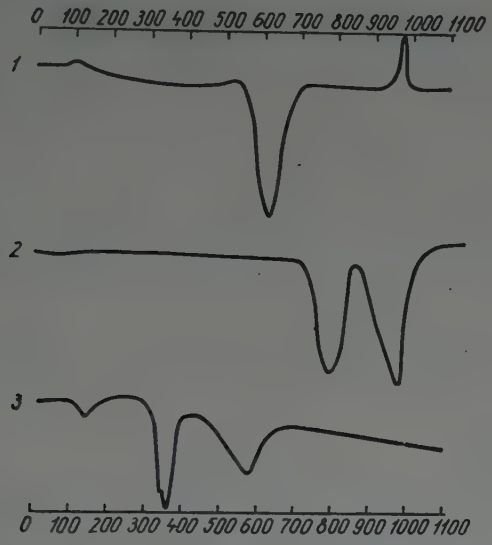

Abb. 2. Durch thermale Schnellanalyse erzielte Thermodiagramme. (Erwärmungsgeschwindigkeit 100 °C/min) 1. Kaolinit aus Zettlitz 2. Dolomit aus Gánt 3. Bauxit aus Gánt

Der notwendige elektrische Strom wurde aus einem Transformator entnommen, in dessen Primärseite ein Potentiometer eingeschaltet war, um den Eingangsstrom zwecks möglichst gleichmässiger Erwärmung zu regeln.

Die Temperatur des zerfallenden Materials wird mit der Vermittelung des Thermoelementes auf einen höchst genauen Millivoltmeter von ungefähr 130 Ohm Innenwiderstand übertragen. Wie schon im vorhin angeführten Aufsatz [2] erwähnt wurde, ist es wichtig, dass die Lötkugel der Thermoelemente möglichst klein sind, sonst können sie infolge ihrer grossen Wärmekapazität den eintretenden Temperaturunterschieden nicht rasch genug folgen. Grundsätzlich sollte man möglichst dünne Drähte der Thermoelemente wählen, jedoch ist ein Durchmesser unter 0,3 mm aus Festigkeitsgründen unerwünscht.

Die Temperaturunterschiede zwischen Probe und Inertmaterial werden durch ein Thermoelementenpaar in Differentialschaltung registriert, das seiner-

seits auf einen Galvanometer mit kurzer Schwingungsperiode einwirkt. Die Schwingungsseite des Galvanometers soll nach Möglichkeit die Grössenordnung 0,1 sec betragen. Diese Forderung ist im gegebenen Falle von grosser Wichtigkeit, denn ein Galvanometer mit langer Schwingungsperiode würde bei schnellem Erhitzen verzerrte, abgeflachte Thermalkurven liefern. Um die schnellstmögliche Reaktion zu erzielen, wird der Grenzwiderstand des Instrumentes so gewählt, dass die Schwingung nahezu aperiodisch ausfällt. Der von uns angewandte Galvanometer besitzt einen inneren Widerstand von 60 Ohm und einen Manganinwiderstand von 60 Ohm in Shuntschaltung. Zwischen Differenzialthermoelement und Galvanometer liegt ein Widerstand von 100 Ohm in Serienschaltung. Der Galvanometer ist ein Instrument vom Typ «Miravi» mit einer Empfindlichkeit von 10^{-8} A/mm.

Die Registrierung der Galvanometerausschläge erfolgt auf einer Registriertrommel von ungefähr 14 cm Durchmesser. Eine volle Umdrehung beansprucht 15 Minuten. Die schnelle Registrierung erforderte eine aussergewöhnlich starke Lampe zur Erzeugung des Lichtsignals. Die Registriertrommel wurde von einem Synchronmotor betrieben. Die Aufnahme der Thermokurven geschah auf einem angehefteten lichtempfindlichen Papierstreifen.

2. Kritische Untersuchung der durch Schnellanalyse erzielten thermischen Kurven

Die Anwendbarkeit der Methode hängt im Endergebnis davon ab, ob die gewonnenen thermischen Kurven, ebenso wie die Kurven der üblichen Prozedur ausfallen, weiterhin, ob sie sich zuverlässig reproduzieren lassen. Um diese Fragen beantworten zu können, haben wir zahlreiche experimentelle Analysen durchgeführt. Einige sind in Abb. 2. dargestellt. Laut den beigelegten Kurven erwies sich die Methode der Schnellanalyse anwendbar. Die Form der Kurven stimmt mit denen der allgemein bekannten thermischen Kurven überein. Der einzige Unterschied ist, dass sich die Spitzen infolge des schnellen Erwärmens etwas nach rechts verschoben haben, diese Verschiebung aber nicht mehr als 20—30° C beträgt. Da durch unsere spezielle Thermoelementschaltung die Spitzentemperaturen der einzelnen Reaktionen sowieso theoretisch um 20° C nach links verschoben werden, entstehen bei der Schnellanalyse als Resultante der beiden entgegengesetzten Wirkungen Kurven, die im allgemeinen die durchschnittlichen Spitzentemperaturen der Literaturangaben zeigen. Die Form der Kurven zeigte auch keinen wesentlichen Unterschied gegenüber der üblichen Prozedur : die Form der Spitzen blieb ähnlich. Der einzige bemerkbare Nachteil bestand darin, dass sich die sehr naheliegenden Spitzen nicht so leicht trennen liessen.

Die in grosser Zahl ausgeführten Paralleluntersuchungen mit der thermischen Schnellanalyse beweisen, dass die Reproduzibilität der Ergebnisse genügt

und dass die Ausmessung der Spitzenflächen sogar semiquantitative Schätzungen ermöglicht. Dieser Umstand ist bei der Ausführung von serienmässigen industriellen Untersuchungen äusserst vorteilhaft.

Die gründliche Erforschung dieser Fragen erwies sich als notwendig, da die Fachliteratur nur eine einzige kurze Anweisung enthält, nach der die Forscher Berg und Rassunskaia die Schnellanalyse mit Erfolg angewandt haben [3].

Als Summierung der Ergebnisse kann festgestellt werden, dass die beschriebene einfache und billige Apparatur zur Ausführung einer thermischen Analyse in 10—15 Minuten geeignet ist. Die derart gewonnenen thermischen Kurven lassen sich gut reproduzieren und können sogar zur semiquantitativen Schätzung von Bestandteilen angewandt werden.

ZUSAMMENFASSUNG

Die vom Verfasser entworfene und erbaute und mit geringen Kosten herstellbare thermische Einrichtung ist für die Ausführung von thermischen Schnellanalysen geeignet. Eine Bestimmung dauert etwa 10 Minuten. Die Spitzen der gewonnenen thermischen Kurven verschieben sich um ungefähr 20° C in Richtung der höheren Temperaturen. Ausserdem erwiesen sich die thermischen Kurven der Schnellanalyse als charakteristisch und reproduzierbar, in Kürze, als anwendbar. Apparat und Methode lassen sich besonders bei routinenmässigen industriellen Untersuchungen mit Vorteil anwenden. Die erzielten Kurven gestatten ebenfalls semiquantitative Schätzung der aktiven Bestandteile.

SCHRIFTTUM

1. Murray, P.—White, J.: Trans. of Brit. Cer. Soc. **54**, 4, 1955.
2. Földvári-Vogl, M.—Kliburszky, B.: Acta Geologica, Tom. II, fasc. 3—4, 215—230, 1954.
3. Berg, L. G.—Rassunskaia, I. S.: Doklady Akad. Nauk. SSSR, **73**, 113—115, 1950.

УСКОРЕННЫЙ ТЕРМИЧЕСКИЙ АНАЛИЗ: ПРИБОР ДЛЯ ДИФФЕРЕНЦИАЛЬНО-ТЕРМИЧЕСКОГО АНАЛИЗА, ПРИМЕНЯЕМЫЙ ПРИ СЕРИЙНЫХ ИССЛЕДОВАНИЯХ ПРОМЫШЛЕННОГО ХАРАКТЕРА

Б. КЛИБУРСКИ

Резюме

Данная простая и дешево изготовляемая термическая установка, проектированная и построенная автором, пригодна для ускоренного исполнения исследований. Продолжительность одного определения равняется примерно 10 мин. Пики полученных термических кривых смещены вверх приблизительно на 20°C. За исключением этого, термические кривые являются показательными и воспроизводимыми и ввиду этого оказались хорошо используемыми. Прибор и способ особенно пригодны для ускоренного исполнения серийных исследований промышленного характера. Полученные термические кривые пригодны и для грубо-количественных оценок.

CRYSTAL ORIENTATION OF TWO PHOSPHATES IN THE SCALES OF PERMIAN FISH OF THE GROUP PALAEONISCIDAE

J. KONTA,

INSTITUTE OF PETROGRAPHY, CHARLES UNIVERSITY, PRAGUE

The studied fish scales of the group *Palaeoniscidae* occur in the copper-bearing series of the Permian of the piedmont region of the Krkonoše, in the area of Horní Kalná and Rudník in Northern Bohemia. The fish scales, and often also completely preserved imprints of whole fish, occur in large quantities in rocks ranging from blackish gray marly limestone to marlstone, to a smaller extent also in the overlying, fine-grained violet-pink limestone. Both rocks are disintegrating into thin sheets to plates.

The accumulation of great quantities of fish in relatively thin layers, coloured blackish gray by a dense organic pigment, may be accounted for by a sudden setting in of unfavourable conditions and the mass dying of the organisms. The volcanic activity of the melaphyres constituted most probably an intervention of this kind; it brought with it strongly toxic products of the volcanic activity, especially solutions of copper compounds (J. KONTA, 1953).

The scales of the fish of the group *Palaeoniscidae* have in a view of the largest surface the shape of a rhombus with moderately rounded sides. The size of the scales is found most frequently between 0,5 and 3 mm. There occur, however, also scales with the length of the side of up to 5 mm. The colouration of the fish scales is twofold, according to the nature of the pigmentation substance of the rock in which the scales are deposited. Thus, in the blackish gray, marly limestone to marlstone the scales are blackish gray with a vitreous lustre. In the violet-red limestone the scales are brownish red from the fine ferruginous pigment, which is concentrated mainly at the periphery of the scales.

A cross section of a scale perpendicular to its largest surface shows the well-known flow shape (Fig. 1). Its details can be observed well under the microscope. The kind of fish scales studied is designated in the literature as ganoid.

In the microscopical investigation of the scales thin sections were used oriented perpendicularly to the stratification of the rocks. In the thin sections the section across the scales appears differently according to the character of the section, but most often there occur elongated flow shapes. The substance of the fish scales of the group *Palaeoniscidae* is formed by two different phosphates. The upper, covering layer of the scales is very thin, most often between

0,015 and 0,05 mm., and in the thin sections it is pure and perfectly transparent. By its optical characters it differs from the inner, thick layer, which forms the predominant substance of the fish scales. This inner or lower part of the fish scales studied is most often of a thickness of 0,08 to 0,3 mm., and is finely fibrous in the direction of the length of the scales. In it can be observed the distinct concentric growth of new layers, and it is almost always rendered somewhat impure by a fine organic or ferruginous pigment (Fig. 2).

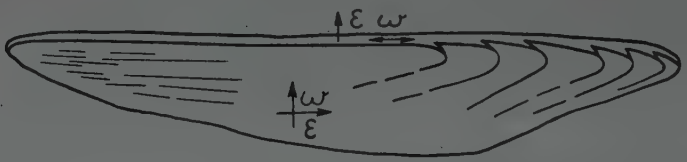

Fig. 1. Section through a scale perpendicular to its largest surface. The phosphates have opposite optical orientation

The *upper layer*, sometimes also called the enamel, sclerite or dorsal layer (F. NEAVE, 1936 ; A. S. ROMER, 1950) has in all cross sections a higher refraction and double refraction than the lower fibrous layer. The substance of the upper layer is called by most of the authors (E. S. GOODRICH, 1907 ; E. K. SUVOROV,

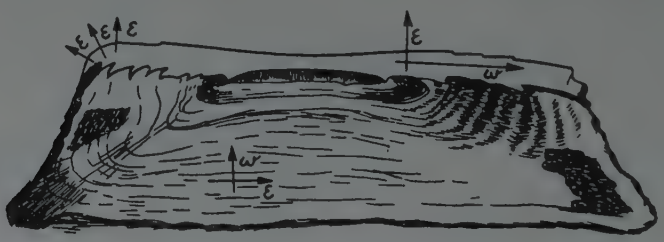

Fig. 2. Another section through a scale with a distinct concentric growth of the following layers of francolite. The covering layer of hydroxy-fluor-apatite is more homogeneous

1948, a. o.) ganoin (designation from WILLIAMSON) ; the composition of the latter is, according to some authors, near to that of dentine, according to others, to that of hyalodentine (cp. e. g. F. NEAVE, 1936). Details concerning the morphology of the scales of recent and extinct fish are given in the work of E. S. GOODRICH (1907), which remains the standard work on this subject.

Optical constants of the phosphate of the upper layer :

$\varepsilon\ (n_\alpha) = 1{,}639 \pm 1$
$\omega\ (n_\gamma) = 1{,}643 \pm 1$ } in Na-light
(n_β is near n_γ), double refraction $= -0{,}004$
anomalously biaxial.

When we project the indices of refraction and the value of the double refraction into a diagram after A. G. Betechtin (1950) or W. E. Trőger (1952), we see that the composition of the phosphate of the upper layer corresponds best to hydroxy-fluor-apatite, $Ca_5(PO_4)_3(OH, F)$.

The indices of refraction were measured, on the one hand, on the uncovered thin section from which the Canada balsam had been removed by alcohol and, on the other hand, in powder preparations of fish scales in various immersion oils. The indices of the refraction of the immersion oils have been controlled simultaneously on the refractometer.

The upper layer is, however, not a monocrystal of hydroxy-fluor-apatite. When we peel it off and place it in immersion oil, we observe between crossed nicols that it is composed of a rather large quantity of irregularly delimited flat formations of hydroxy-fluor-apatite, which are mutually firmly connected. The individual formations have in their plane the direction $\omega(n_\gamma$ and $n_\beta)$ and, perpendicular to their plane, the direction $\varepsilon(n_a)$.

In all sections of the covering layer of the scales, parallel and perpendicular to the optical direction ε, we observe in the otherwise pure hydroxy-fluor-apatite tiny rhomboids or irregular grains of calcite. Their size is mostly below 1 micron, at most up to 2 microns.

Sometimes the *lower, fibrous layer (Francolite)* is designated also as the lamellar or ventral layer, or also as the basal plate (e. g. F. Neave, 1936). It is composed of very thin and long fibres elongated in the plane of the scales and densely arranged.

Optical constants of the phosphate of the lower layer: mean refractive index, $n = 1{,}611 \pm 1$ double refraction $= 0{,}001$ (and less).

The fibrous phosphate substance shows such a slight double refraction that actually it is possible to determine only the mean refractive index. The double refraction is, however, in most sections distinctly perceptible between crossed nicols and when using sensitive violet gypsum plates.

According to the very low refraction of light and the slight double refraction to pseudoisotropy (term after J. Konta, 1951) and the fibrous habit of the crystals as well as according to the roentgenometric analysis we have here the substance designated as francolite $Ca_{10}F_2(P, C)_6O_{24}$.

Fine, variously ramified canals are still preserved in the lower, fibrous layer.

The qualitative (chemical) tests for phosphorus and fluor were in both phosphates strongly positive. Phosphorus was proved by ammonium molybdate. The tests for fluor were carried out in a glass test tube with finely powdered phosphate (0,2 and 0,5 gr) under the influence of acidic perchloricum (5 ccm). The finely powdered samples in the test tube were heated with acidic perchloricum for three hours on a sand bath (about 80° C). The test tubes were placed in a slanting position, about 30°. The escaping fluor hydrogen distinctly etched the glass in both test tubes (Fig. 3).

The same tests for fluor were carried out as control under equal conditions with finely powdered siliceous hornstone and marly limestone from the same copper-bearing series, where neither of the samples contained fish scales. The result of the fluor test was in both cases negative.

Table I*

Francolite (KONTA)		Francolite (McCONNELL, 1938)		Fluor-apatite (McCONNELL, 1938)		Dahllite (McCONNELL, 1938)	
d	I	d	I	d	I	d	I
3,37	2	3,431	2	3,432	2	3,437	2
3,08	0,5	3,157	0,5	—	—	—	—
3,02	1	3,044	2	3,060	3	3,077	3
		2,957	0,5	2,975	0,5	2,990	1
		2,844	0,5	2,884	0,5	—	—
2,75	10	2,765	>10	2,798	>10	2,811	>10
				2,769	4	2,778	3
		2,683	7	2,702	6	2,712	6
2,62	2	2,618	4	2,616	3	2,628	1
2,54	1	2,508	0,5	2,517	0,5	2,524	0,5
		2,462	0,5	2,477	0,5	2,493	0,5
		2,277	1	2,289	0,5	—	—
2,23	3	2,238	3	2,248	2	2,256	4
2,11	1	2,127	2	2,135	1	2,145	2
		2,060	1	2,057	1	—	—
		2,020	1	2,026	0,5	2,031	0,5
		1,996	1	2,001	0,5	—	—
		1,967	0,5	—	—	1,993	0,5
1,92	3	1,928	3	1,937	3	1,941	4
1,87	1	1,876	1	1,883	1	1,888	1
1,82	3	1,835	3	1,838	6	1,840	2
1,78	0,5	1,788	2	1,795	3	1,805	1
		1,762	2	1,769	3	1,778	1
1,75	0,5	1,760	2	1,745	3	1,753	1
1,70	1	1,720	2	1,720	3	1,721	1
1,63	1	1,631	0,5	1,637	1	1,645	0,5
		1,601	0,5	1,605	0,5	—	—
1,52	0,5	1,525	0,5	1,533	0,5	1,538	1
		1,515	0,5	1,521	0,5		
1,49	0,5	1,496	0,5	1,498	1	1,502	1
1,46	1	1,462	1	1,468	2	1,473	1
1,45	1	1,453	1	1,452	1	1,455	1
		1,441	1	1,445	1		
1,42	0,5	1,419	1	1,424	1	1,434	2
1,30	0,5						
1,27	0,5						
1,25	0,5						
1,23	2						
1,21	1						
1,15	2						
1,11	1						
1,10	1						

* The values «d» of the francolite studied are in new units (A), the values of McCONNELL in old kx units. CuK_α radiation, $2r = 57{,}3$ mm.

The test for CO_2 was carried out only with the fibrous francolite, as the hydroxy-fluorapatite is intergrown with fine calcite. Finely powdered pure francolite was placed on the bottom of the test tube, covered with about 5 ccm of distilled water, and then a few drops of concentrated HCl were added with a pipette. The escaping bubbles confirmed the presence of CO_2.

We have today already an extensive literature on the roentgenometrical investigation of biogenic phosphates. But the results obtained by different authors differ considerably. This is due especially to the difficulty of obtaining quite pure material of all biogenic phosphate for all kinds of research (optical, roentgenometrical, chemical, etc.), and also to the difficulty of an exact quantitative determination of the volatile components, i. e. Cl, F, CO_2, and lattice water (OH').

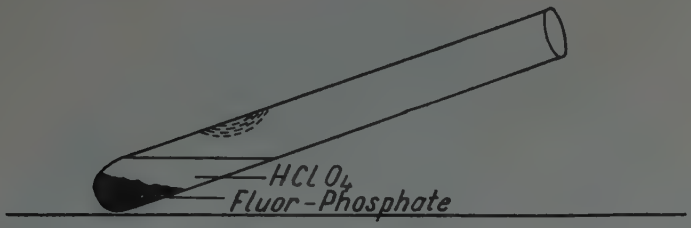

Fig. 3. Quick test for the presence of fluorine in minerals of the apatite group

Thus, the comparison of the new results with the results already published is not simple. D. McConnell (1938, 1952) deals in several papers in some detail with the problems of the study of minerals of the apatite group. This author worked for a long time thoroughly on the chemism and structure of the minerals of the apatite group and gave reliable roentgenometrical data with which we can compare our francolite.

Of all of McConnell's phosphates (1938) it is the francolite with which the values «d» and the intensity (determined visually) of the fibrous phosphate of the fish scales studied agree best. This applies to most of the stronger interference lines and especially to the most intensive line ($d = 2{,}75$).

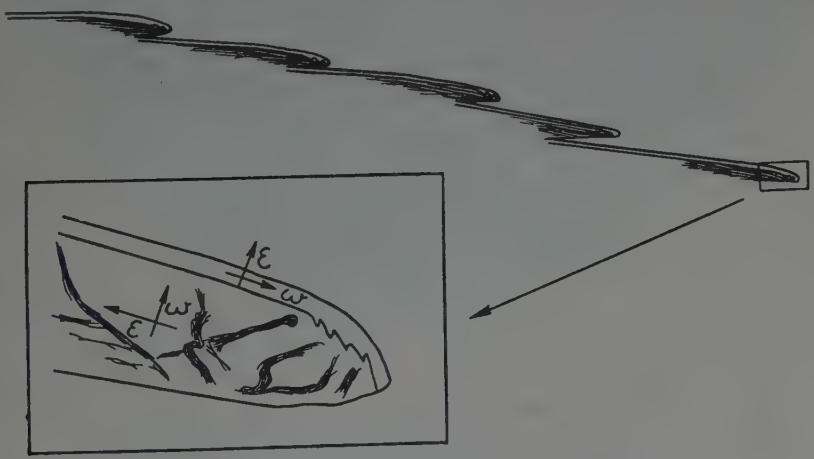

Fig. 4. The protective function of the covering layer is enhanced by its appropriate optical orientation. The elasticity of the scale is maintained by the fibrous structure of the lower layer (with the canals preserved) and the appropriate orientation of the *c* axis (direction ε) in the plane of the scale

Both biogenic phosphates in the scales of fish of the group *Palaeoniscidae* are remarkable not only for their different optical constants and the different

chemism resulting from them, but even more for their being grown together in the scales according to a law. The hydroxy-fluor-apatite in the upper, covering layer has always the optical direction of the smallest refractive index $\varepsilon(n_\alpha)$ oriented perpendicular to the surface of the scale, the direction of $\omega(n_\gamma$ and $n_\beta)$ lies in the plane of the scale (Fig. 4). The lower fibrous layer composed of francolite has, on the contrary, in the direction of the length of the fibres, i. e.

Fig. 5a. Sections through fish scales of the group *Palaeoniscidae.* 15×nat. size

in the plane of the scales, the direction of the smallest index $\varepsilon(n_\alpha)$, whereas the direction of $\omega(n_\beta$ and $n_\gamma)$ is oriented perpendicularly to the length of the fibres (Fig. 4).

The appropriateness of the different composition, habit, mutual arrangement and different optical orientation of the two phosphates in the fish scales studied is best shown by the following facts:

1. The hardness of the two phosphates is different. The more compact hydroxy-fluor-apatite, which protects the scale against outer influences, has

after MOHS' scale the hardness 5, whereas the fibrous varieties, and thus also the francolite, have a somewhat lower one (data after C. DOELTER, 1918).

2. The fine fibres of the francolite forming the main substance of the scales are oriented with the vertical axis in the plane of the scales (optical direction ε). Thus a phosphate structure of a considerable elasticity is formed.

Fig. 5b. The same object between crossed nicols. The thin white covering layer is easy to distinguish from the fibrous francolite layer

3. The main substance of the scale, the fibrous francolite, is covered by a more homogeneous covering layer of hydroxy-fluor-apatite, which has a minimum optical direction ε, and thus also the axis c oriented perpendicularly to the surface of the scale. C. DOELTER (1918, p. 343) gives valuable data for the heat conductivity of apatite after F. M. JAEGER (1906). He designates as λ the heat conductivity in the direction of, and as λ_a the same perpendicular to the main axis. The ratio of the heat conductivity in the two main directions

$\frac{\lambda c}{\lambda a} = 1{,}35$. Also the hardness in the direction of the axis c is in the apatite somewhat higher than in the directions perpendicular to the vertical.

The law-governed orientation of the two different phosphates in the scales of the group *Palaeoniscidae* is thus obvious from the facts given. The covering layer has above all a protective function, which is given by the greater chemical resistance and greater hardness of the hydroxy-fluor-apatite as compared with the francolite. This function is still enhanced by the fact that in the direction of the axis c (optical direction ε) oriented perpendicularly to the surface of the scales the heat conductivity, and thus also the hardness, is in the apatite higher than in the direction of the axes a (optical direction ω). Also the cleavage in the direction of the axis c is in the apatite relatively small. The lower layer, on the contrary, formed of finely fibrous francolite, gives the whole scale elasticity, and thus also firmness. It is not excluded that in addition to a protective function the upper hydroxy-fluor-apatite layer may have also a certain signalling function on the basis of the greater heat conductivity in the direction of the axis c oriented perpendicularly to the surface of the scales.

In some sections we observe in the lower fibrous layer between the fine fibres also more refractive parts with a higher double refraction. After the optical characters they correspond to the covering phosphate, hydroxy-fluor-apatite. But this occurs only in sporadic cases and in very thin scales. Also in these hydroxy-fluor-apatite fibres, situated in the lower layer, the optical orientation agrees with the optical orientation of the francolite fibres, i. e. the direction ε is in the direction of the fibres.

SUMMARY

In the scales of Permian fish of the group *Palaeoniscidae* from the copper-bearing series of the North Bohemian Permian two kinds of phosphates have been ascertained :

a) the thin covering layer of the scales is hydroxy-fluor-apatite ;

b) the lower fibrous layer is francolite.

Both phosphates have been identified by the determination of the optical constants and qualitatively chemically, the francolite also roentgenometrically.

The two phosphates have in the scales differently, however, law-governed oriented principal optical directions. By this law-governed orientation the protective function of the covering layer is enhanced, which is given already by the greater chemical resistance and hardness of the hydroxy-fluor-apatite as compared with the francolite. The discovery of the law-governed oriented concrescence of the two phosphates in the fish scales of the group *Palaeoniscidae* can have a certain importance also for the biomineralogy of the teeth of vertebrates and thus also of the teeth of man, as the fish scales and the teeth have an analogous phylogenetic development.

BIBLIOGRAPHY

Бетехтин, А. Г. (1950) : Минералогия. Москва, стр. 601 – 602.

Doelter, C. (1918) : Handbuch der Mineralchemie. Bd. III, 1 Abt., Dresden u. Leipzig, pp. 339—343.

Goodrich, E. S. (1907) : On the Scales of Fish, Living and Extinct, and their Importance in Classification. Proceed. Zool. Soc. London (May 1908), pp. 751—774.

Jaeger, F. M. (1906) : after C. Doelter (1918).

KONTA, J. (1951): Investigation of the deweylites from the fissure fillings in the serpentine of Mladotice. Bull. internat. de l'Acad. Tchèque des Sciences, LII, No. 31, pp. 1—13.
KONTA, J. (1953): Hydrothermaler Analcim der kupferhaltigen Schichtenfolge des Perms aus dem Vorland des Riesengebirges und seine Bedeutung für die Herkunft des Kupfers. Geologie, **2**, Nr. 4, p. 237—252, Berlin.
MCCONNELL, D. (1938): A structural investigation of the isomorphism of the apatite group. Am. Min., **23**, p. 1—19.
MCCONNELL, D. (1952): The problem of the carbonate apatites. IV. Structural substitutions involving CO_3 and OH. Bull. Soc. Franç. Min., **75**, p. 428—445.
NEAVE, F. (1936): The Development of the Scales of Salmo. Transact. Royal Soc. of Canada, Sect. V, Biolog. Sci., 3. Series, vol. XXX, p. 55—72.
ROMER, A. S. (1950): Vertebrate paleontology. The University of Chicago Press, on pp. 77—78,.
Суворов, Е. К. (1948): Основы ихтиологии. «Совет. Наука», стр. 48—54.
TRÖGER, W. E. (1952): Tabellen zur optischen Bestimmung der gesteinsbildenden Minerale. Stuttgart, p. 27.

ЗАКОНОМЕРНО ОРИЕНТИРОВАННОЕ СРАСТАНИЕ ДВУХ ФОСФАТОВ В ЧЕШУЯХ РЫБ ПЕРМСКОГО ПЕРИОДА, ГРУППЫ PALAEONISCIDAE

И. КОНТА

Резюме

В чешуях пермских рыб, группы Palaeoniscidae, из мединосного яруса северочешского пермского периода были опознаны два вида фосфатов:
а) кроющий, тонкий слой чешуй — гидроксил-флюор-апатит,
в) нижний, волокнистый слой — франколит.

Оба фосфата идентифицировались методом установления оптических постоянных величин и качественно-химически, а франколит еще и рентгенометрически.

Оба фосфата имеют в чешуях различные, однако закономерно-ориентированные главные направления. Этой закономерной ориентацией увеличивается защитная функция кроющего слоя, обладающего ею, благодаря еще большей химической устойчивости и твердости гидроксил-флюор-апатита, чем франколит. Новое открытие о закономерно ориентированном срастании двух фосфатов в рыбьих чешуях группы Palaeoniscidae может иметь определенное значение и для биоминералогии зубов позвоночных, а следовательно и человека, так как рыбьи чешуи и зубы имеют аналогичное филогенетическое развитие.

THE CRYSTAL STRUCTURE OF A-BAYERITE, $Al(OH)_3$

By

K. Sasvári

RESEARCH INSTITUTE FOR TELECOMMUNICATION, BUDAPEST

Fricke [1] has shown, that there exist two kinds of bayerite, which he distinguishes as *a*- and *b*-bayerite. The two forms exhibit X-ray diffraction patterns, differing from each other essentially but in the intensity of a few reflexions. After their behaviour *b*-bayerite may be considered as a transition from *a*-bayerite to hydrargillite. H. Kraut and his collaborators [2] found, in addition to the two forms mentioned, another one, which they called *c*-bayerite but their statements have not as yet been confirmed by any other instances. Recently a description of the preparation of *a*-bayerite was published by Schmäh [3].

Up to the present we have found only a few references about the crystal structure of bayerite. Montoro [4] stated in 1942 that bayerite was of a hexagonal crystal structure with cell dimensions: $a_H = 5{,}01$ Å and $c_H = 4{,}76$ Å, each of these unit cells comprising two molecules. According to him, this crystal, similar to hydrargillite, is of a layer structure, whose layers consist of two hexagonal close-packed $(OH)^-$ ionic planes. Aluminium lies between these planes in the centers of octahedra. In 1952 K. Funaki and Y. Shimizu [5] found bayerite to consist likewise of hexagonal cells, the edges of which differ from those found by Montoro only by 0,01 Å.

The data of cell dimensions given and the considerations suggested by Montoro seem to exhibit great probability, because the $\sin^2\vartheta$ values of the reflexions of *a*- and *b*-bayerite could be readily identified with those calculated from the hexagonal unit cell dimensions suggested by him. His assumptions appear the more probable, because his hexagonal unit cell allows to be easily derived from that of hydrargillite.

The monoclinic lattice of hydrargillite [6] is built of layers situated parallel to the planes (001), the layers consisting, in the sequence A—B and B—A, of close-packed hexagonal $(OH)^-$ ion planes, between which, in the centers of two third of the octahedra, there is aluminium. A projection of such a layer is presented in Fig. 1 by omitting to show the distortions of the hydrargillite lattice. The arrangement of the ions allows to prepare, in the layer and parallel to it, a hexagonal network corresponding, as we shall see, with the basis of the hexagonal unit

cell of MONTORO. If we take every second of the consecutive layers A—B, B—A, A—B ... in the hydrargillite lattice and shifting the two $(OH)^-$ ion planes opposite to each other in the direction $[11\bar{2}0]$ as referred to the hexagonal network, by a distance of $a_H/3$, and let the cations remain in their places, then in the hydrargillite lattice all the consecutive layers will follow the anion arrangement according to A—B or B—A. This, however, will reduce the identity period in the direction [001] of the hydrargillite lattice to half of that of the original hydrargillite lattice.

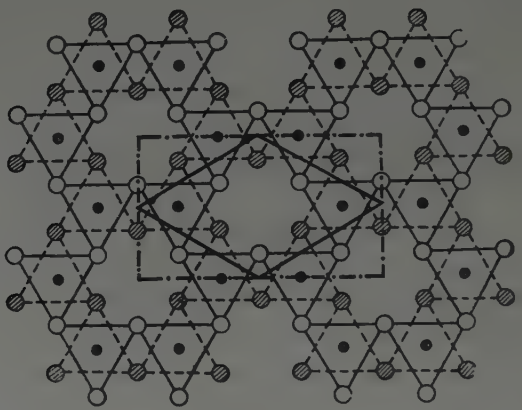

Fig. 1

In the hydrargillite lattice $\frac{c}{2} = 4{,}85$ Å. This fairly well approximates the hexagonal c axis of bayerite, $c_H = 4{,}76$. If we construct now the orthorhombic cell belonging to the hexagonal cell of bayerite, then we obtain for it nearly the same axes a and b as in the hydrargillite lattice. This is shown in the following schedule presenting the monoclinic unit cell of hydrargillite with halved c axis, and the orthorhombic unit cell of bayerite derived from MONTORO's hexagonal cell. On considerations expounded later, we had to choose the transformation from hexagonal to orthorhombic in such a way that as compared to hydrargillite the orthorhombic a and b axis of bayerite should be interchanged.

The monoclinic halved unit cell of hydrargillite		The orthorhombic cell of bayerite	
a	= 8,624 Å	$a_0 = a_H$	= 5,01 Å
b	= 5,06 Å	$b_0 = a_H \cdot \sqrt{3}$	= 8,68 Å
$\frac{c}{2}$	= 4,85 Å	$c_0 = c_H$	= 4,76 Å
β	= 94°34′ Å		

Let us consider one layer of hydrargillite lattice in which anions are without any distortion close-packed in a hexagonal arrangement, as it is seen in Fig. 1. Taking repeatedly such layers parallel to each other at equal distances of 4,76 Å will result in an anion arrangement to which a hexagonal, or, corresponding to it, an orthorhombic cell may be assigned, which latter contains 4 molecules of $Al(OH)_3$ similar to one half of the hydrargillite unit cell.

Taking in the undistorted layer of Fig. 1 the length of the assigned hexagonal axis a to be 5,01 Å, as given by MONTORO for the bayerite unit cell, then in the hexagonal arrangement of the close-packed anion layers, the distance between the anions will be 2,87 Å, the same as the greatest edge of the distorted octahedra found in the hydrargillite lattice, to be 2,88 Å.

To this ionic arrangement three-fold rotation axes parallel to the hexagonal axis c may be assigned, without, however, the cell being of hexagonal symmetry. Accordingly, there exists in the bayerite crystal lattice but a pseudohexagonal symmetry like in hydrargillite.

In the undistorted ionic arrangement of Fig. 1, besides the threefold rotation axes there are in three directions (at angles of 120° to each other) twofold rotation and screw axes and perpendicular to them are symmetry and glide planes, with correlated symmetry centers.

If we consider the threefold rotation axes to be the actual symmetry elements of bayerite, and the other symmetry elements all or partly absent, then the crystal lattice of bayerite may be described with a rhombohedral unit cell possessing the hexagonal dimensions given by MONTORO. If only the twofold rotation and screw axis are left to be considered beside the threefold rotation axis, the space group will be D_3^1 — C312. However, if there are no other symmetry elements to consider, besides the three fold axes the ionic arrangement may be described with the space group C_3^1 — C3.

It may be assumed with great certainty that similar to the hydrargillite lattice and the other aluminium hydroxide lattices, the octahedra $(OH)^-$ of the bayerite lattice is also distorted. This means that in order to come to the true lattice of bayerite we must adequately deform the ionic arrangement of Fig. 1. The kind of distortion that is necessary to obtain the bayerite structure determines which symmetry elements remain in the bayerite structure of those of Fig. 1. Considering that the structure of bayerite is in very close relation to hydrargillite, it seems that we best approach the structure of bayerite by turning from the hexagonal unit cell of MONTORO to the orthorhombic unit cell, in which there are, parallel to the plane (010), mirror planes in $y = O$ and $\frac{1}{2}$ and glide planes in $y = \frac{1}{4}$ and $\frac{3}{4}$, then twofold rotation axes parallel to [010] in OyO

$\frac{1}{2}\,yO$, $Oy\,\frac{1}{2}$ and $\frac{1}{2}\,y\,\frac{1}{2}$ and twofold screw axes parallel to the same direction in $\frac{1}{4}\,yO$, $\frac{3}{4}\,yO$, $\frac{1}{4}\,y\,\frac{1}{2}$ and $\frac{3}{4}\,y\,\frac{1}{2}$. There are also symmetry centers in the mirror and glide planes and in addition the unit cell is C centered.

This symmetry combination of the orthorhombic cell allows more deformation in the arrangement of the ions presented in Fig. 1, and in this way we can easily arrive at the distorted octahedra of the aluminium hydroxide crystals.

If we convert the indices of the reflexions of bayerite into those of an orthorhombic cell, we can see that there are only reflexions with $h + k = 2n$, which is the extinction of the space group of C_{2h}^3 — C2/m. From this and what we concluded above it follows that bayerite crystallizes according to the monoclinic system. The ionic arrangement of the unit cell may be derived from the hydrargillite structure by the repetition of only one hydrargillite layer, where the monoclinic angle β is 90°. It was necessary to change axes a and b in the orthorhombic cell contrary to hydrargillite in order to achieve that the mirror plane should be rectangular to axis b, as it is customary in the monoclinic crystal system.

The parameters of the regular ionic arrangement of Fig. 1 are according to the «Internationale Tabellen» (Bornträger, 1935) as follows:

4 Al : (*g*) *OyO* $\qquad y = \frac{1}{3}$

4 O_1 : (*i*) *xOz* $\qquad x = \frac{1}{3}, \qquad z = -0{,}22$

8 O_2 : (*j*) *xyz* $\qquad x = \frac{1}{6}, \qquad y = \frac{1}{6} \qquad z = +0{,}22$

The choice of coordinate z was made so as to have the distance of the two close-packed ion planes be 2,12 Å, the same as in hydrargillite. The neighbouring layers may, however, come somewhat closer to each other than in hydrargillite, because in the bayerite lattice there are layers ordered in the same sequence which follow each other. Accordingly, axis c will be somewhat shorter than that of hydrargillite. The other two cell dimensions change too, but to a smaller and equal extent and in a direction opposite to each other, therefore the density calculated from the X-ray data is a little higher ($s_x = 2{,}487$) than with hydrargillite ($s_x = 2{,}440$). The measured density of bayerite according to FRICKE and SEVERIN is $s = 2{,}529$.

The ideal structure of bayerite is shown in Fig. 2. The length of the octahedral edges reaching from one ionic plane into the other is 2,69 Å, i. e. by 6,3% longer than those lying in the close-packed ion planes. This means that the octahedra are to a certain extent distorted even at the ideal ionic arrangement given above. In these octahedra the distance Al-O is equal to 1,98 Å, i. e. the same as the greatest distance Al-O in hydrargillite. In the layers the neighbouring octahedra join each other with a common edge, just as in hydrargillite.

The intensities of the reflexions calculated with the ideal coordinates given above are seen in Table I. The atomic scattering factors are taken from the «Internationale Tabellen» (Bornträger, 1935) without any correction.

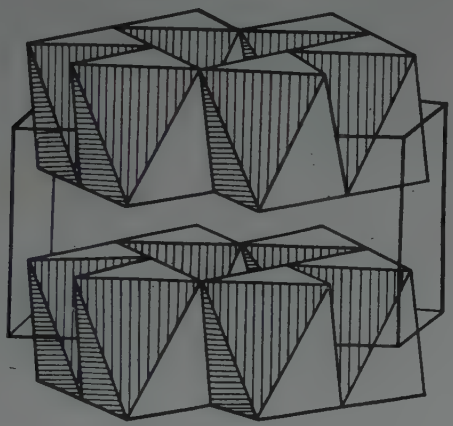

Fig. 2

It is evident from Table I that the calculated intensities agree well with those estimated on the powder photographs by FRICKE and by us. The greatest difference is exhibited at the coinciding reflexions of (200) and (130). We found a weak intensity for this double reflexion, whilst FRICKE describes it as a medium one. This difference finds an explanation in that FRICKE had not filtered the *X*-ray radiation whereby at the place of this reflexion the line $K\beta$ of the very strong reflexions (201) and (131) appeared too.

The little difference between the estimated and calculated intensity means that the ideal parameters of the structure given in Fig. 2 approximate the true structure fairly well. This requires, however, a slight distortion of the ideal ionic arrangement, as already pointed out before when concluding from another consideration.

The *X*-ray reflexions of bayerite could be readily identified by those calculated from the monoclinic cell as derived from the cell dimensions of MONTORO, with the only exception of one weak reflexion existing in both *a*- and *b*-bayerites. This reflexion appears with FRICKE as well as with us

and cannot be explained by the given cell dimensions. Besides, it is very near to the inadmissible reflexion (211).

Table I

The estimated and calculated intensity of the X-ray reflexions of α-bayerite

Refl. (hkl)	Intensity		Refl. (hkl.)	Intensity		Refl. (hkl)	Intensity	
	Est.	Calc.		Est.	Calc.		Est.	Calc.
001	12	77,0	060 330	5	26,0	402 262	2	8,3
110 020	7	23,0	061 331	2—3	12,0	080 440	0,5	0,5
111 021	3	27,0	242 152 312	0,5	3,4	204 134 422		
200 130	1	0,2	203 133	4—5	17,4	172 352 063	1—2	4,9
002	0,5—1	3,4	013 223	0,5	1,4	333 081	—	0,2
201 131	15	99,0	400 260	0,5	0,3	044 224	—	0,8
040 220	0,5	4,0	062 332	—	0,1	280 370 510	—	0,8
022 112	0,5	4,2	401 261	3—4	9,9	082	—	0,2
041 221	1	6,6	420 170 350	—	0,5	403 263 281	1—2	6,6
202 132	8	47,0	004	1	2,4	371 511	—	1,4
240 150 310	0,5—1	3,5	171 421 351	0,5—1	2,0	244 154 314	—	1,4
042 222	1	2,1	024	—	0,4	173 423	0,5	1,4
003	—	0,1	114	—	0,6	353 460		
241 151 311	1—2	5,5	243 153 313	1	1,0	530 190	0,5	0,6
023 113	0,5	2,7				005	—	1,0

The calculated intensity of the reflexions showing the greatest difference between *a*- and *b*-bayerite comes nearest to that of *a*-bayerite. From the reflexions (002) and (201) it may be stated with certainty that the structure described above is identical with that of *a*-bayerite.

SUMMARY

It has been shown, that from the hydrargillite layer lattice an ideal crystal structure may be derived for bayerite. This lattice contains the hexagonal unit cell given by MONTORO for bayerite, the real structure, however, proved monoclinic $C_{2h}^3 - C2/m$, with 4 molecules in it. The observed and calculated intensities agree very well. From the calculated intensity it is evident that the structure described is identical with that of a-bayerite.

LITERATURE

1. FRICKE, R.: Z. anorg. allg. Chem., **179**, 287, 1929; **175**, 249, 1928.
2. KRAUT, H., FLAKE, E., SCHMIDT, W., VOLNER, H.: Ber. Deutsch. Chem. Ges. **75**, 1357, 1942.
3. SCHMÄH, H.: Z. Naturforschung **1**, 323, 1946.
4. MONTORO, V.: Ric. Sic. Progr. Techn. **13**, 565, 1942.
5. FUNAKI, K., SHIMIZU, Y.: J. Chem. Soc. Japan, Ind. Chem. Sect. **55**, 135, 1952.
6. MEGAW, H. D.: Z. Krist. A. **87**, 185, 1934.

КРИСТАЛЛИЧЕСКАЯ СТРУКТУРА А-БАЙЕРИТА $Al(OH)_3$

К. ШАШВАРИ

Резюме

Монторо в 1942 г. установил для байерита гексагональную ячейку, с которой рентгеновская пылевая диаграмма хорошо может быть индексирована. Исходя из этого, кристаллическую решетку байерита можно вывести из решетки гидраргиллита, а именно таким образом, что анионные плоскости в каждом втором ионном слое решетки гидраргиллита — оставляя катионы на месте — сдвигаем параллельно с направлением $[11\bar{2}0]$ соответствующим гексагональному, плотно сопряженному распределению слоя, но в обратном смысле на растояние $a_H/3$, вследствие чего все последующие слои будут относяться к типам А—В или В—А. Одновременно все слои сдвигаются один по сравнению с другим лишь в небольшой мере таким образом, чтобы моноклинный угол β был ликвидирован. Выведенная таким образом решетка может быть построена из гексагональной решетки Монторо, однако согласно присутствующим элементам симметрии решетка не обладает гексагональной симметрией.

Выведенная из гидраргиллита решетка предоставляет немного идеализированное строение байерита. Однако ввиду хорошего совпадения интенсивностей оно приближается к настоящей решетке. Симметрии, обнаруживаемые в идеальном распределении ионов, вследствие вероятных небольших искажений, ведущих к настоящей решетке, отчасти исчезают. Смотря по тому, какие симметрии сохраняются после искажения, могут осуществляться две ромбоэдрические и одна моноклинная комбинации симметрий. Ввиду значительного сходства с гидраргилитом весьма вероятно, что сохраняется симметрия моноклинной пространственной группы $C_{2h}^3 - C2/m$, которую можно связывать с орторомбической ячейкой, относящейся к ячейке Монторо. На основании расчетных и измеренных интенсивностей данная структура идентична с структурой а-байерита.

A kiadásért felelős: az Akadémiai Kiadó igazgatója Műszaki felelős: Farkas Sándor
A kézirat beérkezett: 1955. XI. 4. — Terjedelem: 11¾ (A/5) ív, 52 ábra, 2 melléklet

37990/56 — Akadémiai Nyomda, V., Gerlóczy u. 2. — Felelős vezető: ifj. Puskás Ferenc

Les *Acta Geologica* paraissent en russe, français, allemand et anglais et publient les travaux du domaine des sciences géologiques.

Les *Acta Geologica* sont publiés sous forme de fascicules qui seront réunis en un volume par an.

On est prié d'envoyer les manuscrits destinés à la rédaction et écrits à la machine à l'adresse suivante :

Acta Geologica, Budapest, 62. *Postafiók* 440.

Toute correspondance doit être envoyée à cette même adresse.

Le prix de l'abonnement annuel est de 110 forints.

On peut s'abonner à l'Entreprise du Commerce Extérieur de Livres et Journaux «Kultúra» (Budapest VI., Sztálin út 21. Compte-courant No. 43-790-057-181) ou à l'étranger chez tous les représentants ou dépositaires.

The *Acta Geologica* publish papers on geological and relative subjects in Russian, French, German and English.

The *Acta Geologica* appear in parts of various size, making up one volume yearly.

Manuscripts should be typed and addressed to :

Acta Geologica, Budapest, 62, *Postafiók* 440.

Correspondence with the editors and publishers should be sent to the same address.

The rate of subscription to the *Acta Geologica* is 110 forints a volume. Orders may be placed with «Kultúra» Foreign Trade Company for Books and Newspapers (Budapest, VI., Sztálin út 21. Account No. 43-790-057-181) or with representatives abroad.

Die *Acta Geologica* veröffentlichen Abhandlungen aus dem Bereiche der geologischen Wissenschaften in russischer, französischer, deutscher und englischer Sprache.

Die *Acta Geologica* erscheinen in Heften wechselnden Umfanges. Mehrere Hefte bilden jährlich einen Band.

Die zur Veröffentlichung bestimmten Manuskripte sind, mit Maschine geschrieben, an folgende Adresse zu senden :

Acta Geologica, Budapest 62, *Postafiók* 440.

An die gleiche Anschrift ist auch jede für die Redaktion und den Verlag bestimmte Korrespondenz, zu senden.

Abonnementspreis pro Band 110 Forint. Bestellbar bei dem Buch- und Zeitungs-Aussenhandels-Unternehmen «Kultúra» (Budapest, VI., Sztálin út 21. Bankkonto Nr. : 43-790--057-181) oder bei seinen Auslandsvertretungen und Kommissionären.

32,— Ft

INDEX

CRISTALLOGRAPHIA – MINERALOGIA – PETROGRAPHIA – GEOCHEMIA

FÖLDVÁRI-VOGL, M. — KOBLENCZ, V.: Sur les possibilités de l'analyse thermique différentielle des minéraux de manganèse — Возможности применения дифференциально-термического анализа при изучении марганцовых минералов ... 85

GEDEON, T. G.: Bayerite in Hungarian Bauxite — Байерит в венгерском боксите 95

KLIBURSZKY, B.: Thermische Schnellanalyse, ein DTA-Apparat für industrielle Serienprüfungen — Ускоренный термический анализ: прибор для дифференциально-термического анализа, применяемый при серийных исследованиях промышленного характера 107

KONTA, J. (Prague): Crystal Orientation of two Phosphates in the Scales of Permian Fish of the Group *Palaeoniscidae* — Закономерно ориентированное срастание двух фосфатов в чешуях рыб пермского периода, группы *Palaeoniscidae*..... 113

SASVÁRI, K.: The Crystal Structure of A-Bayerite, $Al(OH)_3$ — Кристаллическая структура А-байерита..... 123

GEOPHYSICA

AUJESZKY, L.: Détermination des valeurs numériques pour le moment d'inertie, le moment angulaire et l'énergie cinétique rotatoire de l'atmosphère terrestre — Определение момента инерции, углового момента и кинетической энергии вращения атмосферы 1

BARTA, GY.: A 40—50 Year Period in the Secular Variation of the Geomagnetic Field — О периоде 40–50 лет вековой вариации геомагнитного поля 15

EGYED, L.: A New Theory on the Internal Constitution of the Earth and its Geological-Geophysical Consequences — Новая теория внутреннего строения Земли и ее геологические и геофизические результаты..... 43